A DEVICE FOR MEASURING THE SPATIAL ORIENTATION BETWEEN TWO SEPARATING STAGES OF A SPACE VEHICLE

NUCLEAR AEROSPACE RESEARCH FACILITY

operated by

GENERAL DYNAMICS | *Fort Worth Division*

NUCLEAR AEROSPACE RESEARCH FACILITY

A DEVICE FOR MEASURING THE SPATIAL ORIENTATION BETWEEN TWO SEPARATING STAGES OF A SPACE VEHICLE

Prepared for the

AVIONICS BRANCH of the
GEORGE C. MARSHALL SPACE FLIGHT CENTER
HUNTSVILLE, ALABAMA

Contract NAS8-11995

GENERAL DYNAMICS

Fort Worth Division

ABSTRACT

A device for measuring the spatial orientation between two separating stages of a space vehicle has been designed, developed, and tested by the Fort Worth Division of the General Dynamics Corporation. The device was developed for the Avionics Division of the George C. Marshall Space Flight Center. The design is based on its use between the S-IVB and S-II stages of Saturn V. The measuring capabilities of the system were determined by testing on a full-scale test rig. The theory and fabrication techniques are discussed to assist in any design changes that may be required if the device is to be used for another vehicle configuration.

TABLE OF CONTENTS

TABLE OF CONTENTS (Cont'd)

vi

LIST OF FIGURES

LIST OF FIGURES (Cont'd)

LIST OF TABLES

I. INTRODUCTION

The Fort Worth Division of the General Dynamics Corporation has designed, fabricated, and tested a device for measuring the changing spatial orientation between two separating stages of a space vehicle. The program was performed for the George C. Marshall Space Flight Center and the system was designed for use between the S-IVB and S-II stages of Saturn V.

Operation of the device is based on making six distance measurements between the separating stages. Each distance is that between a detector and a radiation source, where the signal from the detector is a function of the inverse square of the distance. These six measurements are sufficient for calculating the spatial orientation of one stage relative to the other.

The system was designed and tested to meet the severe vibration environment of the Saturn V launch. All electronic components and detector parts are embedded in potting compounds.

A full-scale test rig was constructed and the limits of distance, tilt, rotation, slip, and velocity were determined by actual measurements.

II. THEORY OF DETECTOR AND SOURCE ARRAY

A number of different source-detector arrays were considered before the one described in this document was selected. These varied from one source and one detector to six sources and six detectors. The one-source and one-detector array would give one distance measurement only, whereas the larger number of measurements would provide an abundance of information but would also require more instrumentation or, more specifically, more telemetry channels. The problem was to find an array that would give the required information with the minimum amount of instrumentation.

The measurements required of the system are as follows:

1. A separation rate of 0-400 in./sec with an accumulative measuring error of ±8 in./sec.

2. The included angle between the longitudinal axes of the two stages of the vehicle, measured as a function of time, over a maximum angle of ±15 deg with a maximum accumulative measuring error of 0.5 deg.

3. A separation distance of 15 ft with maximum errors as follows: 0-0.5 ft ± 0.5 in.; 0.5-7.5 ft ± 0.5 in.; 7.5-15 ft ± 1.0 in.

The least complex system capable of meeting the above requirements is one that would provide two distance measurements and one angular measurement. However, such an array is limited in its ability to measure movement between the two stages and, because of the particular configuration of the S-IVB/II stages, the sources and detectors would have to be intermixed on each stage. This is undesirable for two reasons: (1) detectors on both stages would complicate the telemetry problem and (2) the detectors on the S-IVB stage would not have access to the much greater electrical power supply that is available on the S-II stage.

The six-distance measurement array described in this document will measure any movement between the two stages, and there is a large enough circumference on the S-IVB/II stages to measure a 15-deg tilt at 15 ft without interference between sources.

The one distance, one-angle measurement was considered in some detail for this task, but was discarded and the six-measurement array was used for the following reasons:

1. The centerline of the vehicle could not be used because of the gimbled location of the S-IVB engine. This would require detectors on both stages and a complex computation for the angle between the vehicles.

2. The angle-distance array has limitations on measuring the spatial orientation if the distance between the centerlines of the stages becomes excessive.

3. The six-distance measurement array has no restrictions on its movement within magnitude limits.

4. Although the six-distance measurement array has more electronic channels, it has only one type of channel.

5. The angle-measuring channel would require a larger dynamic range than the distance-measuring channel.

The result of the angle-distance array work is presented in Appendix A, since it could be useful for other applications.

2.1 Properties of Six-Measurement Array

The relative position between any two planes requires a minimum of six selective values. These values can be obtained using six detectors and three sources, as shown in Figure 2-1.

The sources are located at the corners of an equilateral triangle, GHJ, and the detectors at the corners of a regular hexagon, ABCDEF. The source and detector arrays, of course, are known. The measured values are the distances $\overline{AG}$, $\overline{BG}$, $\overline{CH}$, $\overline{DH}$, $\overline{EJ}$, and $\overline{FJ}$. The voltage from each detector is proportional to the inverse of the distance squared. The desired values are the distance $\overline{OO'}$ between the centers of the detector and source planes, and the angle θ between the normals to the above planes.

Since the sources are rigid in one plane and the detectors are rigid in the other plane, the number of degrees of freedom for the source triangle is six, corresponding to six independent measurements. Pitch, yaw, and roll are possible in this

4
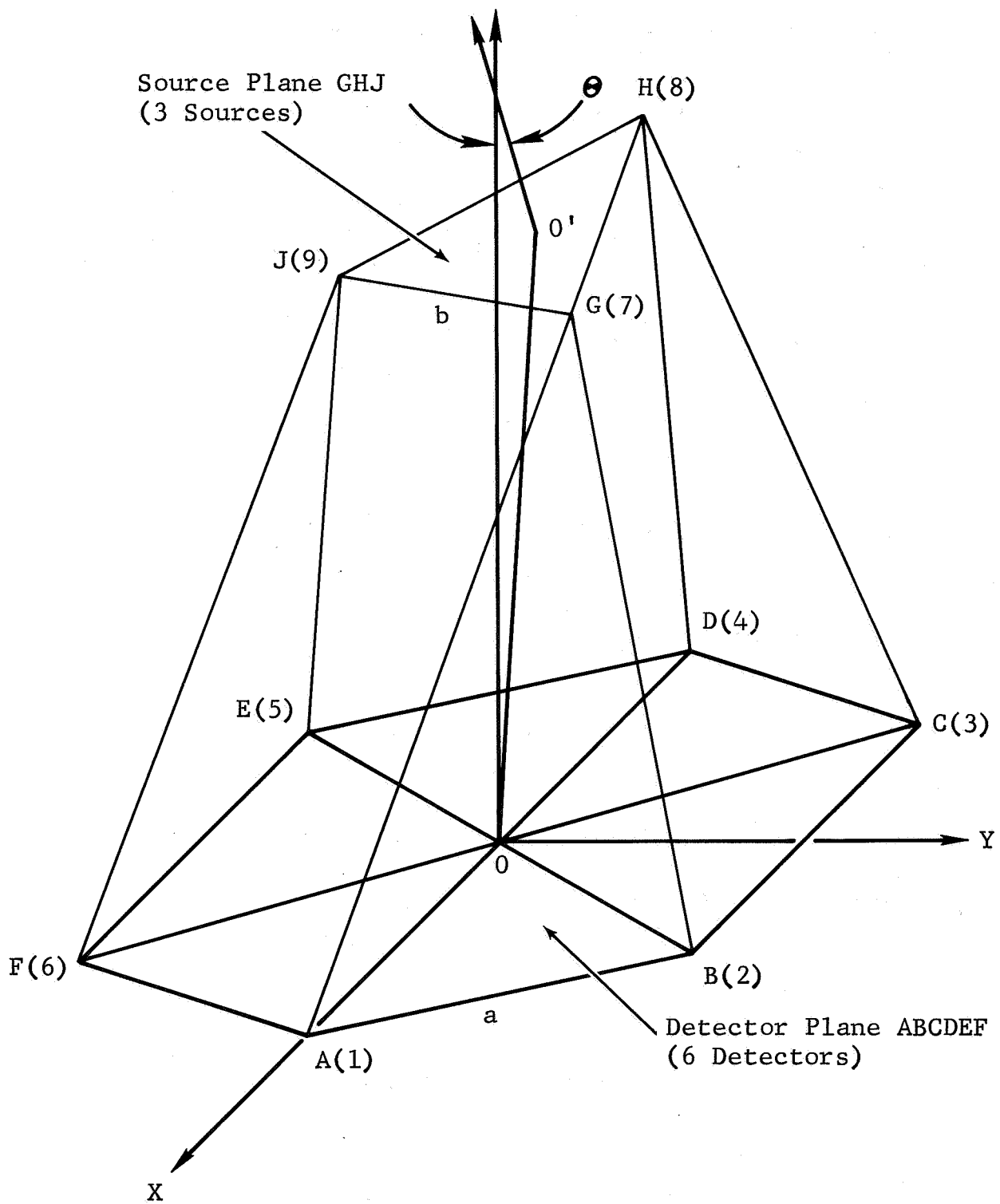
Figure 2-1 Source-Detector Relationship for
Six-Distance Array

configuration. The equations to be solved are

$$(x_7 - x_1)^2 + (y_7 - y_1)^2 + (z_7 - z_1)^2 = r_{17}^2$$

$$(x_7 - x_2)^2 + (y_7 - y_2)^2 + (z_7 - z_2)^2 = r_{27}^2$$

$$(x_8 - x_3)^2 + (y_8 - y_3)^2 + (z_8 - z_3)^2 = r_{38}^2$$

$$(x_8 - x_4)^2 + (y_8 - y_4)^2 + (z_8 - z_4)^2 = r_{48}^2$$

$$(x_9 - x_5)^2 + (y_9 - y_5)^2 + (z_9 - z_5)^2 = r_{59}^2$$

$$(x_9 - x_6)^2 + (y_9 - y_6)^2 + (z_9 - z_6)^2 = r_{69}^2$$

$$(x_8 - x_7)^2 + (y_8 - y_7)^2 + (z_8 - z_7)^2 = b^2$$

$$(x_9 - x_8)^2 + (y_9 - y_8)^2 + (z_9 - z_8)^2 = b^2$$

$$(x_9 - x_7)^2 + (y_9 - y_7)^2 + (z_9 - z_7)^2 = b^2$$

The distance $\overline{OO'}$ is given by

$$x_{0'}^2 + y_{0'}^2 + z_{0'}^2 = (\overline{OO'})^2$$

where

$$x_{0'} = \frac{1}{3}(x_7 + x_8 + x_9)$$

$$y_{0'} = \frac{1}{3}(y_7 + y_8 + y_9)$$

$$z_{0'} = \frac{1}{3}(z_7 + z_8 + z_9)$$

Determination of the angle involves finding the equations for the two planes, namely

$$\alpha_1 x + \beta_1 y + \gamma_1 z + \delta_1 = 0 \quad \text{for the detector plane}$$

and

$$\alpha_2 x + \beta_2 y + \gamma_2 z + \delta_2 = 0 \quad \text{for the source plane}$$

In this case, set $\alpha_1 = \beta_1 = \delta_1 = 0$; $\gamma_1 = 1$ and the detector plane equation is

$$z = 0$$

The source plane equation is easily derived from the determinant

$$\begin{vmatrix} x & y & z & 1 \\ x_7 & y_7 & z_7 & 1 \\ x_8 & y_8 & z_8 & 1 \\ x_9 & y_9 & z_9 & 1 \end{vmatrix} = 0$$

Which corresponds to the equation

$$\alpha_2 x + \beta_2 y + \gamma_2 z + \delta_2 = 0$$

The angle between the normals is given by

$$\cos\theta = \pm \frac{\alpha_1 \alpha_2 + \beta_1 \beta_2 + \gamma_1 \gamma_2}{\sqrt{\alpha_1^2 + \beta_1^2 + \gamma_1^2}\sqrt{\alpha_2^2 + \beta_2^2 + \gamma_2^2}}$$

7

which,by choosing the acute angle and substituting $\alpha_1 = \beta_1 = \delta_1 = 0$, $\gamma_1 = 1$ gives

$$\cos \Theta = \frac{\gamma_2}{\sqrt{\alpha_2^2 + \beta_2^2 + \gamma_2^2}}$$

2.2 Computer Method

An IBM 7090 digital computer program was set up and checked for use in solving for $\overline{OO}'$ and Θ when the six distances are known. The routine, designated A12 by the Fort Worth Division, consists of two decks, as follows:

1. Library Deck (Initial Conditions)

This deck of cards contains the position of the detector plane, e.g., (X1, Y1, Z1) is the position of detector 1, and the distance between sources, B. In the cases programmed this was the x-y plane.

Card

1   LIBRARY

	1-7	9-15	17-23	25-31	33-39	41-47	49-55	63-68	69	70-72	73-77	78-80
2	X1	X2	X3	X4	X5	X6	Y1	JOBNO	L	DECKNO	SEQ	PRO
3	Y2	Y3	Y4	Y5	Y6	Z1	Z2					
4	Z3	Z4	Z5	Z6	B							

FORMAT (2A4)

FORMAT (6(F7.2,1X), F7.2)

2. Problem Deck

This deck of cards gives the library deck to be used; a constant which is greater than any R^2, where R is the distance from a source to detector; a convergence factor, CONV; a scale

8

factor for the six distances; and an indicator, IRCD, for reading in a guess or using the last answer calculated. If IRCD < 0 the old answer from the previous problem is used as a guess. For example, $(X_7Y_7Z_7)$ etc. is a guess for the solution to the problem. In the example below,

$$R_i{}^2 = VC/SV_i \quad \text{where } i = 1,6$$

$$= \text{the square of the distance} \\ \text{between detector and source} \\ \text{for each of the six detectors.}$$

1-7	11-16	17-19	21-30	31-40	46-50
PROBLEM	LIB.JOB.NO.	DECK NO.	VC	CONV	IRCD
1-10	11-20	21-30	31-40	41-50	51-60
SV1	SV2	SV3	SV4	SV5	SV6
X7	Y7	Z7			
X8	Y8	Z8			
X9	Y9	Z9			

FORMAT (2A4, 2X, I6, I3, 1X, 2E10.0, 5X, I5)

FORMAT (6E10.0)

FORMAT (3F10.0)

Three test cases were successfully computed using this routine:
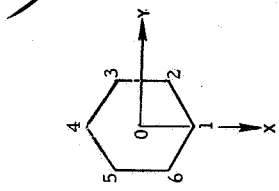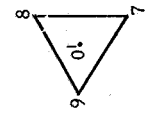
> Case 1 Separation, no tilt, no translation
>
> Case 2 Separation, tilt, no translation
>
> Case 3 Separation, tilt, translation

The detectors are represented as points 1 through 6 on the detector plane and 0 in the center of the detector circumference. The sources are points 7, 8, and 9 relative to detector center 0. The center of the source circumference is 0'. The data for each case, including hand-calculated results, are shown in Table 2-1. Figure 2-2 is a photograph of the 7090 outputs for each case.

Table 2-1

COMPUTER INPUT AND OUTPUT FOR IBM 7090 PROCEDURE A12 TEST CASES

Geometry	Case 1 Separation (in.)			Case 2 Separation and Tilt (in.)			Case 3 Separation, Tilt, & Translating (in.)		
	x	y	z	x	y	z	x	y	z
Detectors: Lower Stage									
0	0	0	0						
1	115.9	0	0						
2	57.95	100.37	0						
3	-57.95	100.37	0						
4	-115.9	0	0						
5	-57.95	-100.37	0						
6	57.95	-100.37	0						
Sources: Upper Stage									
7	99.75	57.59	36	99.75	55.63	201.10	109.75	75.63	201.10
8	-99.75	57.59	36	-99.75	55.63	201.10	-89.75	75.63	201.10
9	0	-115.18	36	0	-111.26	245.81	10	-91.26	245.81
0'	0	0	36			216	10	20	26
Results									
$r_{OO'}$		36			216			217.154	
θ		0°			15°			15°	
Distance Between Detectors									
r^2_{17}	4,873.4			43,797			46,199		
r^2_{27}	4,873.4			44,190			43,737		
r^2_{38}	4,873.4			44,190			42,065		
r^2_{48}	4,873.4			43,797			46,845		
r^2_{59}	4,873.4			63,899			65,123		
r^2_{69}	4,873.4			63,899			62,805		

Case 1: Separation, No Tilt or Translation

R17**2	R27**2	R38**2	R48**2	R59**2	R69**2	B
4.8734+03	4.8734+03	4.8734+03	4.8734+03	4.8734+03	4.8734+03	1.9950+02

X1	X2	X3	X4	X5	X6	X7	X8	X9
1.1590+02	5.7950+01	-5.7950+01	-1.1590+02	-5.7950+01	5.7950+01	9.9750+01	-9.9750+01	1.3894-07

Y1	Y2	Y3	Y4	Y5	Y6	Y7	Y8	Y9
0.	1.0037+02	1.0037+02	0.	-1.0037+02	-1.0037+02	5.7590+01	5.7590+01	-1.1519+02

Z1	Z2	Z3	Z4	Z5	Z6	Z7	Z8	Z9
0.	0.	0.	0.	0.	0.	3.6000+01	3.6000+01	3.5997+01

DISTANCE BETWEEN PLANES = 3.599908+01 INCHES

THETA = -0. DEGREES

Case 2: Separation and Tilt, No Translation

R17**2	R27**2	R38**2	R48**2	R59**2	R69**2	B
4.3797+04	4.4190+04	4.4190+04	4.3797+04	6.3899+04	6.3899+04	1.9950+02

X1	X2	X3	X4	X5	X6	X7	X8	X9
1.1590+02	5.7950+01	-5.7950+01	-1.1590+02	-5.7950+01	5.7950+01	9.9750+01	-9.9750+01	-5.9494-08

Y1	Y2	Y3	Y4	Y5	Y6	Y7	Y8	Y9
0.	1.0037+02	1.0037+02	0.	-1.0037+02	-1.0037+02	5.5632+01	5.5632+01	-1.1126+02

Z1	Z2	Z3	Z4	Z5	Z6	Z7	Z8	Z9
0.	0.	0.	0.	0.	0.	2.0110+02	2.0110+02	2.4581+02

DISTANCE BETWEEN PLANES = 2.160034+02 INCHES

THETA = 1.499741+01 DEGREES

Case 3: Separation, Tilt, and Translation

R17**2	R27**2	R38**2	R48**2	R59**2	R69**2	B
4.6199+04	4.3737+04	4.2065+04	4.6845+04	6.5123+04	6.2805+04	1.9950+02

X1	X2	X3	X4	X5	X6	X7	X8	X9
1.1590+02	5.7950+01	-5.7950+01	-1.1590+02	-5.7950+01	5.7950+01	1.0975+02	-8.9749+01	1.0001+01

Y1	Y2	Y3	Y4	Y5	Y6	Y7	Y8	Y9
0.	1.0037+02	1.0037+02	0.	-1.0037+02	-1.0037+02	7.5628+01	7.5627+01	-9.1259+01

Z1	Z2	Z3	Z4	Z5	Z6	Z7	Z8	Z9
0.	0.	0.	0.	0.	0.	2.0110+02	2.0110+02	2.4581+02

DISTANCE BETWEEN PLANES = 2.171585+02 INCHES

THETA = 1.499759+01 DEGREES

Figure 2-2 IBM 7090 Computer Printout of Test Cases

11

III. SOURCE SELECTION

3.1 Source Type

The selection of the source energy involved consideration of the following factors:

1. High-energy radiation suffers less attenuation in air and exhaust gases than low-energy radiation.

2. High-energy radiation is scattered less by air and surrounding structures than low-energy radiation.

3. The detector output current per incident flux pulse increases as the radiation energy increases.

4. High-energy sources require more shielding, resulting in a higher weight system.

5. The counting efficiency in a scintillating crystal increases with decreasing energy. The efficiency is essentially 100% for energies less than 0.15 MeV in a 2- by 2-in. NaI(Tl) crystal.

6. A relatively long half-life is required to eliminate recalibration of the associated electronics within a minimum time of about two weeks between installation of sources and launch.

Since alphas would suffer too much attenuation by air and rocket gases, only gamma emitters were considered. Table 3-1 lists four having characteristics suitable for systems similar to the one developed in this project. Of those listed, cesium-137 was considered to be the most practical for this particular application. Cobalt-60 gammas have too high an energy; cerium-144 has too short a half-life; and americium-241 gammas have too low an energy, considering the 0.5% accuracy requirement.

Table 3-1

CHARACTERISTICS OF POTENTIAL GAMMA SOURCES

Source	Max Energy (Mev)	Half-Life	Specific Activity (Ci/g)	Dose Rate from 2.5-Ci Source at 1 m (R/h)	Shielding Required for Dose Rate of 10 mR at 1 m (in.)		
					Pb	Cu	Fe
Cs^{137}	0.661	33 y	7.94×10^1	0.89	1.14	2.8	3.01
Co^{60}	1.33	5.27 y	1.14×10^3	3.3	4.12	5.12	7.41
Ce^{144}	0.134	282 d	3.22×10^3	1.7	0.04	0.76	1.02
Am^{241}	0.0597	470 y	3.16	0.104	0.024	0.065	0.098

3.2 Source Strength

The equation which governs the response of a pulse integrating amplifier is as follows:

$$Q_T = qN_oRCe^{-T/RC} + \int_0^T q \frac{N_o r_o^2 e^{-(T-t)/RC}}{r^2(t)} \, dt$$

where Q_T = charge on condenser at time T

q = increment of charge

N_o = initial count rate

RC = circuit time constant (product of resistance and capacitance of circuit)

r_o = initial separation distance

$r(t)$ = separation distance at time t

14

The equation cannot be solved directly. However, since RC must necessarily be small for tracking purposes, the function $1/r^2(t)$ can be expanded by a Taylor series about the point $r(T)$ and an integration performed. By keeping RC small, only two terms need to be retained. The equation cannot be solved because $r(t)$ is not known; however, a relatively simple and accurate solution can be reached after a few simple assumptions are made. For tracking purposes it is assumed that RC must be made small and that the separation velocity can then be considered constant over a period of several mean lifetimes (the RC time period is analogous to the mean life). The function $r^2(t)$ is then expanded about the point $r(T)$, giving

$$\frac{1}{r^2(t)} = \frac{1}{r^2(T)}\left\{1 + 2\left[\frac{v\epsilon}{r(T)}\right] + 3\left[\frac{v\epsilon}{r(T)}\right]^2 + 4\left[\frac{v\epsilon}{r(T)}\right]^3 + \ldots\right.$$

where $r(T)$ = distance at time T

   v = velocity at time T, approx. constant

   ϵ = T-t time interval

The integral is divided into two intervals: 0 to t_1, and t_1 to T. The integral reads

$$\int_0^T f(t)\, dt = \int_0^{t_1} f(t)\, dt + \int_{t_1}^T f(t)\, dt$$

$$= \int_T^{T-t_1} g(\epsilon)(-d\epsilon) + \int_{T-t_1}^0 g(\epsilon)(-d\epsilon)$$

which, for $T-t_1$ = KRC, with K some number, gives

$$\int_0^T f(t)\, dt = \int_{KRC}^T g(\epsilon)\, d\epsilon + \int_0^{KRC} g(\epsilon)\, d\epsilon$$

15

The integrable equation incorporating the Taylor expansion of $r(t)$ about $r(T)$ in terms of the variable is

$$Q_T = qN_oRCe^{-T/RC} + qN_or_o^2 \int_{KRC}^{T} g(\epsilon) \, d\epsilon + qN_or^2 \int_0^{KRC} g(\epsilon) \, d\epsilon$$

where

$$g(\epsilon) = \frac{e^{-\epsilon/RC}}{r^2(T)} \left\{ 1 + 2\left[\frac{v\epsilon}{r(T)}\right] + 3\left[\frac{v\epsilon}{r(T)}\right]^2 + 4\left[\frac{v\epsilon}{r(T)}\right]^3 + \ldots \right.$$

For $t > t_1 \gg RC > 0$, only the last integral is important. For $K > 1$, say 5, $e^{-K} \ll 1$, and the last integral reduces to

$$Q_T = \frac{qN_o \, r_o^2}{r^2(T)} RC\left(1 + 2RC \frac{v}{r(T)}\right)$$

Substituting the right-hand side of the above equation into

$$V_T = \frac{Q_T}{C}$$

and replacing $\frac{2v}{r}$ by its equivalent, $\frac{-1}{V} \frac{dV}{dt}$ or $\frac{-1}{V} \frac{\Delta V}{\Delta T}$, obtained by

differentation of the uncorrected relation $V(t) = \dfrac{V_o r_o^2}{r^2(t)}$,

gives $\quad r_T^2 = \dfrac{qN_oRr_o^2}{V_T} \left[1 - \dfrac{RC}{V_T}\left(\dfrac{\Delta V}{\Delta t}\right)\right]_T$

The second term within the brackets represents a first order correction term for velocity-detector response effects.

In order to prevent amplification of the statistical variation in V, Δt should be ≥ 10 RC. The overall error in r^2 is then

16

primarily dependent on V alone. It is easily shown that

$$\frac{PE(r^2)}{r^2} \approx \frac{2PE(r)}{r} \approx \frac{PE(V)}{V} \approx \frac{PE(N)}{N} = \frac{0.6745}{\sqrt{2NRC}}$$ where PE is the

probable error. Accuracy requirements are $\frac{PE(r)}{r} = 0.5\%$ or

$\frac{PE(V)}{V} = 1\%$.

With this restriction, and by limiting the lag correction term to a maximum of 3%, the minimum source strength is 2.5 curies per source and the minimum time constants for each of the three channels are as follows:

Channel			
1	1.4 msec	3	- 5.45 ft
2	2.5 msec	5.45	- 9.9 ft
3	4.5 msec	9.9	- 18 ft

The accuracy is directly proportional to the curie strength of the source, if the velocity requirement (RC time constants) remains constant.

IV. ELECTRONIC DESIGN

4.1 System Description

A block diagram of one of the six separation channels is shown in Figure 4-1. Each channel consists of a scintillation detector (sodium iodide crystal and photomultiplier tube) which drives a preamplifier which, in turn, drives three spreader amplifiers. The three spreader amplifiers, rather than one amplifier or one telemetry channel, are used to increase the accuracy. Eighteen telemetry outputs are required for the six separations channels.

The output of the scintillation detector is inversely proportional to the square of the distance separating the source and the detector. The signal from the photomultiplier tube is fed into an integrating feedback preamplifier which converts the excitation pulses to a voltage.

The output of each spreader amplifier covers approximately one-third of the total measured separation distance: amplifier A , from 0 to 5 ft; amplifier B , from 5 to 10 ft; and amplifier C , from 10 to 15 ft.

The complete electronics system (six detectors and the electronics package) requires 400 mA of current at 28 V dc for a total power consumption of 11.2 watts. The electronics unit and one of the six scintillation detectors are shown in Figure 4-2.

4.2 Scintillation Detector

The scintillation detector consists of a thallium-doped sodium iodide crystal and a photomultiplier tube. The incident gamma rays produce ionization and excitation within the scintillator and are subsequently absorbed within it. The conversion of this energy to light flashes is brought about by the luminescent process. By means of a light pipe most of the light is transmitted to the photocathode of the photomultiplier tube. The photoelectrons emitted at the photocathode are multiplied many times (1.7×10^5) by the dynodes of the tube. The output of the photomultiplier tube is inversely proportional to the square of the distance separating the detector and the source.
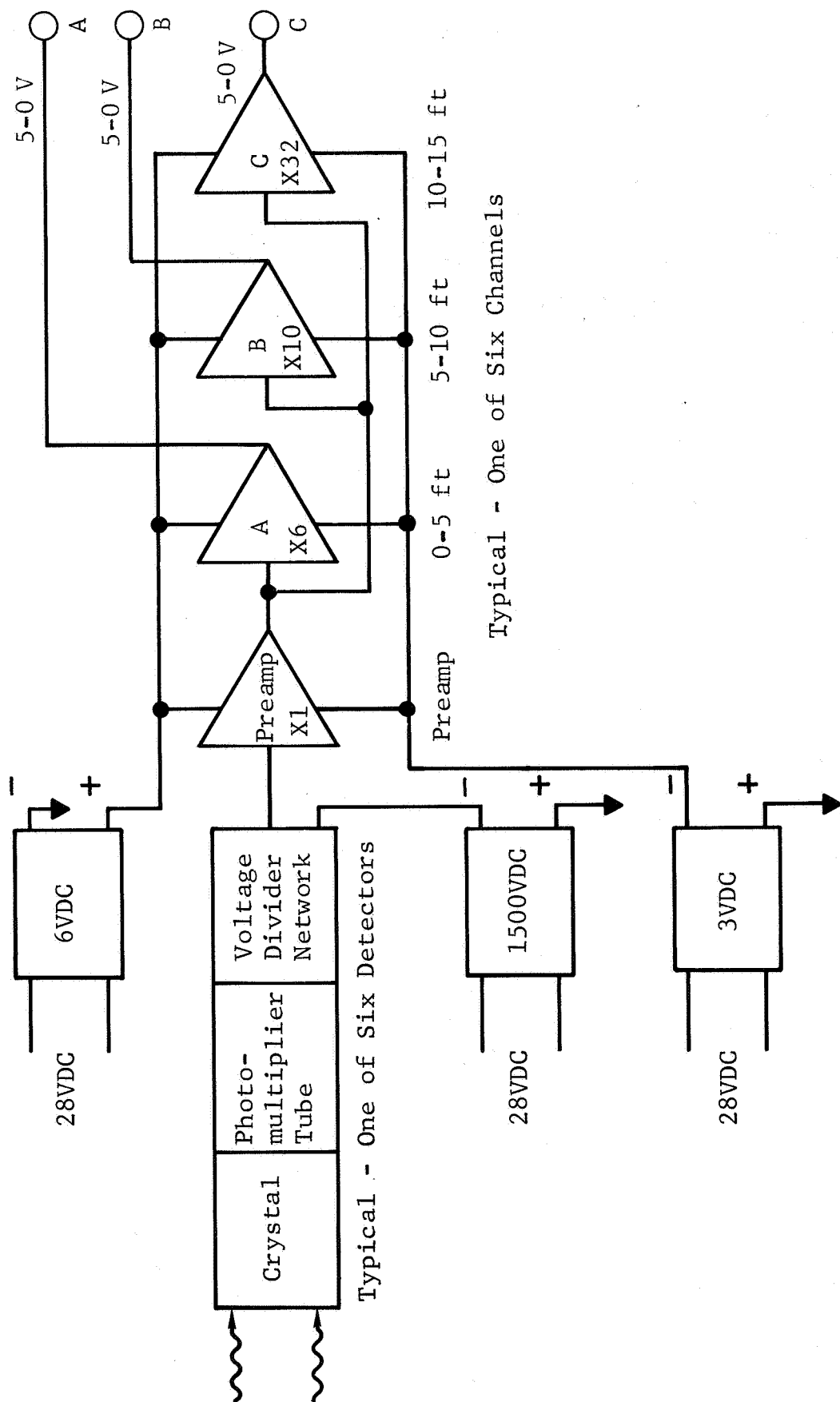
Figure 4-1 Block Diagram of Separation Unit
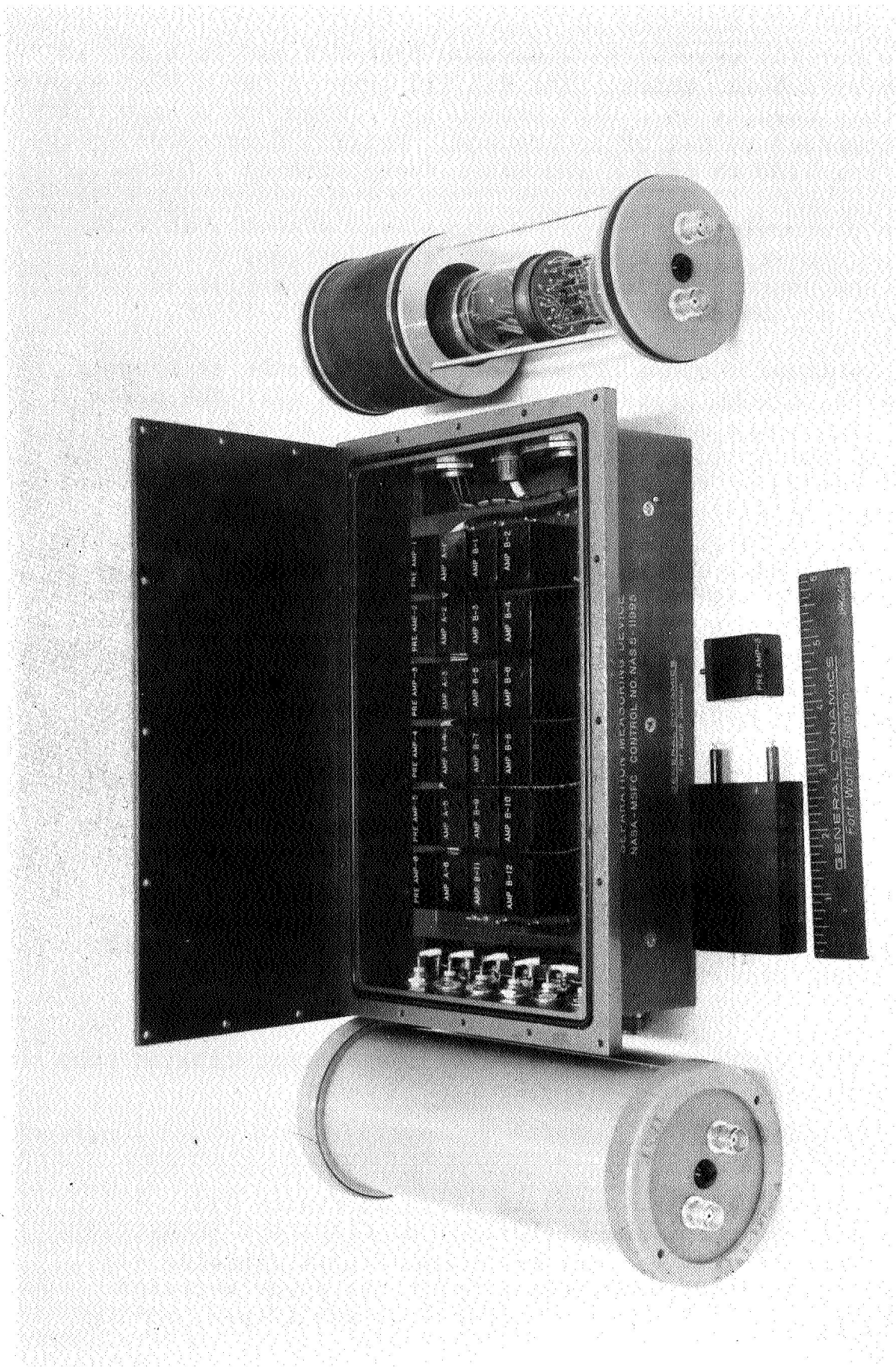
Figure 4-2 Electronics Unit and Detector

The NaI(Tl) crystal is a Harshaw 8PA6-21X and is 2 in. in diameter by 1.5 in. thick. The NaI(Tl) crystal has a high atomic number that results in a high proton conversion and a high pulse height compared to CsI or anthracene. NaI(Tl) fluoresces in the region from 4100 to 4350 Å and has a decay time of 250 nsec.

The photomultiplier tube, a ruggedized RCA4461, is a 10-stage, head-on type that was specifically designed for use in missile and rocket applications. Each tube is subjected to a shock test at the factory in accordance with MIL-5272C.

The voltage divider network for the 4461 tube is shown in Figure 4-3. A 1-MΩ resistor (R12), in series with the zener diodes, limits the maximum current the tube can draw to 0.0015 A. The divider network is composed of zener diodes instead of resistors for better voltage stability over the temperature range. All diodes operate at 100 V except the one between the photocathode and dynode 1, which is a 200-V zener. These zener diodes establish a minus 1200-V potential across the phototube.

The integrated output current of the scintillation detector as a function of temperature is shown in Figure 4-4 for a source at a fixed distance.

The 1500-V power supply output is plotted as a function of temperature in Figure 4-5. The 28-V input to this power supply was varied ± 3 V at each temperature and this information is shown in the same figure. The 1500-V output of this converter does not change with a ± 3-V swing on the 28-V-dc input voltage. The photomultiplier tube current consumption is dependent upon the count rate, and maximum current at the highest count rate is 250 μA per detector from the 1500-V supply.

The time constant of the crystal and photomultiplier tube is approximately 300 nsec.

4.3 Electronics Unit

The electronics schematic is shown in Figure 4-3. A detailed schematic and the mechanical drawings are submitted under a separate cover. This electronics unit contains six identical channels of electronics and three power supplies. Each channel of electronics contains four amplifiers, giving

22
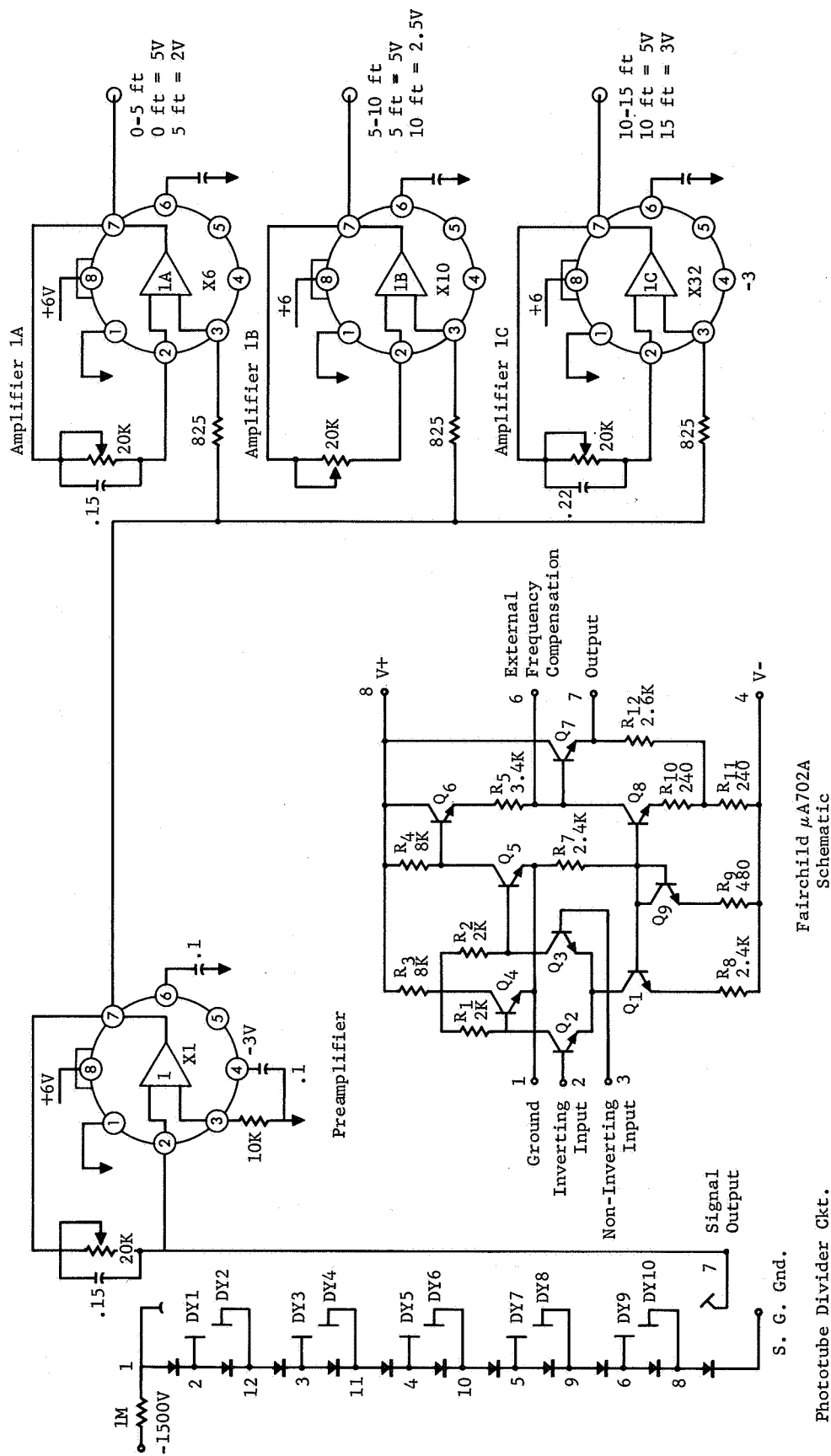
Figure 4-3 Schematic of Detector and One Amplifier Channel

23
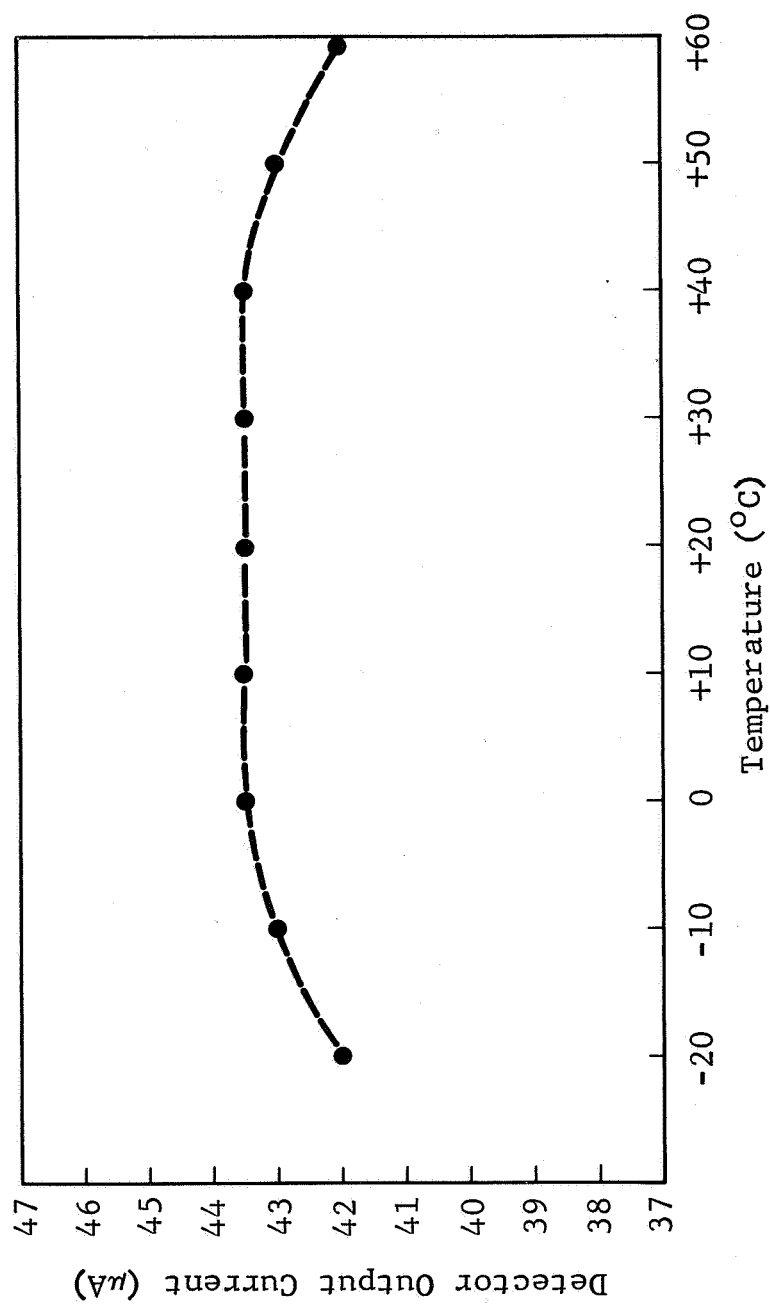
Figure 4-4   Temperature Response of Detector
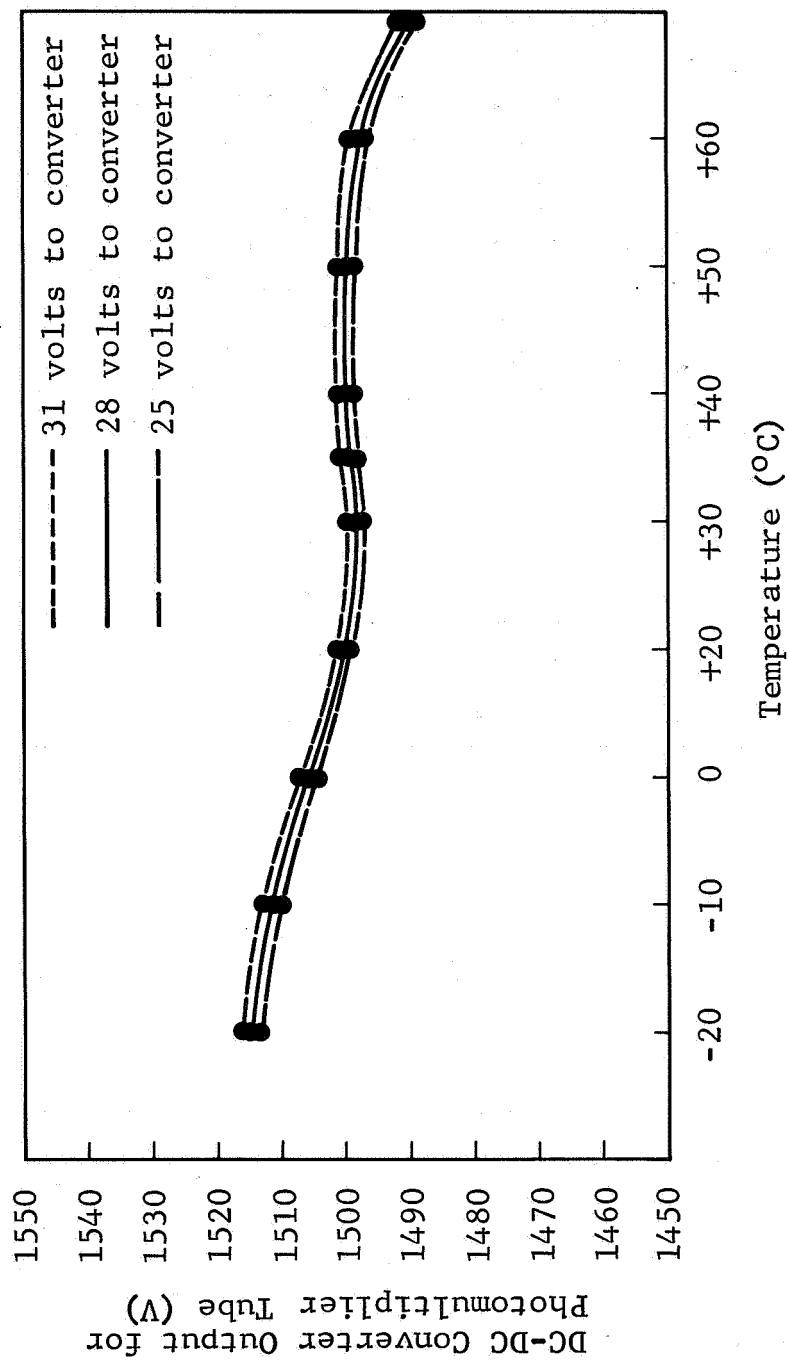
Figure 4-5 Temperature Response of 1500-V Supply

25

a total of twenty-four amplifiers for all six channels. Figure 4-6 shows the printed circuit board, the unencapsulated amplifiers, the power supplies, and a detector.

The output pulses from the scintillation detector arrive at the inverting input (pin 2) of the preamplifier of channel 1 (Fig. 4-3). This preamplifier acts as an integrating amplifier and converts these pulses into a voltage through a feedback network consisting of C1 and R1. It also has a 400-Ω output impedance to drive amplifiers 1A, 1B, and 1C. This preamplifier is adjusted to a gain of $\approx$1 by R1. The positive output drives the succeeding parallel amplifiers. Amplifier 1A accepts the positive voltage on the noninverting input (pin 3) and amplifies with a gain of $\approx$6. This amplifier is near saturation at 5.00 V before the vehicle stages separate. As the stages separate the first 5 ft, amplifier 1A drops from 5.00 V to $\approx$2.00 V, then amplifier 1B takes over for the succeeding 5 ft and, finally amplifier 1C comes out of saturation at 10 ft separation and drops from 5.00 V to $\approx$3.00 V at 15 ft.

The three amplifiers of each channel give the following typical voltage changes for the total separation distance of 15 ft.

Separation Distance (ft)	Amplifier Voltage (V)		
	A	B	C
0	5.00		
5	2.17	5.00	
10		2.75	5.00
15	‗‗‗	‗‗‗	3.23
	2.83	+ 2.25	+ 1.77 = 7.85 volts
15 ft (180 in.) separation = 7.85 V dc			

Amplifier B has a gain of 10 and amplifier C has a gain of 32. Each amplifier has a fixed time constant whose value is determined by a capacitor across the feedback resistors R2, R5, and R9. These capacitors, in combination with the feedback resistors, enable the amplifiers to present a stable dc voltage level at the telemetry output instead of a randomly varying ac level that follows the output pulses of the source.

26
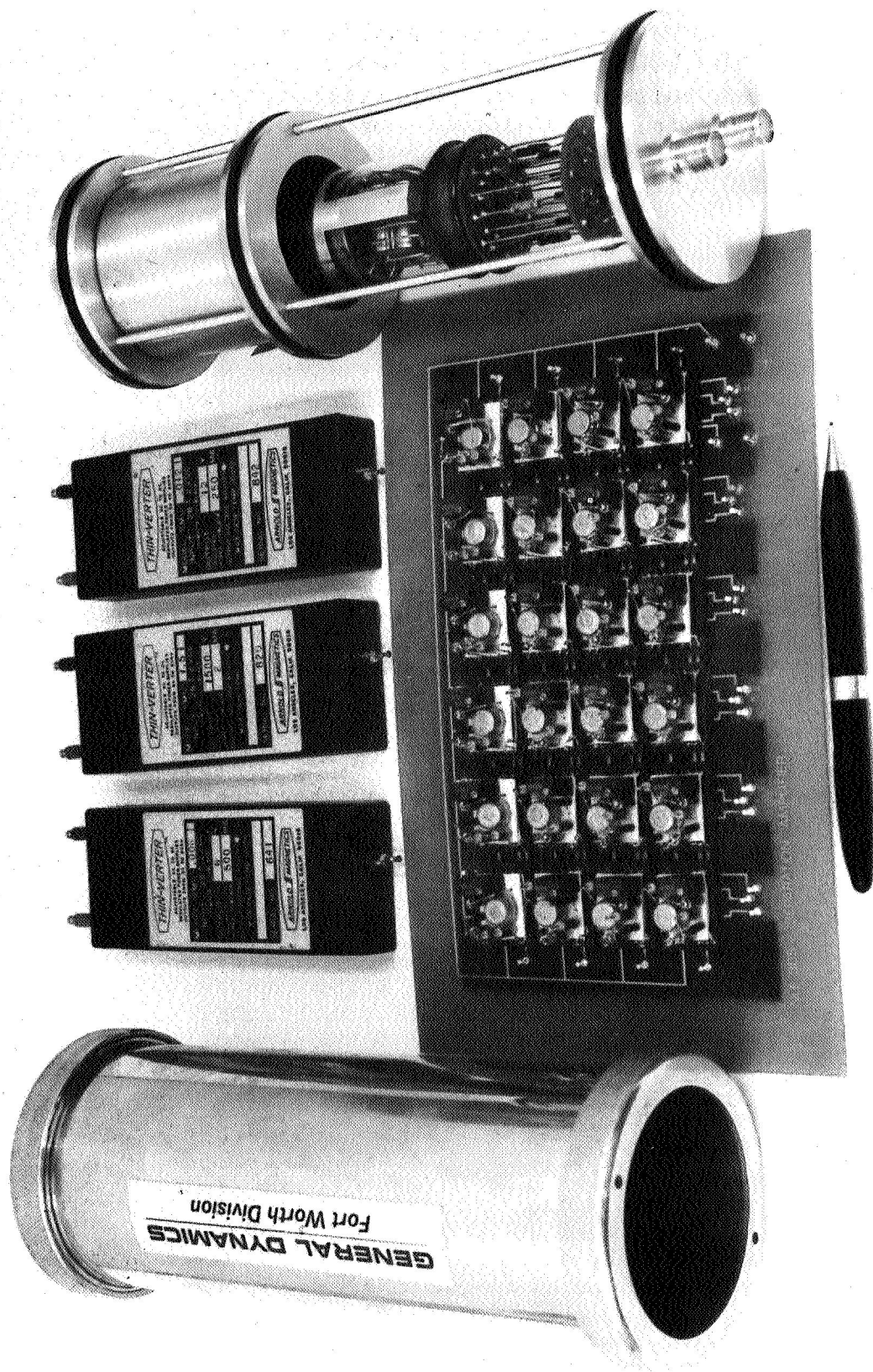
Figure 4-6 Electronics Unit, Power Supplies, and Detector

27

The output impedance of each amplifier is 400Ω and will readily drive the 100-kΩ telemetry input units with less than a 1% change in output voltage. Each amplifier output is connected to a pin in one of the telemetry output connectors, J1 or J2. The outputs of the preamplifiers are connected to test points on the printed circuit board.

The detector and electronics unit were placed in an environmental chamber where the temperature was varied from -20° to +60°C while the outputs of the detector and the amplifiers were monitored. A small cesium-137 source was used to bring the amplifiers up to a stable output voltage. These output voltages are shown as a function of temperature in Figure 4-7. The amplifier outputs are stable from -10° to +50°C, but drop off slightly at -20° and +60°C. This dropoff is not caused by the temperature coefficient of the electronics package, but by the temperature coefficient of the scintillation detector (see Fig. 4-4). Figure 4-8 shows the output of a typical amplifier channel versus temperature, with a constant current input rather than a detector current input. This gives the amplifier response versus temperature independent of the detector current.

The amplifiers used in the modules are the temperature-stabilized Fairchild μA702A units mounted in a TO-5 package. The operating temperature range of these units is from -55° to +125°C. The dc supply voltages for these amplifiers are +6 and -3 V dc. Each amplifier module requires 18 mW of power at these voltages. The input impedance is approximately 15 kΩ. The closed-loop frequency response at a gain of 100 is 9 MHz. Each amplifier has an adjustable gain potentiometer (20 kΩ) that is accessible at the top of the module. The amplifiers (μA702's) and their associated piece parts are mounted on a small module header (type HSSB) developed by MSFC for use in severe environmental conditions.

4.4 Power Supplies

The electronics package contains three solid-state, completely encapsulated power supplies (Fig. 4-6). These supplies are mounted beneath the amplifier printed-circuit board, with the outer shell of the electronics package serving as the heat sink. They are built by Arnold Magnetics Corporation, Los Angeles, California, and are designed to meet MIL-E-5272 specifications.
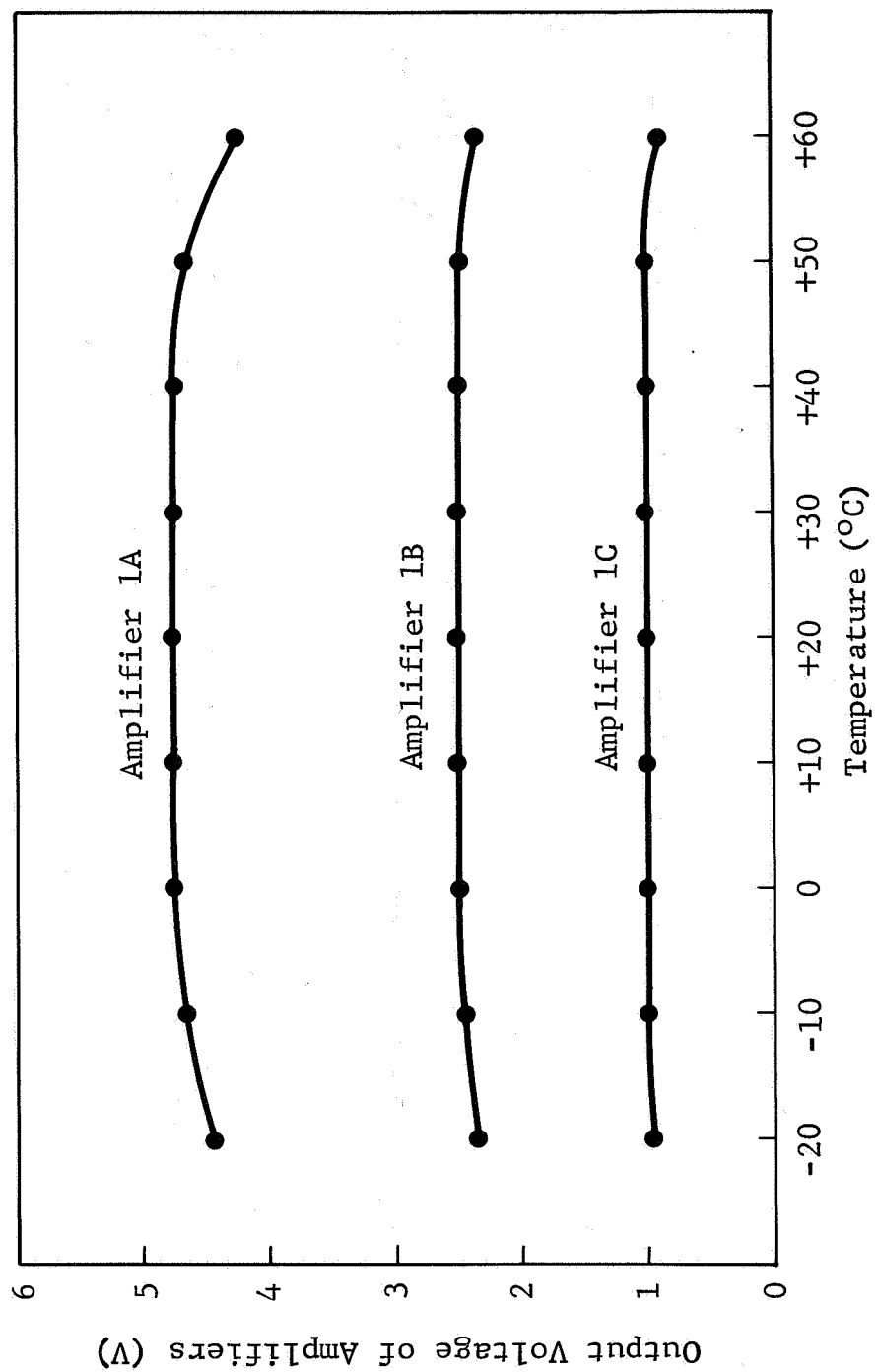
Figure 4-7   Temperature Response of Detector and Amplifiers
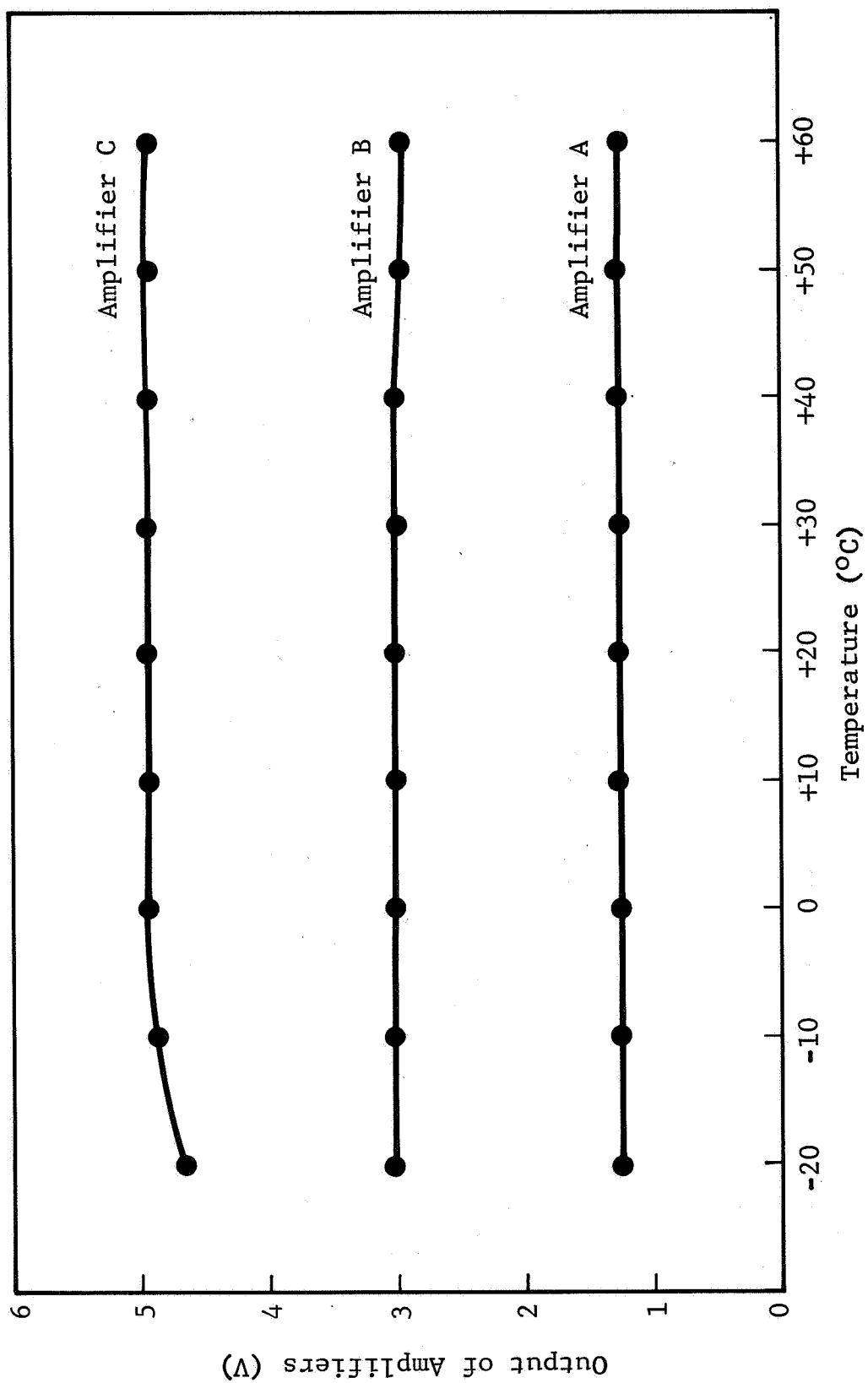
Figure 4-8 Temperature Response of Amplifiers

The model numbers of the power supplies and the current drawn from each are given below.

Model No.	Volts	Max Load Current (mA)	Min Load Current (mA)	Max Load (watts)
SMU- .006	+6.67	103	67	0.69
SMU- .003	-3.13	84	60	0.26
SMU-1.5KV	-1500	1.5	0.3	2.25

Total Output Power Used	3.20 W
Total Input Power @ 28 V dc	11.20 W
Efficiency of the 3 supplies	30%

These power supplies are relatively stable over the operating temperature range (-20° to +60°C). The temperature responses of the 3- and 6-V supplies are shown in Figure 4-9. The temperature response of the minus 1500-V supply is plotted in Figure 4-5. Each power supply has an output voltage adjustment potentiometer that will vary the output approximately +15%. The company that builds these units considers the electronic schematics to be private data and will not furnish these drawings. Since the units are encapsulated, it is probably easier to replace a defective unit than repair it; therefore the drawings are not actually needed.

4.5 Mechanical Design and Fabrication Techniques

4.5.1 Detector

The detector contains a sodium iodide crystal, a photomultiplier tube, and a divider network of zener diodes. The divider network is shown in Figure 4-3. The detector assembly is installed in a hermetically sealed aluminum cylinder that is 3.25 in. in diameter by 8.25 in. in length. The detector weighs 3.5 lb and has a natural anodized finish. The signal and high-voltage coaxial connectors are Amphenol TNC, which provide maximum reliability.

Detailed mechanical drawings of the detector are submitted under separate cover (GDFWD HLM 266 and NLM 263). The Harshaw crystal (8PA6-21X) is mounted between two aluminum wafers with a silicone rubber O-ring between each end of the crystal and the wafers (see Fig. 4-10). This assembly is encapsulated with Emerson & Cummings 1090SI potting compound. The encapsulated crystal is shown in Figure 4-11.

31
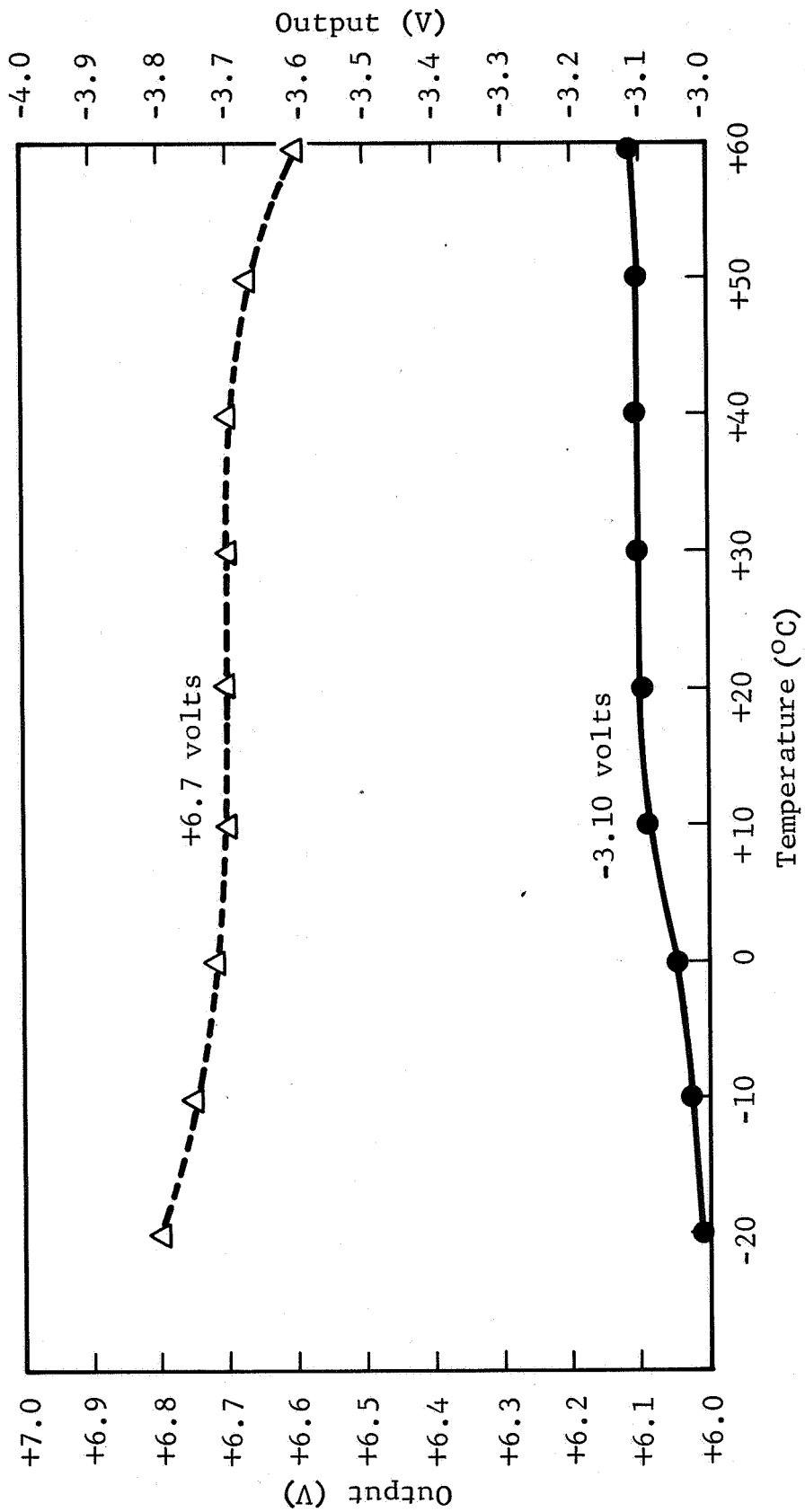
Figure 4-9   Temperature Response of Three- and Six-Volt Power Supplies
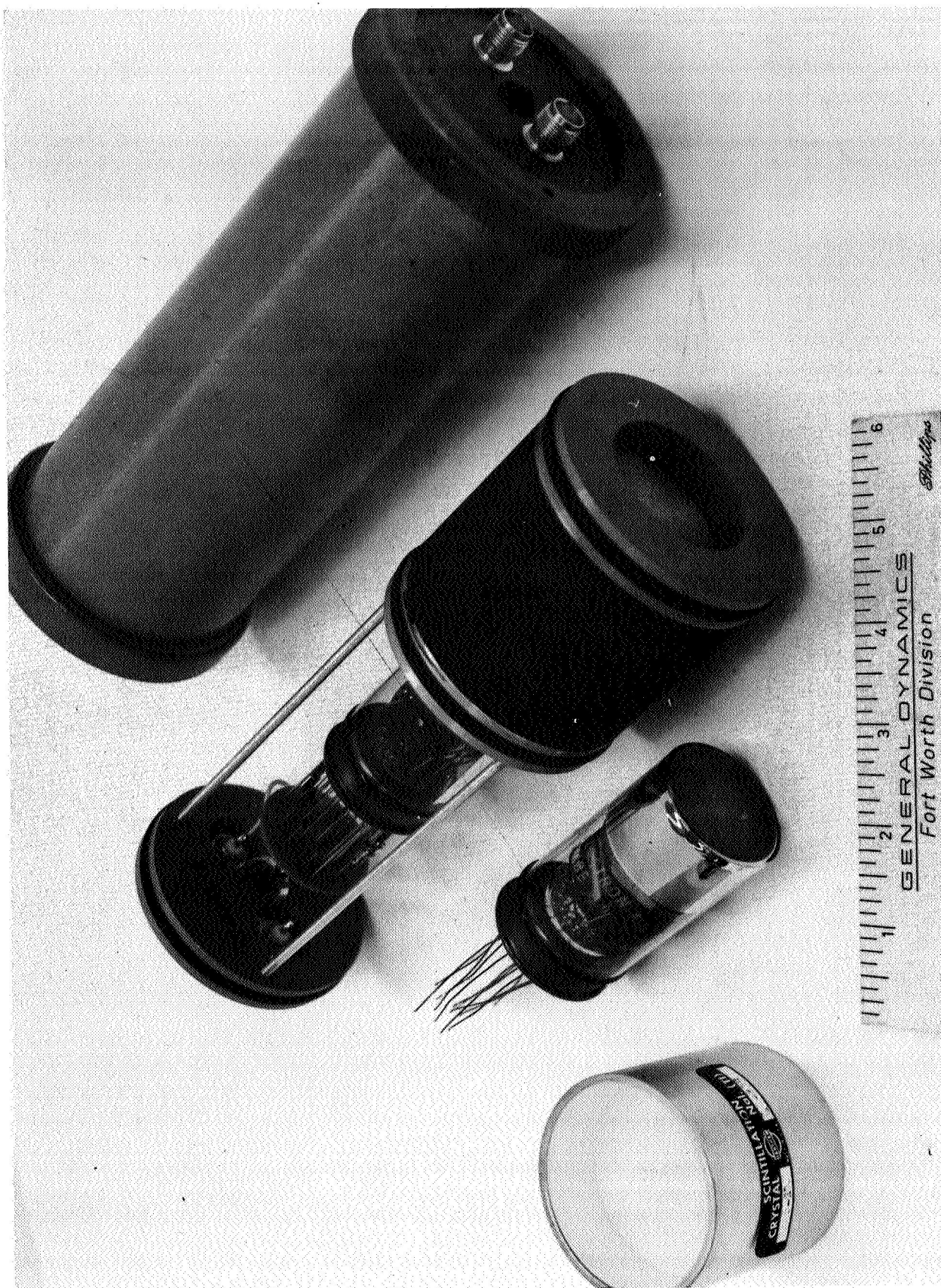
Figure 4-10 Detector Parts

33

Figure 4-11 Encapsulated Sodium Iodide Crystal

Two printed-circuit boards with zener diodes are installed on the photomultiplier tube. The tube is installed on the crystal, given a preliminary electrical check, and removed.

The photomultiplier tube (RCA4461) is then installed in the detector assembly. A small amount of high-quality vacuum grease is spread on the glass surface of the crystal where the face of the photomultiplier tube is mounted. The photomultiplier tube is then inserted into the aluminum wafer and placed firmly against the glass of the crystal.

The crystal and phototube are again given an electrical check. A small amount of E & C 1090SI potting compound is poured around the tube where it meets the glass and a constant pressure is maintained to hold the tube and crystal together while the 1090SI is setting. After 48 hours, the potting compound is quite firm and the detector assembly is given another electrical check. If the detector output current is the same as it was before potting, the assembly is ready for completion. The assembly is leveled and adjusted for the proper length so it will fit its cylindrical shell, and the three silicone O-rings are dipped in vacuum grease and installed. The detector assembly is then forced inside the anodized aluminum cylinder and the end caps are screwed on.

The photomultiplier tube is now ready for encapsulation. The detector assembly in the can is placed, crystal down, on a level work bench. The plastic screw between the signal and high-volume connectors is removed, and the portion of the can around the photomultiplier tube is then filled completely with Dow-Corning Sylgard 185. The potting compound is allowed to cure for 48 hours before handling or using the detector.

A problem was encountered when the photomultiplier tube was first encapsulated with E & C 1090SI. This potting compound is a light-weight, firm epoxy that works well when encapsulating small modules and when used in small quantities. However, when poured in large quantities, as in the container around the photomultiplier tube, the compound cures at a temperature of +250°F and the heat removes the cesium-antimony coating from the cathode of the RCA4461 photomultiplier tube. This reduces the gain of the tube severely. The problem was solved by using only a small amount of E & C 1090SI around the outside of the tube to cement it to the crystal and the aluminum wafer. The epoxy was then allowed to set up (cure) in the refrigerator before encapsulating the entire photomultiplier tube with Dow-Corning Sylgard 185.

Clear Sylgard 182 was also tried between the crystal and the photomultiplier tube instead of vacuum grease. This was allowed to cure and the tube was then encapsulated with Sylgard 185; however, the results were unsatisfactory because air bubbles had a tendency to form between the Sylgard 182 and the phototube and crystal, thereby reducing the sensitivity.

4.5.2 Amplifier Chassis

The chassis for the twenty-four amplifiers and three power supplies is machined from a solid piece of aluminum having dimensions of 10.432 by 6.882 by 2.625 in. This chassis, shown in Figure 4-6, weighs 4.9 lb and has a dark blue anodized finish. The unit is hermetically sealed with a silicone rubber O-ring between the lid and the box. A wiring diagram identifying interconnecting leads and outputs is shown in Figure 4-12.

The amplifier modules are constructed on the cordwood type principle and are soldered to NASA soldering specification NPC200-4 using 60/40 solder. Corning glass resistors and Sprague tantalum capacitors are used in the modules because of their small size and low temperature coefficients. The Fairchild μA702 amplifiers used in the modules are mounted in a TO-5 package and are easily adaptable to the cordwood type construction. These piece parts and amplifiers are mounted on a module base (type HSSB) manufactured by the Burndy Co. Figure 4-13 shows the module before and after mounting to the motherboard. This module base incorporates two bolt studs that protrude through the motherboard and are fastened down with lock washers and nuts. The modules are easily removed from the motherboard and will withstand severe environmental vibration and shock. These module base plates have hard gold-plated contact springs that make firm contact to the motherboard when bolted into place.

The amplifier module is encapsulated in E & C 1090SI after it has been completed and electrically checked. The module measures 0.700 by 1.000 by 1.000 in. in height. Each amplifier module has an adjustable, 20-kΩ, gain potentiometer accessible at the top of the module. These potentiometers, Bourns Model No. 3280W-1-203, have internally welded leads and are high-reliability components.
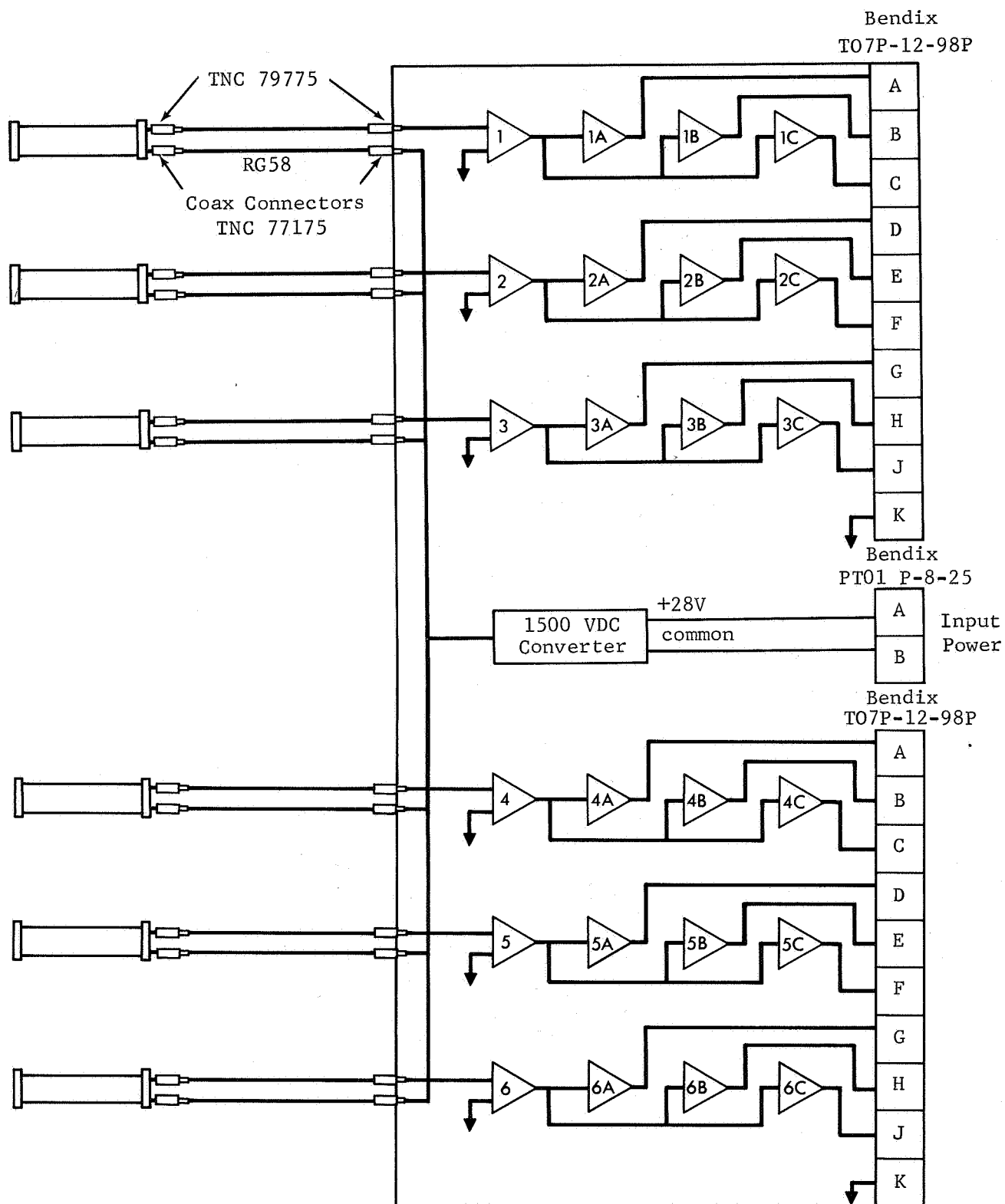
Figure 4-12 Cable and Wiring Diagram
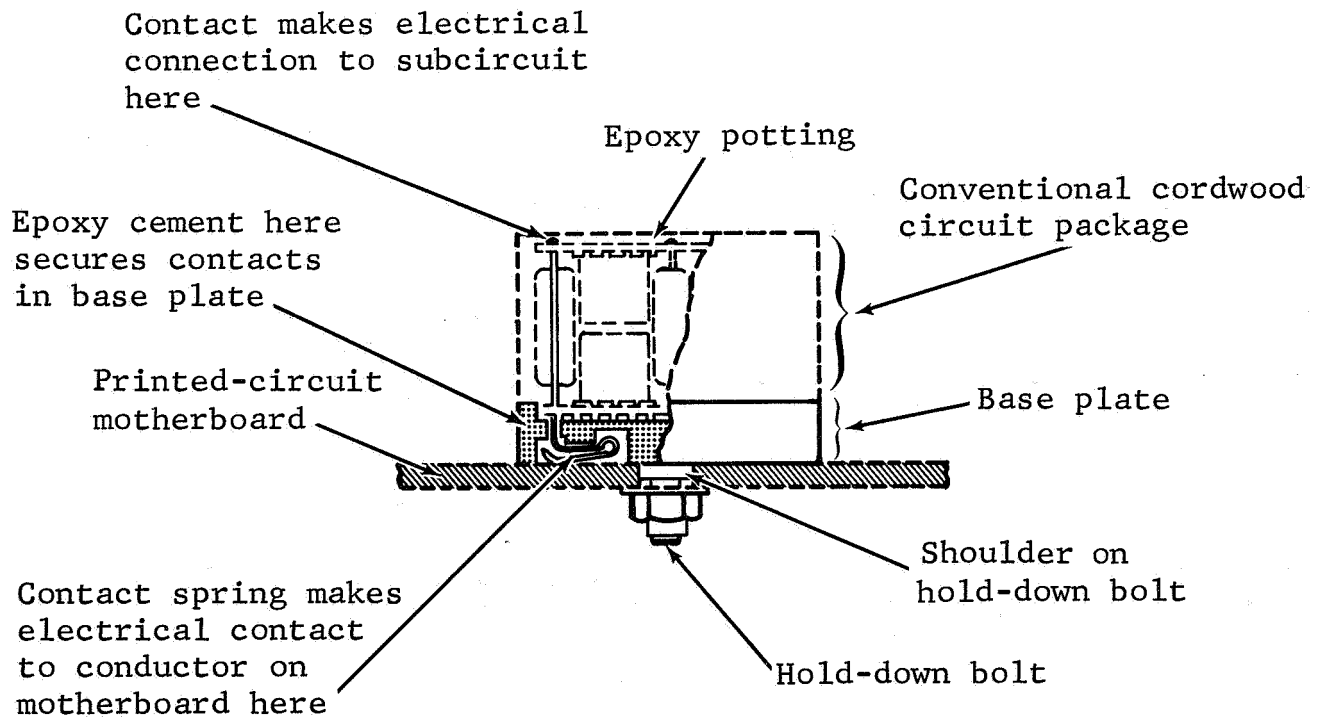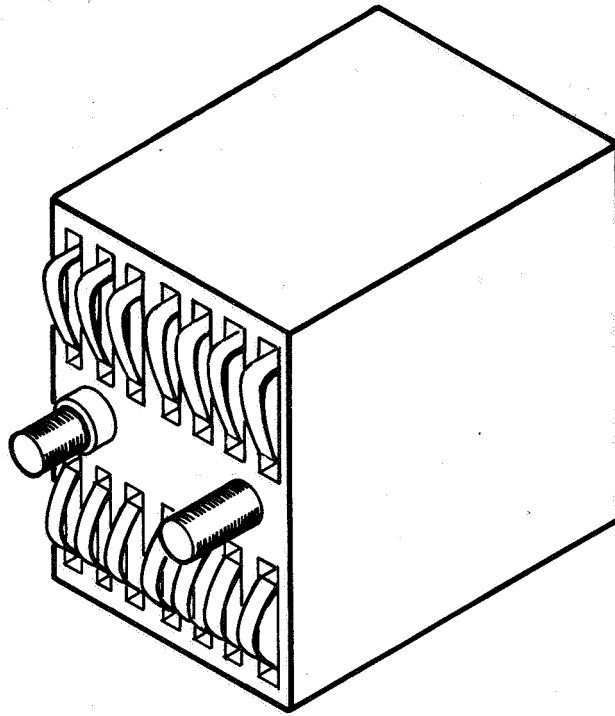
Figure 4-13   Bolt-Down Module

V. SHIELDING DESIGN

The system of three sources and six detectors operates as three independent sets, each consisting of one source and two detectors each. To prevent any interaction between the three sets, shielding must be used.

5.1 Source Shields

Shields can be used on either the sources or the detectors or on both. The first consideration is to shield the three sources only, since this approach results in less weight.

In Figure 5-1 it is seen that the source radiation should be limited to a maximum of 21 deg from the vertical. The 21 deg comprises the 6-deg angle between the source and the detector at 0-deg tilt plus the 15-deg tilt requirement. The source is also shielded at the bottom and sides to reduce scattering. A drawing of the source shield is shown in Figure 5-2.

The ± 15-deg tilt requirement can be met with source shields only up to a separation distance of about 13 ft. The maximum tilt permitted by this arrangement at 15 ft is about 11-deg. These limits are valid only if there is no rotation or translation. In fact, little or no rotation or translation can be tolerated at 15 ft when there is no shielding on the detectors. If the system is to be practical, it must use detector shields.

5.2 Detector Shields

Shielding the detectors will afford considerably more movement, especially in rotation and translation. However, these shields are heavier and the sources must still be shielded to reduce scattering effects.

The detector shield and its relation to the detector are shown in Figure 5-3. The dimension A is determined by the diameter of the detector and the position of the other two sources. The dimension B is determined by the detector size

39
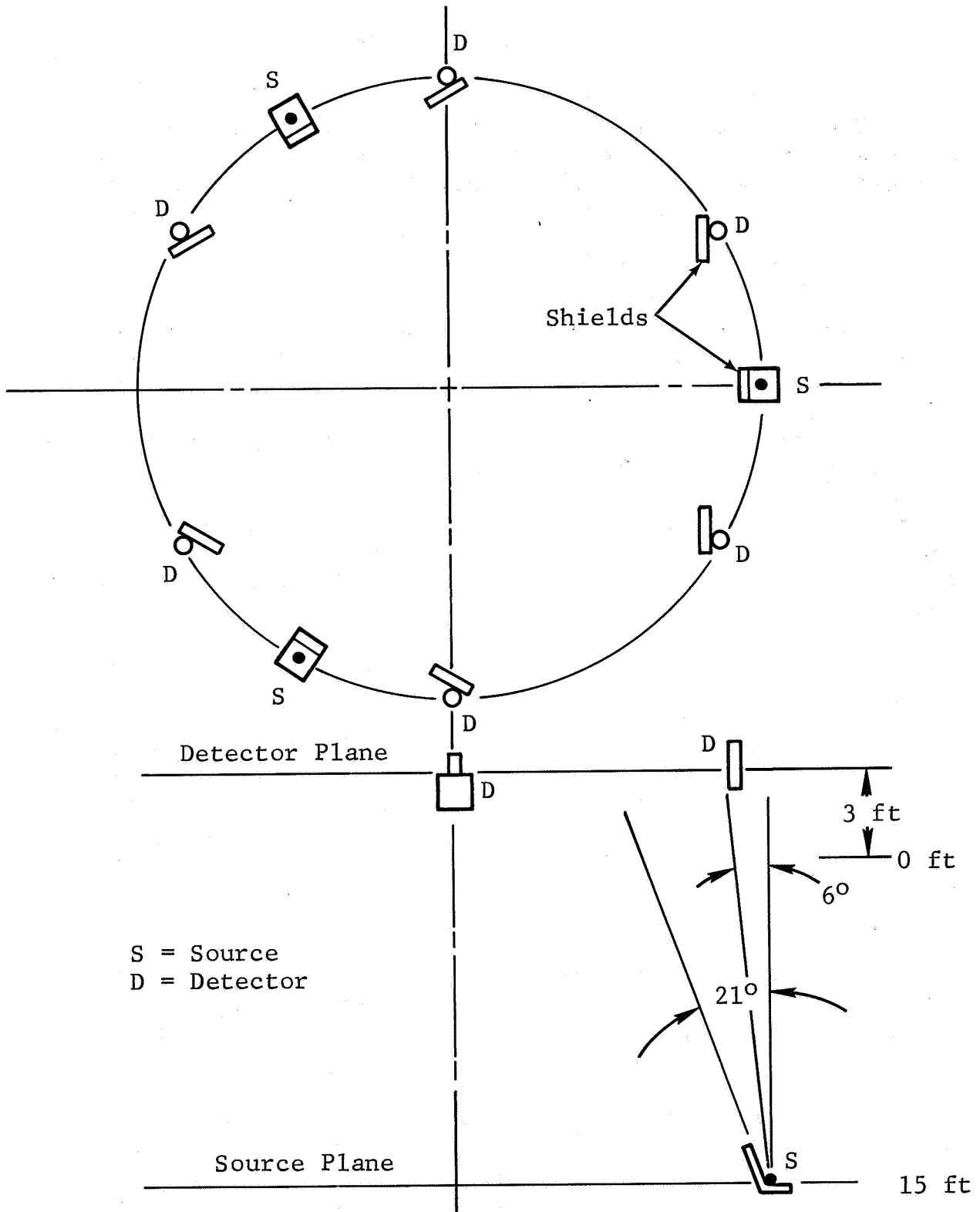
Figure 5-1 Position of Shields

Lead Cover

3.5"

2.5"

2.750"

21°

69°

2"

.335 Dia.
Source
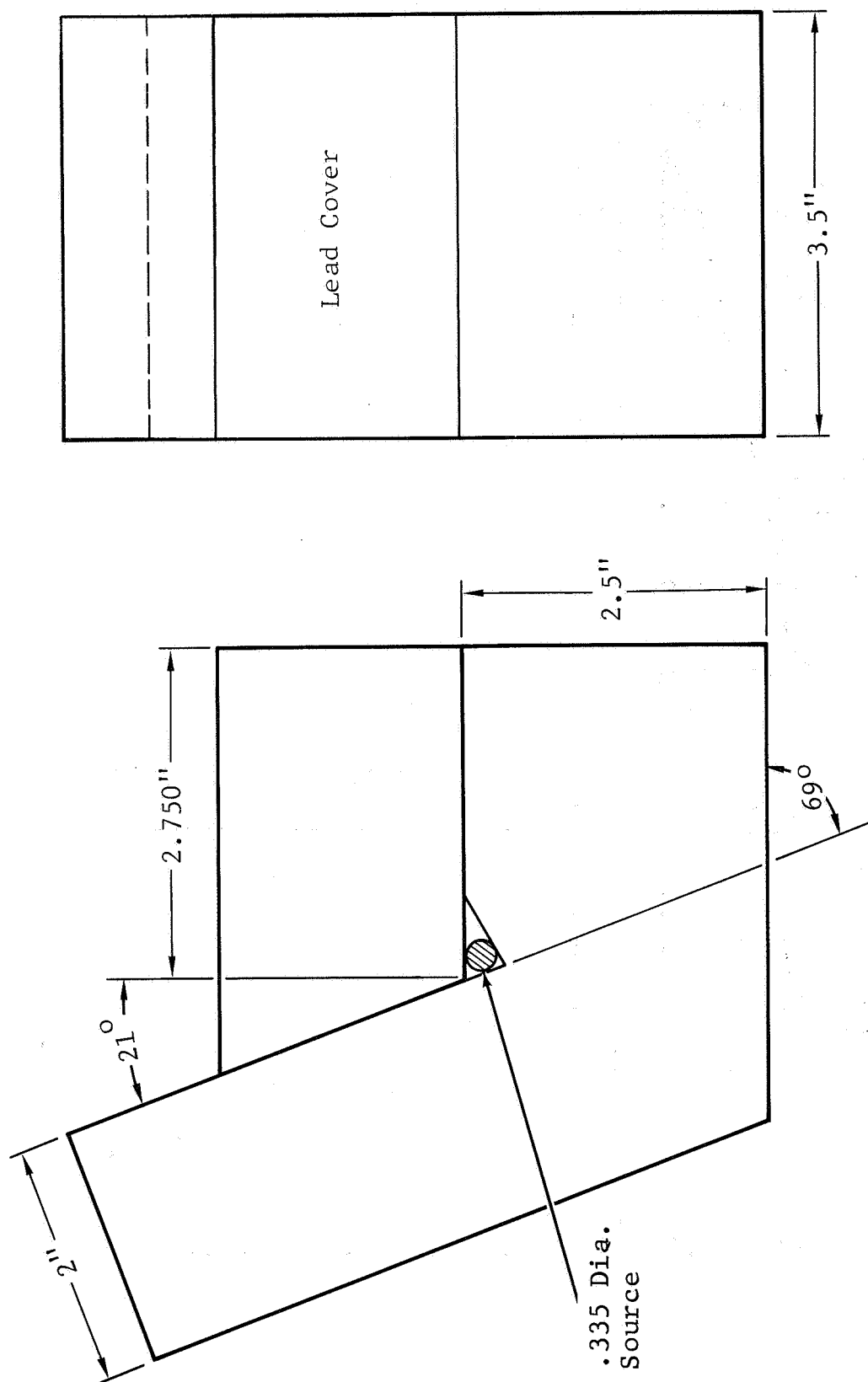
Figure 5-2 Source Shield

41
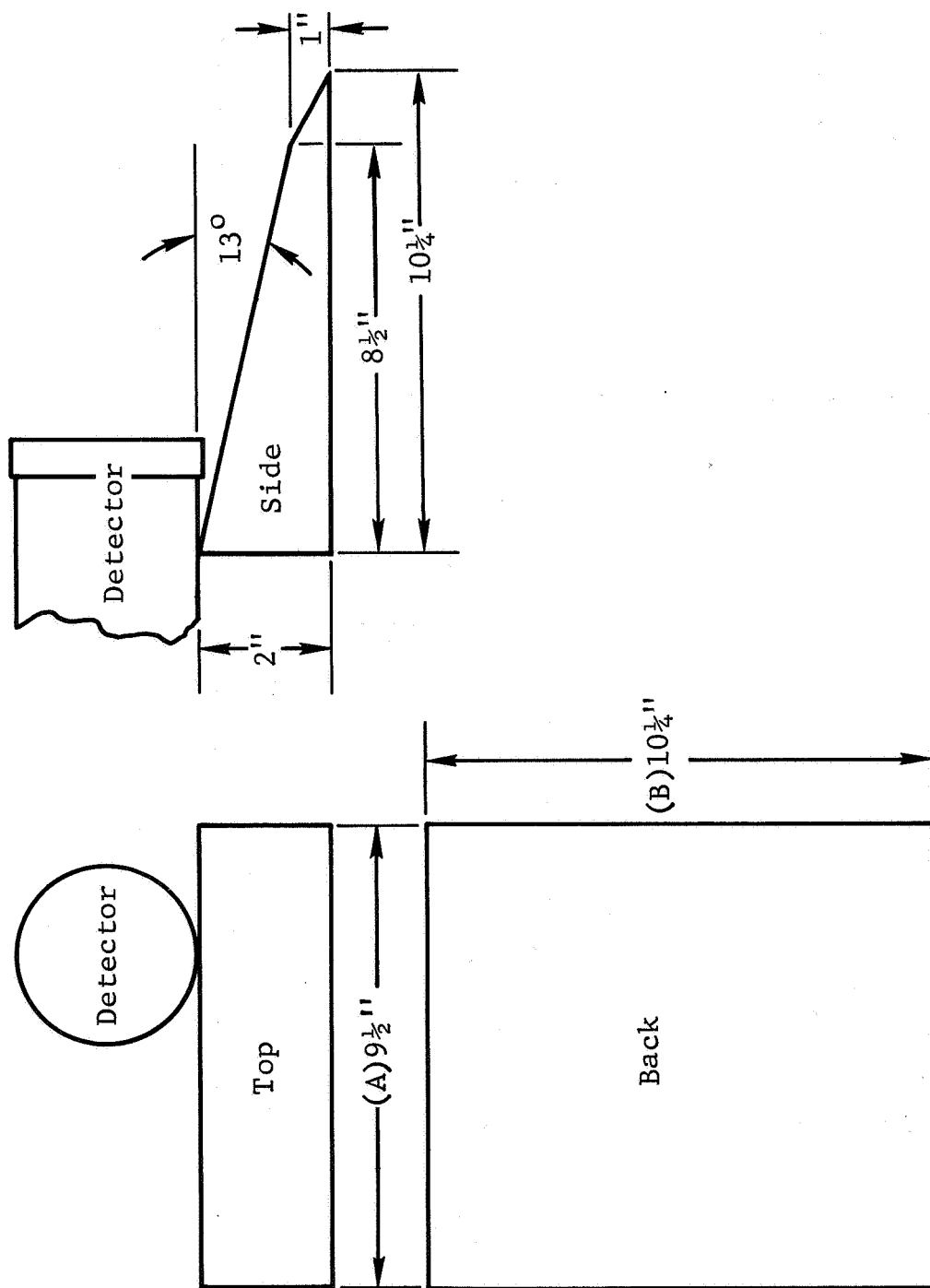
Figure 5-3   Detector Shield

and the position of the sources at 15 ft. The 13-deg slope of the detector shield is necessary to obtain a $\pm$ 15-deg tilt of the detector plane.

Limits of the system are determined experimentally using a full-scale test rig. The limit test and its results are given in the following section.

VI. LIMIT TESTS

The limits of the system could be easily calculated if there were no scattering of radiation by air and structures, including the shields. Since scattering of the source radiation is significant, a full-scale test rig was constructed to determine the limits of separation, tilt, rotation, translation, and velocity.

The test rig was built in the configuration described in Section V and illustrated in Figure 5-1. Since it was necessary to attach signal cables to the six detectors, it was more practical to release the source plane for the velocity test. Thus, the source plane was the lower stage and the one that was moved relative to the detector plane, which was fixed on two large work stands. The test rig and the crane used to position the source plane are shown in Figure 6-1.

A high-voltage cable and six signal cables were routed approximately 60 ft from the detectors to the electronics unit inside the instrumentation building. Digital voltage-measuring equipment was used for static measurements and a CEC oscillograph recorder for the velocity measurements. A photograph of the instrumentation is shown in Figure 6-2.

The static voltages can be recorded with an accuracy of ±0.01 V. The random variation in source strength results in about a ±0.003-V variation in output voltage at 5.00 V. The accuracy of positioning the source-detector distances is about ±2 in.

The tests performed on the rig were:

1. Interaction Between Sources

2. Calibration and Repeatability

3. Tilt

4. Rotation

5. Translation

6. Velocity
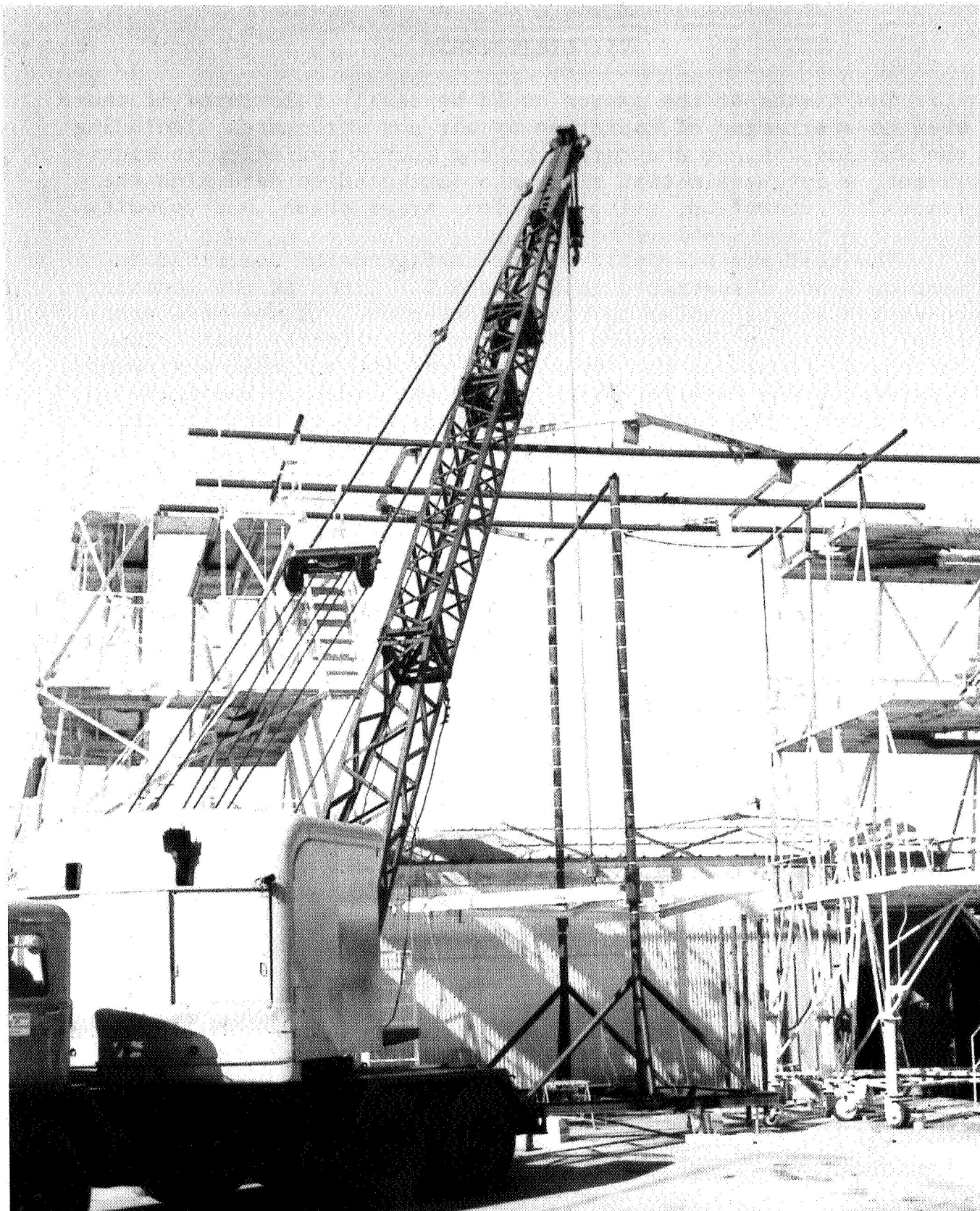
Figure 6-1 Full-Scale Test Rig

46
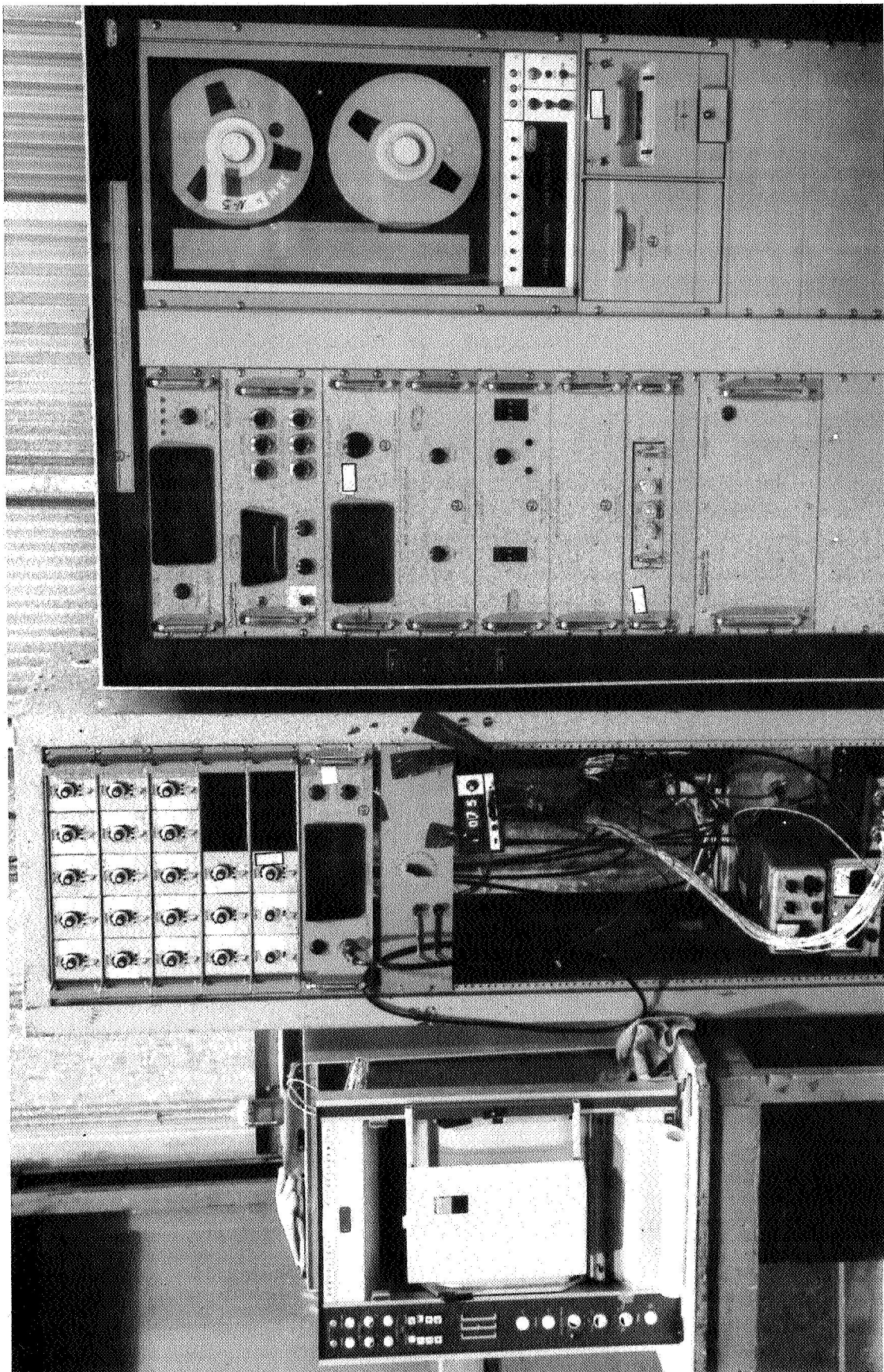
Figure 6-2 Test Rig Data Acquisition Equipment

The primary method of checking the accuracy of the detector readings was to take actual distance measurements between the source and the detector and compare the output voltage as a function of the measured source-detector distance. The various movements are limited by shield interference between the source and the detector. These limits are easy to locate, since the detector output decreases rapidly when shield interference is encountered. The source-detector positions and the coordinates for the various movements are shown in Figure 6-3. The separation distances referred to throughout the tests do not include the initial distance of 3.25 ft between the source plane and the detector plane.

6.1 Calibration of Amplifier Gains

The output of the 1500-, 6-, and 3-V power supplies can be adjusted by approximately +15%. Once these voltages are adjusted, they remain stable if the primary power is 28 + 3 V. The initial step in calibration is to check the 28 + 3 V supply. This primary source should be capable of furnishing 0.5 A.

The -1500 + 20 V supply is checked at one of the high-voltage output connectors. The 6- and 3-V supplies are checked on the printed circuit board and should read 6.60 + 0.02 V and 3.10 + 0.02 V, respectively. Each power supply has a potentiometer for adjusting its output voltage.

After the power supplies are checked, the three 3-Ci Cs-137 sources are placed in their respective positions. Note that each source is color-coded and should always be used with the same pair of detectors. In addition, each source is always oriented in the same position in each shield.

Each of the six channels has a preamplifier that drives three spreader amplifiers, denoted A, B, and C. At separation distances of 0, 5, 10, and 15 ft, the amplifier outputs should have the following values:

48
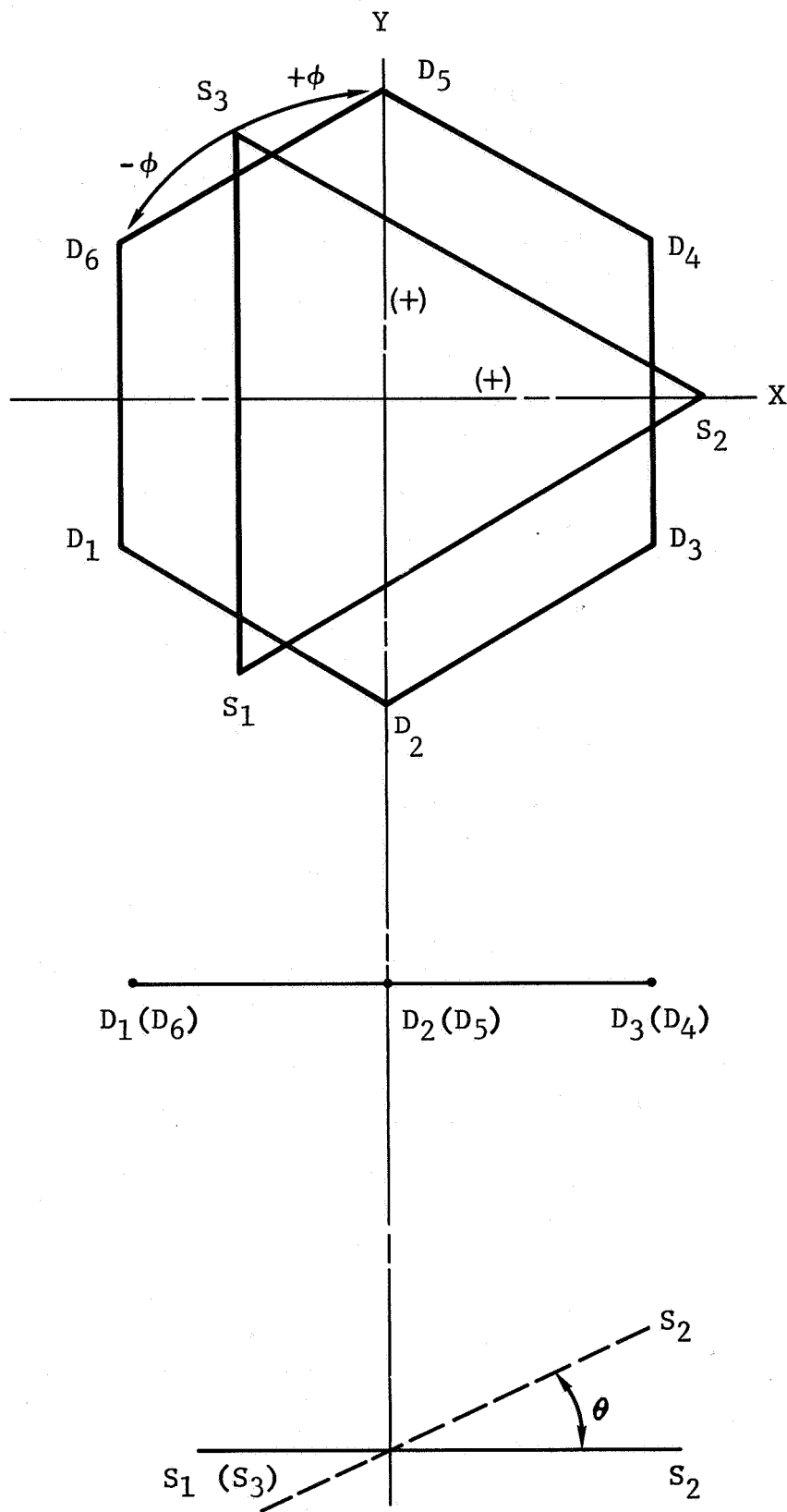
Figure 6-3 Test Rig Coordinates

49

Calibration Set Points

Separation Distance (ft)	Preamplifier (V)	Amplifier A (V)	Amplifier B (V)	Amplifier C (V)
0	1.00 ± 0.01	5.00 ± 0.01	(5.3)	(5.3)
5		$(2.10)^a$	5.00 ± 0.01	(5.3)
10		(1.1)	(2.5)	5.00 ± 0.01
15		(0.6)	(1.5)	(3.2)

[a]Values in parentheses are approximate.

The amplifiers are set at their maximum readings of 5.00 ± 0.01 V by adjusting the potentiometer in each module. The readings in parentheses are approximate and will vary to some extent. Do not adjust the amplifiers after they have been set at 5.00 V.

6.2 Interaction Between Sources

After the system gains and voltages had been set, the source plane was positioned at 0, 5, 10, and 15 ft, first with one source, then with two sources, and finally with three sources. The 0-ft position represents the 3.25-ft perpendicular distance between the source and detector planes. This 3.25 ft is the minimum distance that could be obtained with the test rig. Readings of all channels were recorded at the three positions and no interactions between the sources were noted.

6.3 Source-Detector Distance Calibration and Repeatability

All three sources were installed. The source plane was maintained at zero tilt (parallel to the detector plane) with no rotation or translation. Output voltages were then taken at 1-ft intervals from a 0-ft separation to a 15-ft separation. This test was repeated to establish the repeatability of the test rig and system. A measuring tape was used to set the distance between planes. Figure 6-4 shows the data from both runs for detector D_1. Note that the readings repeat very well and show a variation of a maximum of 1%, or 0.05 V, at the 5-V reading
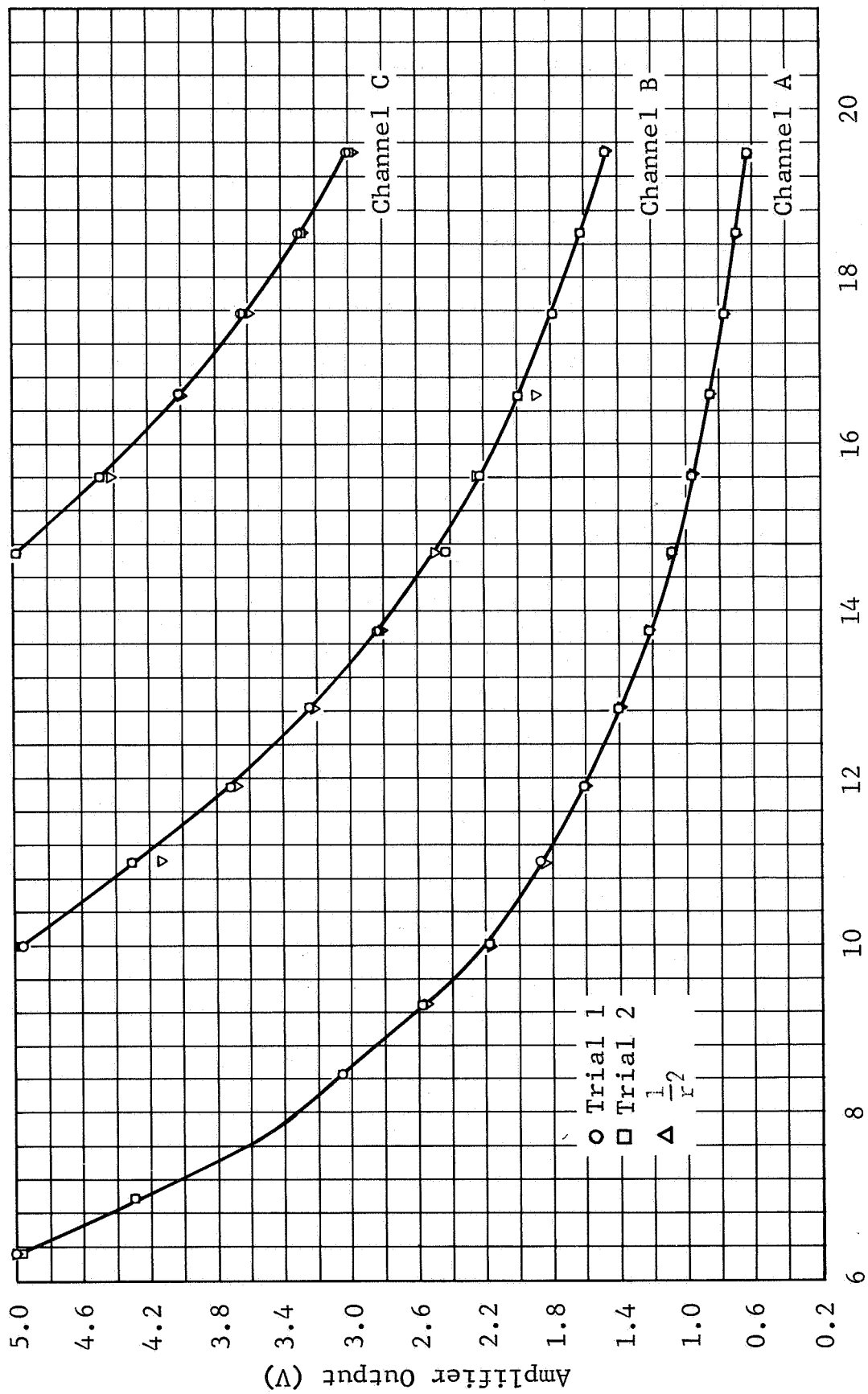
Figure 6-4 Calibration of Detector 1

of amplifier A. This variation is probably due to the variation in source-detector distance of the test rig. Most of the readings were within ± 0.01 V.

The effects of scattering are shown in Figure 6-4 by plotting the inverse of the square of the distance between points. The smaller separations do not fit a $1/r^2$ dependence. A lower energy source would deviate even more from $1/r^2$. A higher energy source would reduce scattering but increase shield weight.

Figures 6-5 through 6-9 show the response of the other five detectors.

6.4 Tilt

Data were taken at two separations distances, 3 and 15 ft, with the tilt angle varying in 5-deg increments from -15 to +15 deg. When tilting, detectors D_1, D_2, and D_3 are symmetrical relative to detectors D_4, D_5, and D_6 (see Fig. 6-3). The actual source-detector distance measurements were made on D_4-S_2, D_5-S_3, and D_6-S_3; the source plane was made level by adjusting distances D_1-S_1 and D_3-S_2.

At 3 ft, which is about the minimum practical separation distance, the responses of D_4, D_5, and D_6 were recorded as a function of source-detector separation distance as the source plane was tilted from -15 to +15 deg.

As is apparent in Figure 6-10, there were no abrupt changes in the detector responses. Consequently, it may safely be assumed that the system has the capability of measuring tilt angles up to ± 15 deg with no danger of shield interference.

At the 15-ft separation distance, the source plane was tilted ± 20 deg with no shield interference. The detector outputs are plotted in Figure 6-11 for a tilt angle varying from -15 to +15 deg.
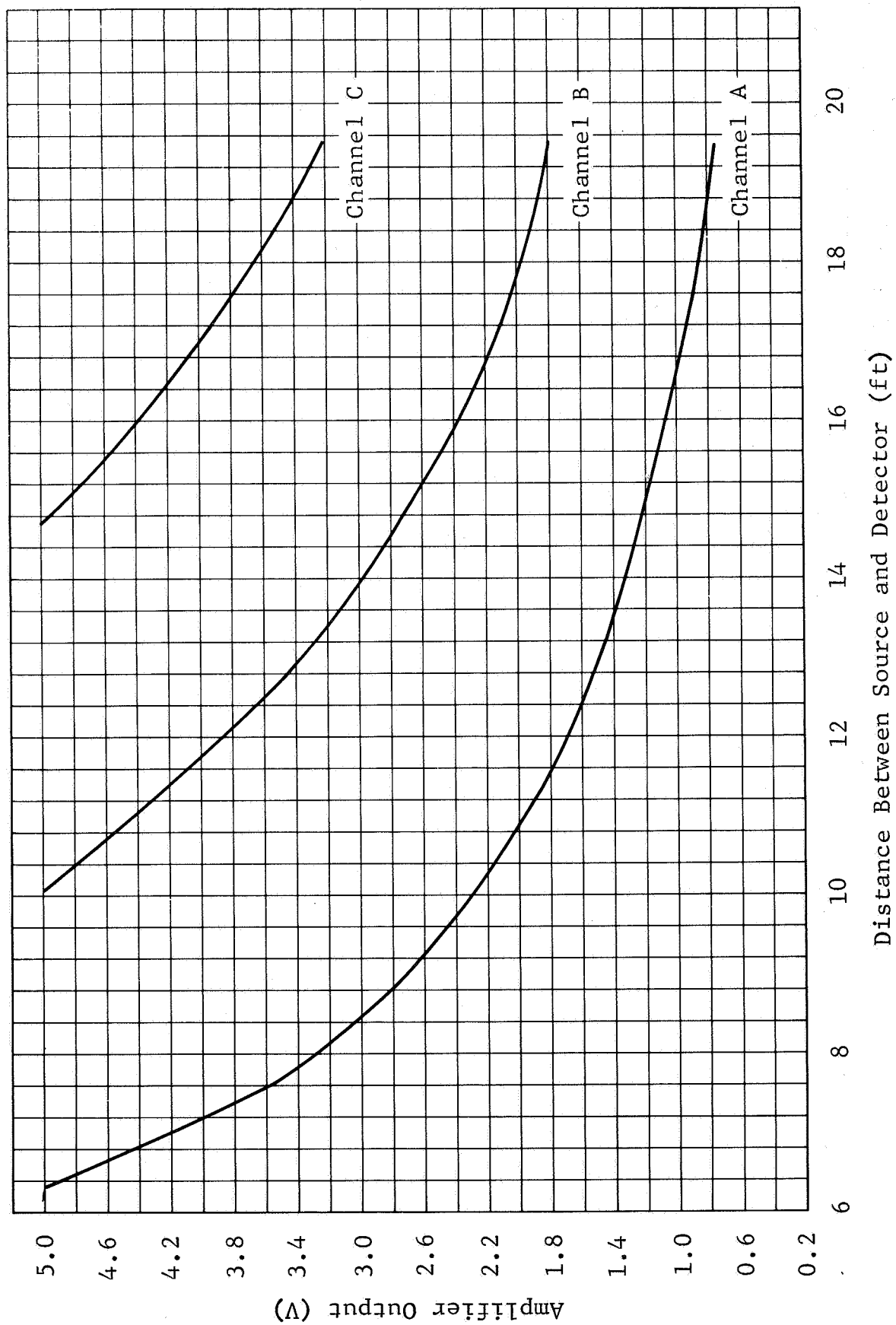
Figure 6-5 Calibration of Detector 2
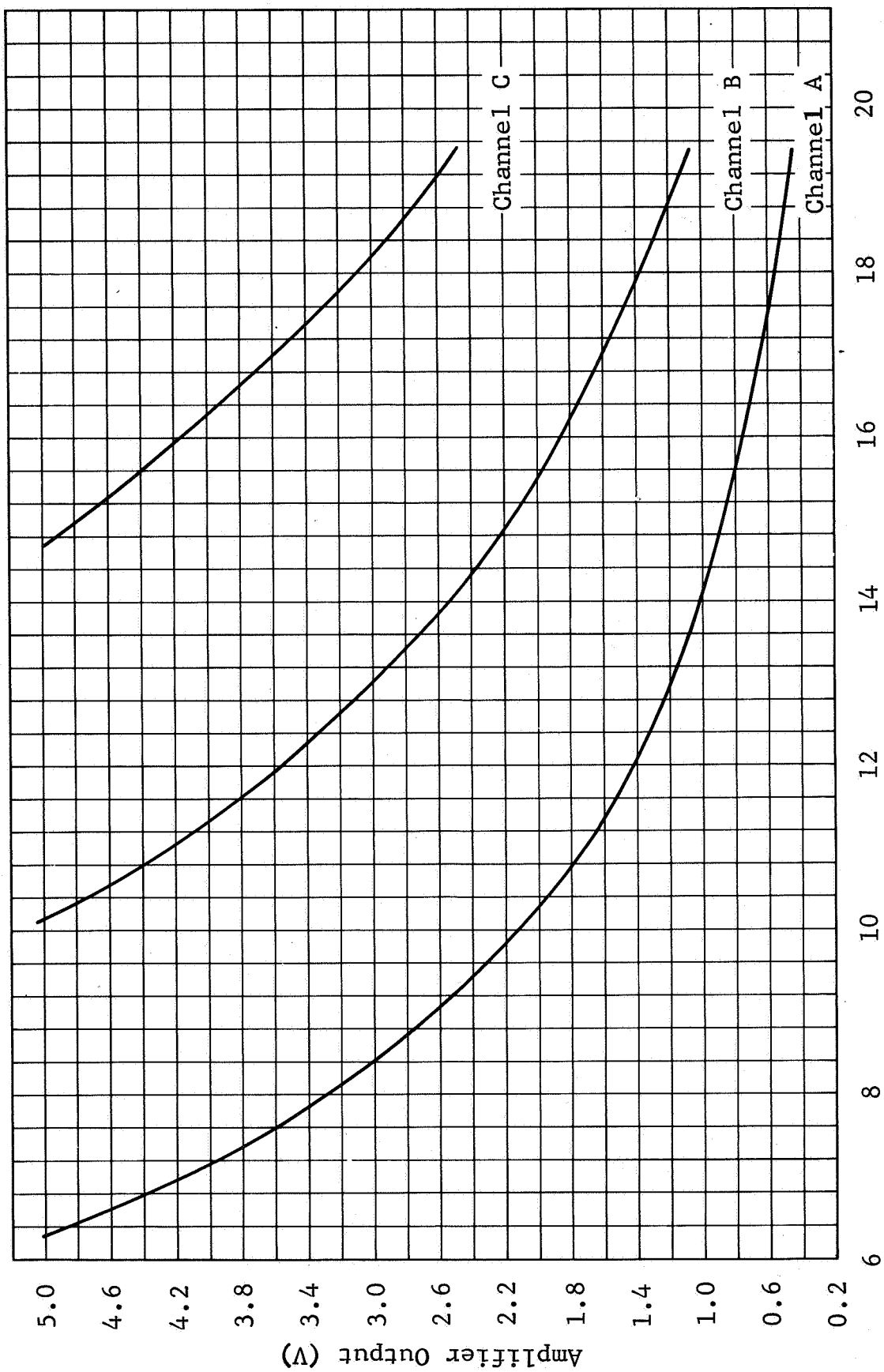
Figure 6-6   Calibration of Detector 3

54
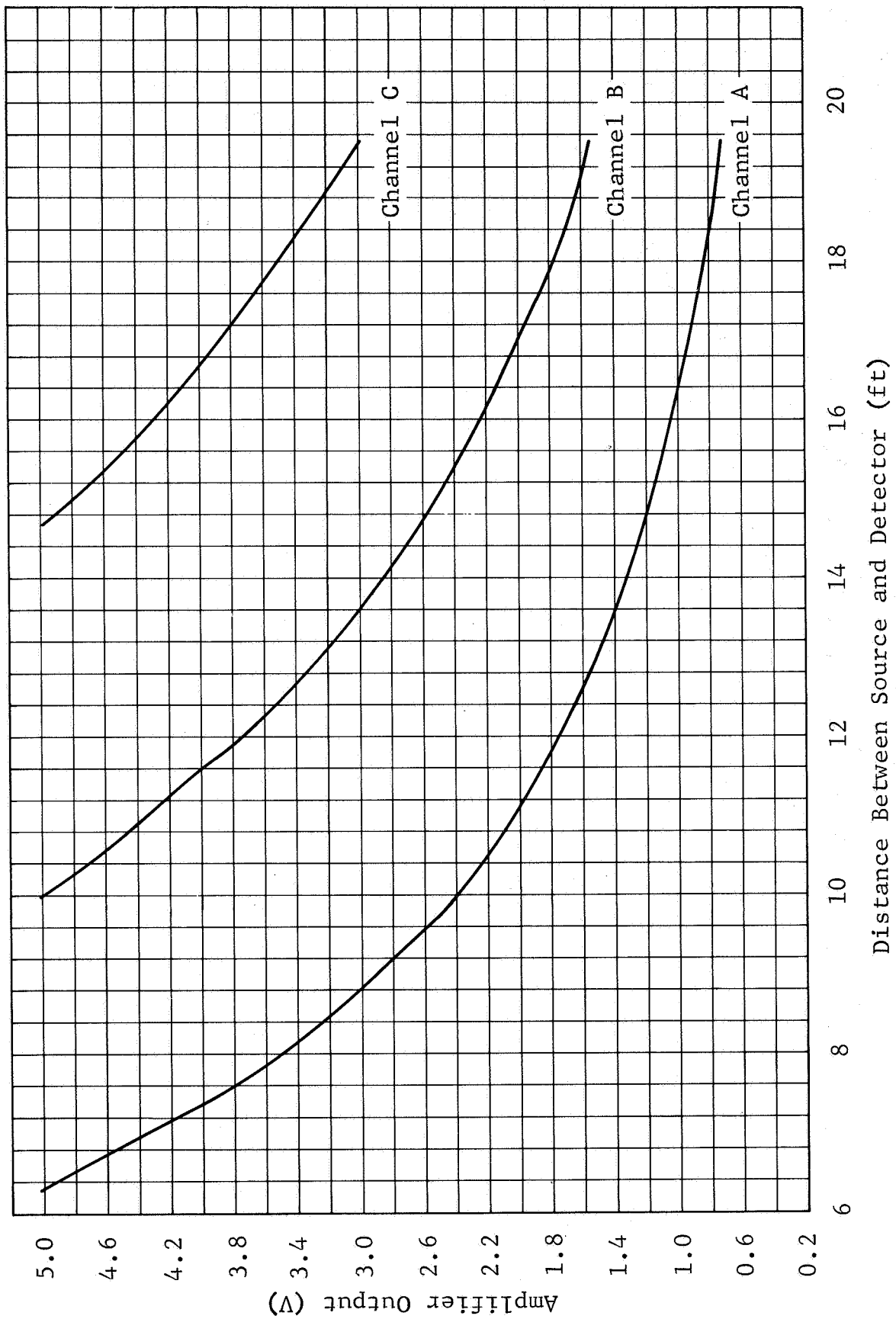
Figure 6-7 Calibration of Detector 4
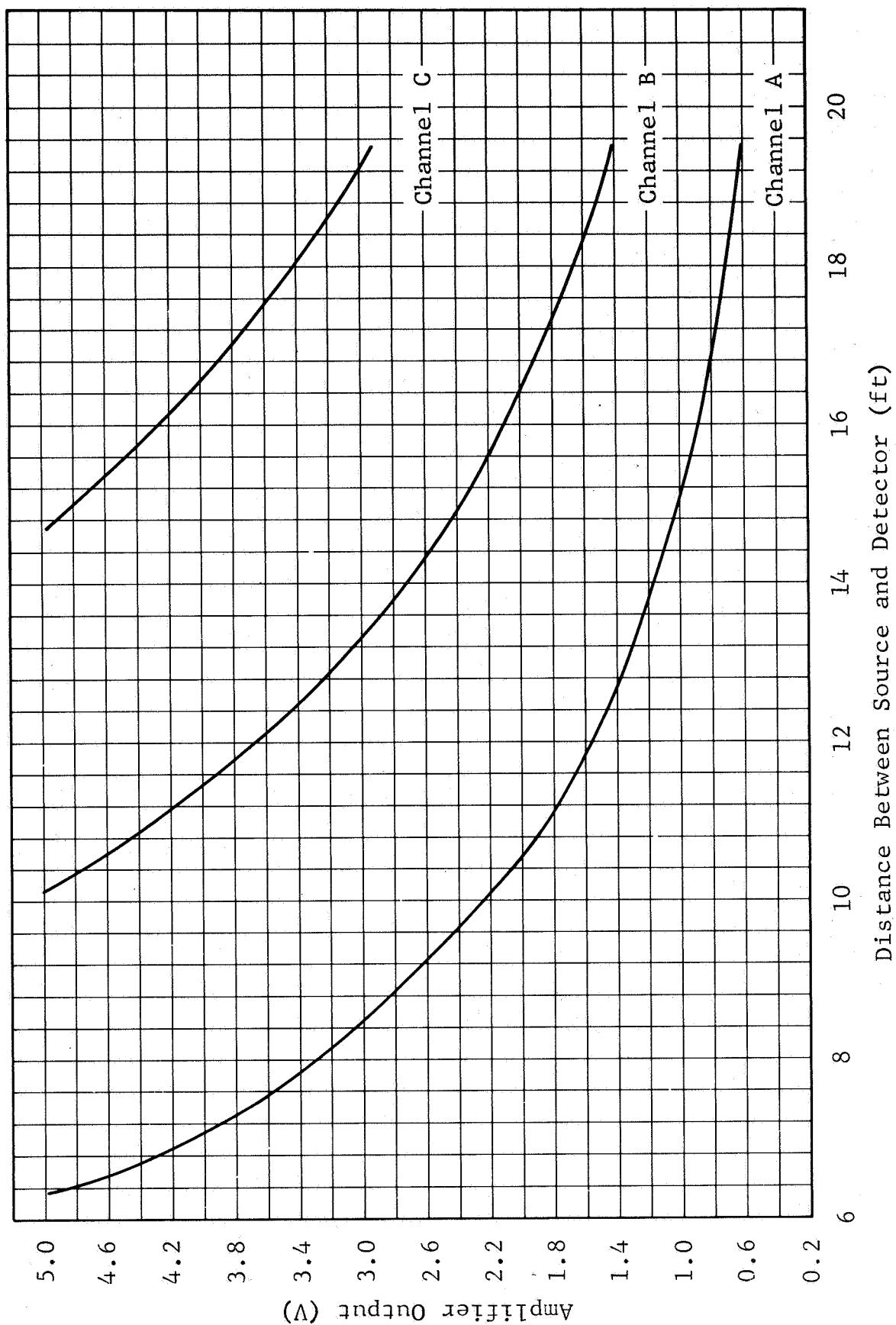
Figure 6-8 Calibration of Detector 5
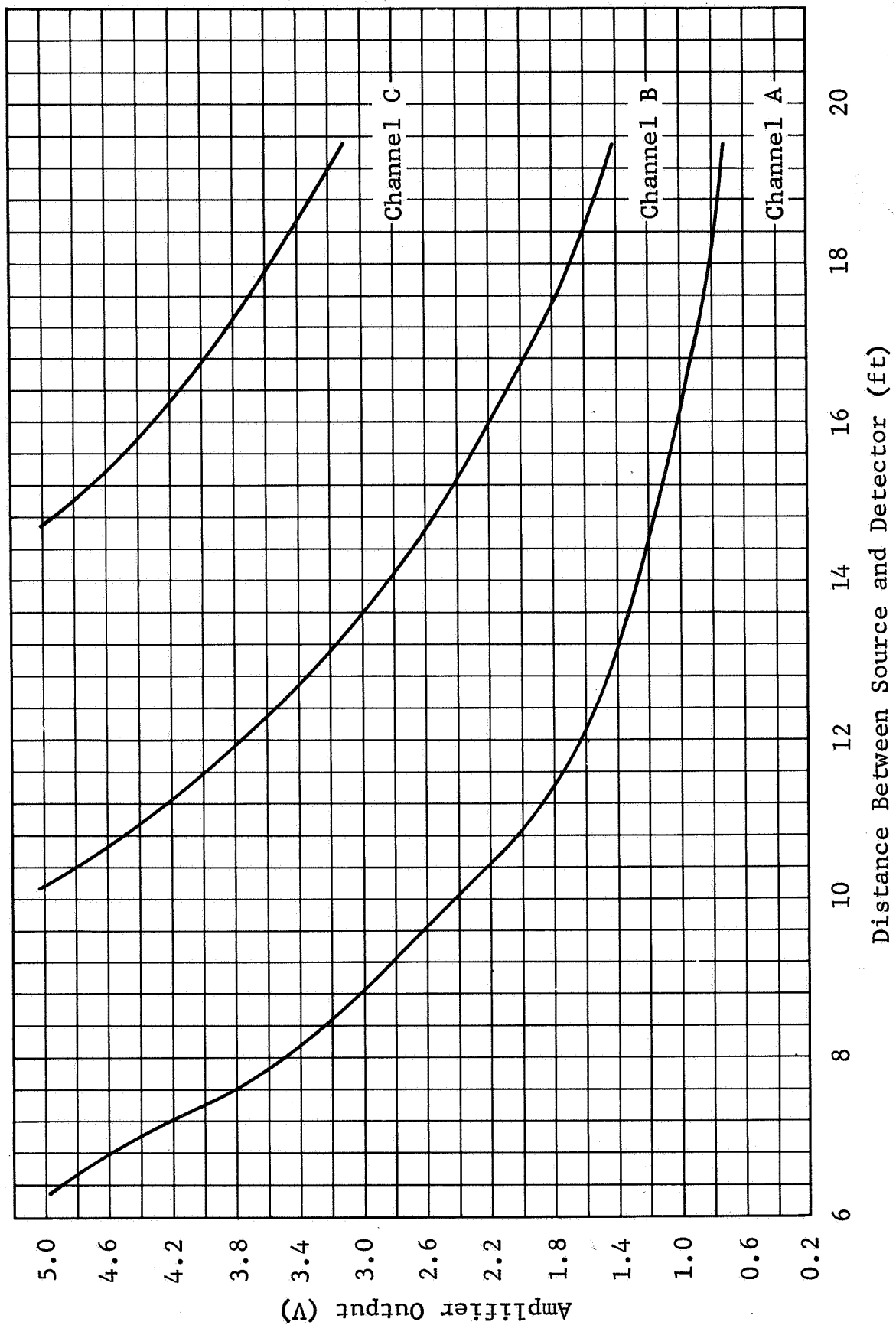
Figure 6-9 Calibration of Detector 6
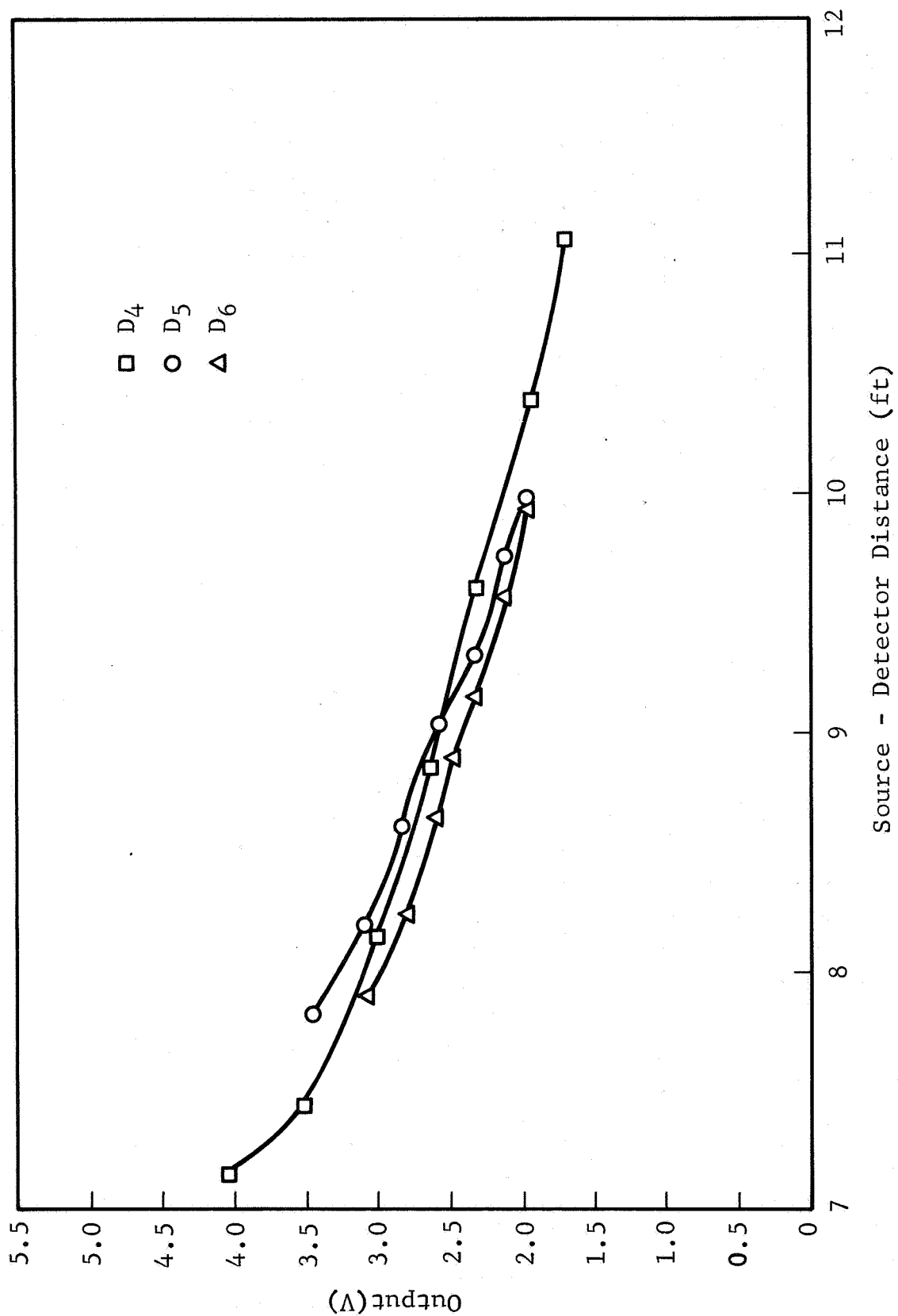
Figure 6-10 Tilt Limits at Separation of 3 Feet
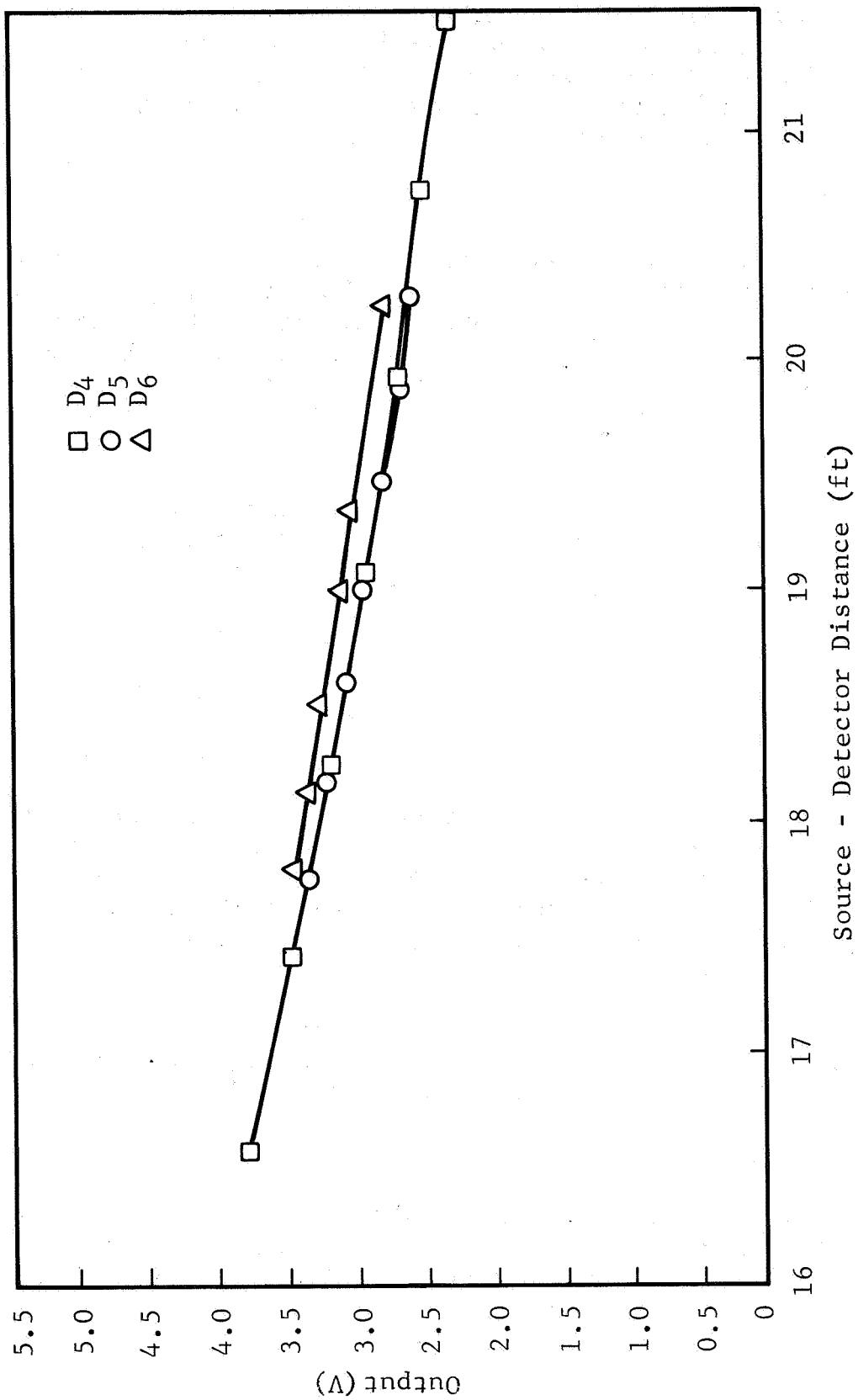
Figure 6-11 Tilt Limits at Separation of 15 Feet

The maximum limits were determined by observing the detector outputs as the plane was tilted. The response of D_5 decreased sharply past -20 deg while D_4 decreased past +20 deg. The sharp reduction in response was due to the source shield. The tilt limits at this position could be increased if source shield angle were increased. However, increasing the source shield angle would increase scattering.

6.5 Rotation

The source plane was maintained at zero tilt (no translation) and was rotated from -30 to +30 deg in 10-deg steps. With the source plane at one rotation setting, the separation distance was decreased until the outputs showed an abnormal change. Thus, the minimum separation distance was located for ±10, ±20, and ±30 degrees of rotation. The minimum distances are:

Minimum Distance of Separation (ft)	Angle of Rotation (deg)
9	±30
8	±20
5	±10

The limit of rotation was reached when the distance between a given source and detector increased to the point where the detector was shadowed by the source shield (see Figures 5-1 and 6-3). The rotation cannot be greater than ±30 deg at any separation distance, since the detector shields would then shadow the source.

If the source shield were almost flat, so that the source could radiate upward in any direction, ±30 deg rotation could be detected at separation distances up to 15 ft.

6.6 Translation

The source plane was translated with no tilt and no rotation at stage separation distances of 2 and 15 ft. The translation was performed along the X and Y coordinates (Fig. 6-3).

At a separation distance of 2 ft, the system will measure translation from X = -2 ft to just less than X = 1.5 ft. The Y coordinate was maintained at Y = 0 ft for the X translation. Detector D_4 is shadowed by the source shield at X = +1.5 ft, as can be seen by Figure 6-12 where the D_4, D_5, and D_6 outputs are plotted for X = -2 to X = +1.5 ft. The D_4 output at a D_4-S_2 of 8 ft 4.5 in. is below what it should be. The response of this detector is normal at an X of about 1.3 ft. At more than 2 ft in the X-direction, D_5 and D_6 become shadowed by the S_3 source shield.

The Y translation limits are from Y = -2 ft to Y = +2 ft with X = 0. Note that the Y translation is symmetrical and the limits can be determined by translating in the positive direction only. At Y = +2 ft, detector D_2 is shadowed from S_1 by its own shield. The Y = +2 ft translation limit is due to the detector shields on D_2 and D_5. The decrease in D_5 at Y = +2 ft can be seen in Figure 6-13 where the D_4, D_5, and D_6 outputs are plotted from Y = -2 ft to Y = +2 ft.

At a separation distance of 15 ft, the system will properly measure translation from X -4.5 ft to X = +3 ft. The limit at X = -4.5 ft is due to the detector shields shadowing D_4 and D_3. The limit at X = +3 ft is due to shadowing of D_5, D_6, D_1, and D_2 by their detector shields.

The Y limits at 15 ft are from Y = -5 ft to Y = +5 ft. The limits are due to shadowing of detectors D_5 and D_6 at -5 ft and detectors D_1 and D_2 at +5 ft by their respective shields.

The data for X = 4.5 ft to X = 3 ft and Y from -2 ft to Y = +5 ft are shown in Figures 6-14 and 6-15, respectively. The data are somewhat inaccurate because of the small change in source-detector distance as the source plane was translated and the difficulty in translating the source plane accurately. However, when the shield limits are reached, the response limits are very evident.

6.7 Velocity

The velocity of separation at time t_o is

$$V_o = \frac{|R_o - R_1|}{|t_o - t_1|}$$
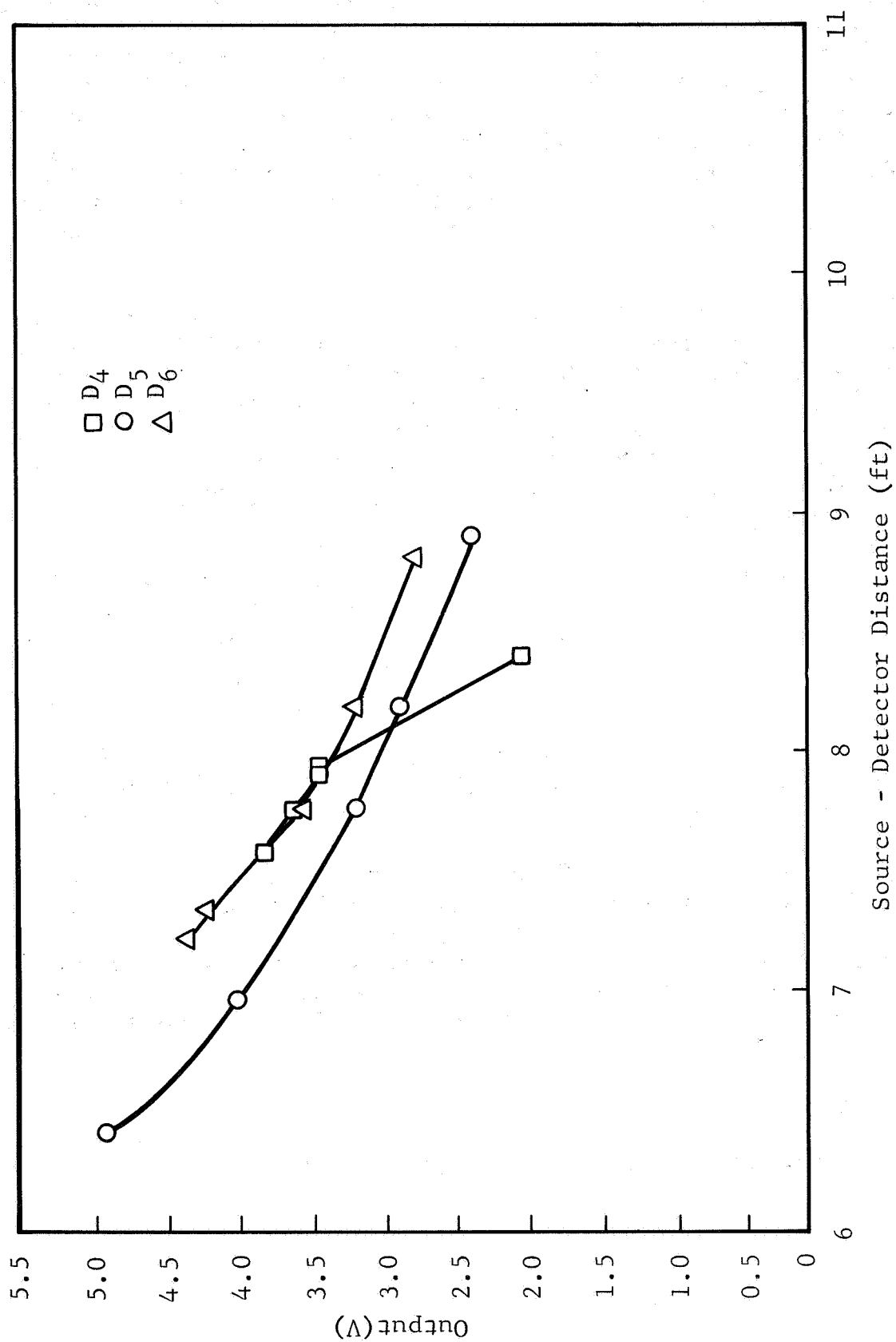
Figure 6-12 X Translation at Separation of 2 Feet
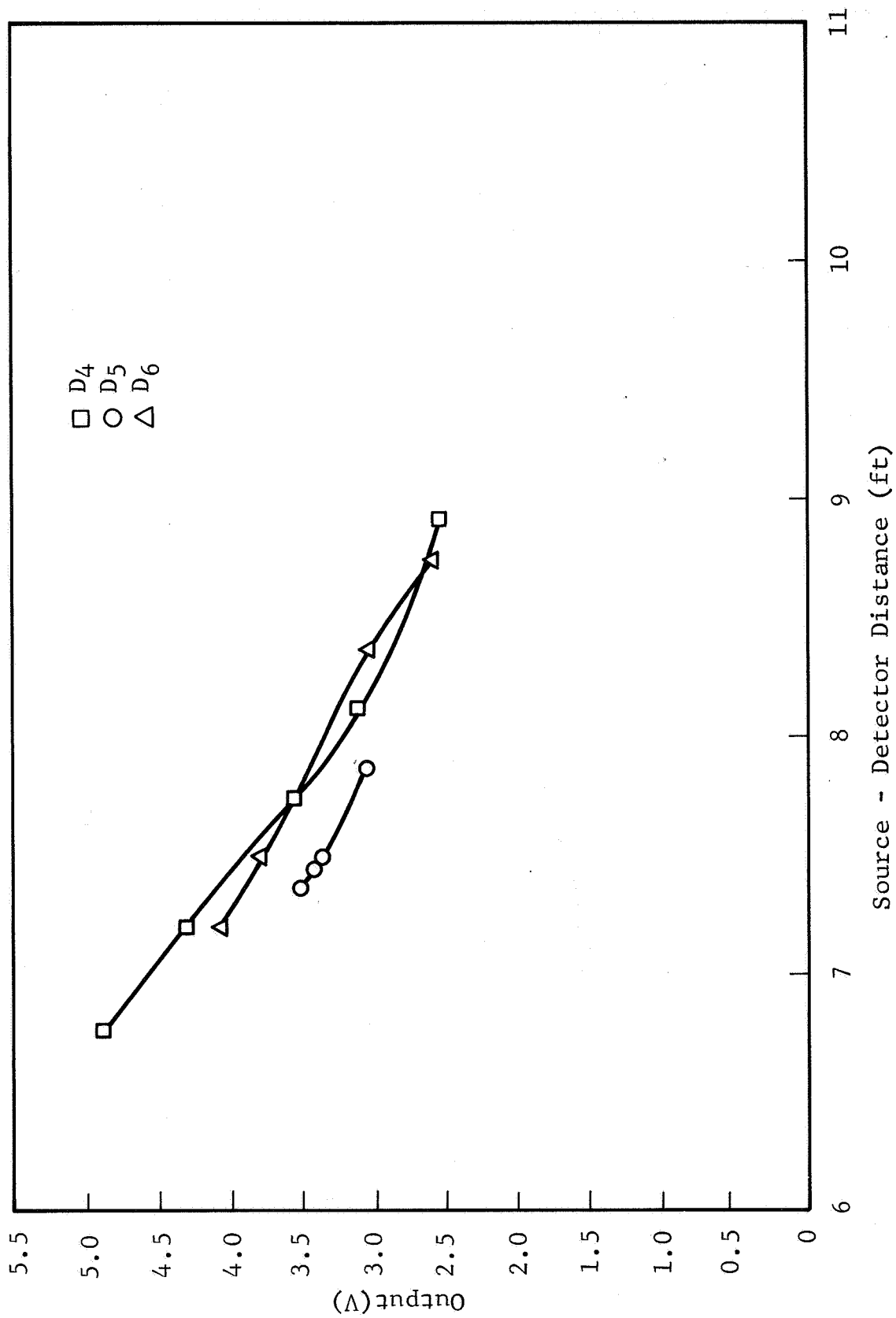
Figure 6-13 Y Translation at Separation of 2 Feet
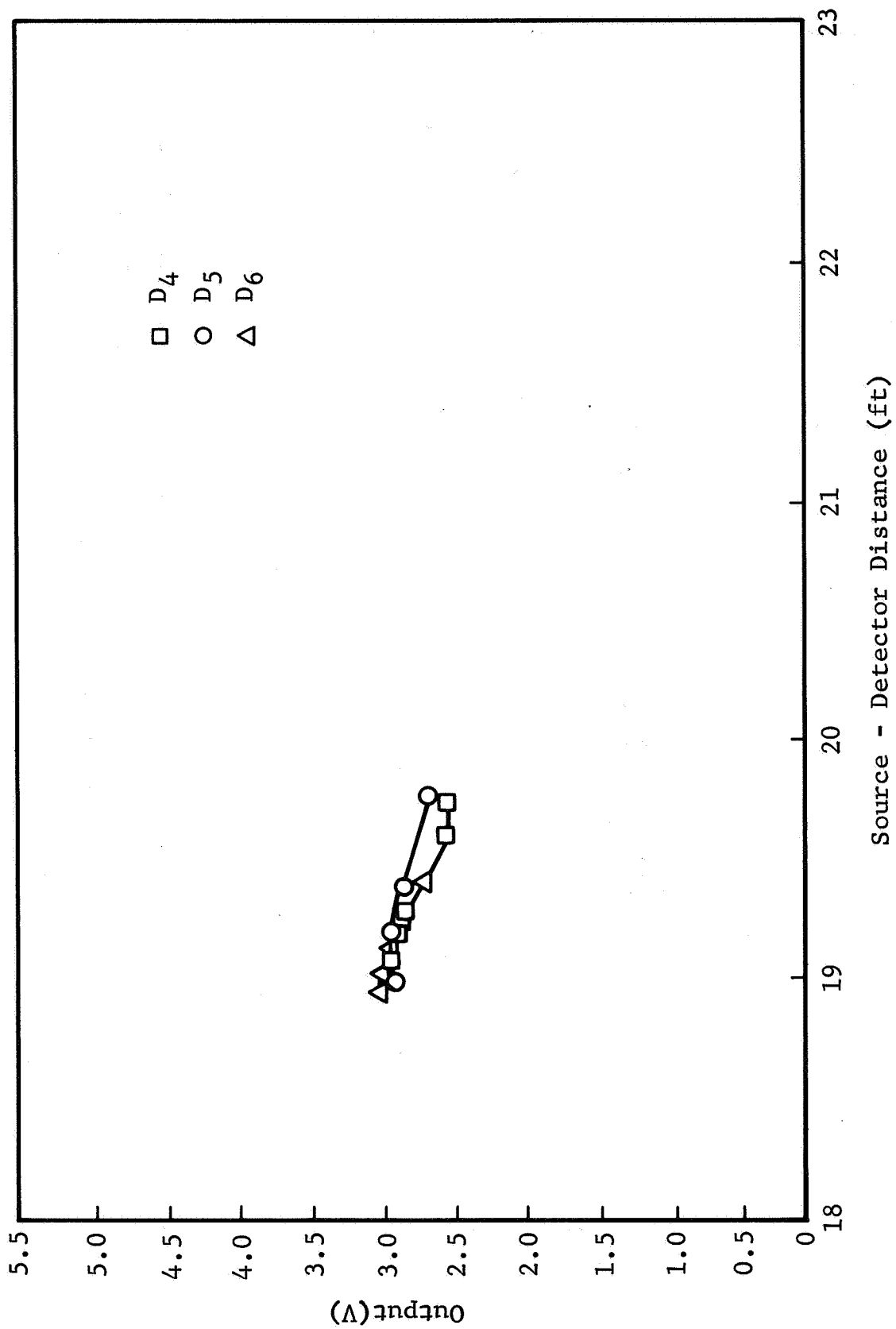
Figure 6-14 X Translation at Separation of 15 Feet
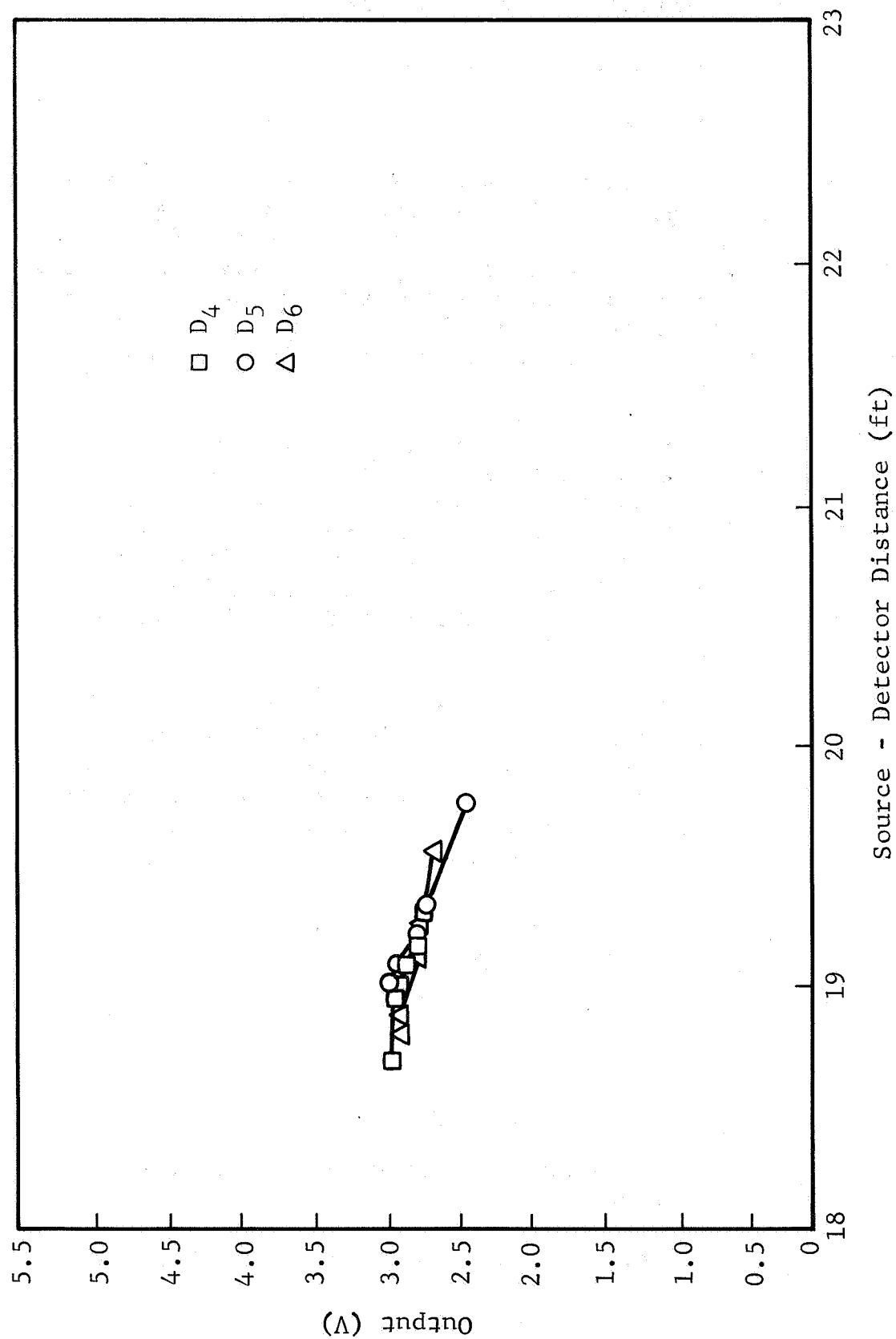
Figure 6-15 Y Translation at Separation of 15 Feet

where R_0 = separation distance at time t_0

R_1 = R_0 + ΔR, where $\Delta R << R_0$

t_1 = time at R_1.

The velocity of the source plane was measured by using two position indicators, one at a 15-ft separation and one at a 16-ft separation. Each position indicator consisted of a photodiode and a light source so arranged that the source plane would interrupt the light beam impinging on the photodiode. The time to travel 1 ft was the time between the interrupted signals of the photodiodes. Two of these light systems were placed near sources S_2 and S_3.

The detector and photodiode signals were fed into a 52-channel oscillograph where there was an internal time base. The output of each detector was accurately measured at the photodiode positions for zero velocity. The source plane was dropped and the velocity at the 15-ft separation distance was measured as 363 in./sec. The velocity was determined by dividing the 1-ft distance between the photodiodes by the time lapse between the two photodiode pips.

The signals from the detectors arrive at the oscillograph a fraction of a second later than the signals from the photodiodes. This time delay is caused by the electronics and recording system. (The delay of a pulse-integrating amplifier is discussed in detail in Section III.) The error in reading the source-detector distance is given by

$$r^2_{ac} = r^2_{det} \left(1 - \frac{RC}{V_T} \frac{\Delta V}{\Delta t} \right)$$

where

r_{ac} = actual distance

r_{det} = distance given by detector voltage reading

$\frac{\Delta V}{\Delta t}$ = rate of change of voltage reading

V_T = voltage reading

RC = delay time

66

The voltage error, as read from the oscillograph, proved to be small - about 0.03 ± 0.01 V high out of 3 V, or about 1%. The delay, as determined from the detector readings before and during the drop, averaged about 2 ± 1 msec.

The delay was measured electronically in the laboratory by feeding a burst of negative pulses into the separation amplifiers and recording the output on an oscilloscope. The frequency of the input pulse train was 1 MHz; this pulse train was gated into the preamplifier for 200 msec.

A 200-msec square wave from one pulser was used to gate on a separate pulser running at a 1-MHz frequency. This 1-MHz pulse train was fed into the preamplifier and the outputs of the preamplifier and the three spreader amplifiers were recorded. A dual-trace oscilloscope was used to determine the exact decay times.

The response of the oscillograph recorder and its preamplifiers was measured as 1.5 msec. The total time delay, not including the detector, as measured electronically, is then

$$\sqrt{1.5^2 + 1.5^2} \quad \text{or 2.1 msec.}$$

The delay in the crystal and phototube should not be more than $0.3 \; \mu$sec. The only remaining delay that has not been measured electronically is the delay in the detector-to-preamplifier cable. The input resistance to the preamplifier is 1.5×10^4 ohms and the input capacitance (≈ 70-ft coax cable) is 2.1×10^{-9} farads. This RC time constant is only 0.03 msec.

The total times measured electronically are 1.5 msec from detector to telemetry output for all three amplifiers and 1.5 msec for the oscillograph recording system. The 2.1 msec agrees with the velocity test on the full-scale test rig.

As a second independent test of the delay time, a detector system was exposed to a pulsed radiation source. The pulsed radioactive source was improvised by rotating a cesium source past an opening in a lead shield. The source was mounted on the end of a rod that was attached to a variable-speed motor shaft. A scintillation detector was located opposite the opening. A light sensitive diode was used to gate the oscilloscope "on" each time the source entered the opening in the lead.

From the source diameter and source velocity, the decay time of the source intensity was estimated to be 3 msec. The delay seen on the oscilloscope was 3.5 msec. This delay is the 3-msec source-strength decay plus the 1.5-msec electronic delay. The cable length from detector to preamplifier was varied from 5 ft to 75 ft with no noticeable change in decay time.

The total decay time in the system is ~1.5 msec. The resulting error in source-detector distance reading is small for velocities up to 400 in./sec and this error can be calculated if the velocity is known.

VII. QUALITY ASSURANCE

A quality control plan based on NASA 200-3 was utilized throughout this program. The plan consists of those functions which ensure compliance with the requirements of the contract. The responsibility for control procedures and inspection was with the Fort Worth Division Quality Assurance Department, which has unimpeded access to the Division Manager. The details of the control plan were established early in the program and were submitted as a separate document entitled, "Inspection Plan for NAS8-11995." A summary of the control functions is given below.

7.1 Control of Procurement

Purchase orders were screened prior to release to ensure adequate quality requirements. Test reports, certifications, and Government Inspection were requested on items of a critical nature. This included raw material and the major electronic components. Government source inspection was requested on the 1500-V, Arnold Magnetics #SMU Series power supply. Certifications of conformance were requested on zener diodes, photomultiplier tubes, crystals, potentiometers, and the Fairchild $\mu A702$ integrated circuit.

7.2 In-Process and Assembly Inspection

All purchased parts, components, and subassemblies were inspected and/or tested prior to encapsulation or enclosure into the prime assemblies. Inspection verified that all machined detail parts were fabricated to the latest engineering specification.

7.3 Final Inspection

Final inspection and testing, including environmental testing, was witnessed 100% by inspection personnel.

7.4 Materials Review

There were no nonconforming articles used in the system and, consequently, no waivers and/or approvals were needed.

7.5 Special Processes

Only trained and certified personnel were used to package and assemble the system. Soldering of the electronic modules was performed by personnel who were certified to NASA NPC-200-4. Each connection was evaluated using a 30-power lens prior to encapsulation in the module.

VIII. RELIABILITY ANALYSIS

This analysis provides (1) failure modes of the piece parts, with a description of the effect of failure of the components as applied within the circuit design; (2) a mathematical prediction of the Mean Time to Failure; and (3) implications of the analysis in the construction and applications of the device. To assist in preparing this analysis, a NASA Literature Search[*] was requested and utilized.

The modes of failure described are those randomly experienced with the various components used in the Separation Unit and reflect the inherent nature of the parts within the specified environment. These random failure modes and rates exclude failures caused by poor design or fabrication or by accidents, abuse, faulty maintenance, operator error, or similar happenings. Such causes of failure are minimized by thorough testing, skilled workmanship, and use of quality-control procedures.

8.1 Major Components

8.1.1 Detector

The detector consists of a sealed container, high-voltage and signal-output connectors, printed circuit boards, resistors, zener diodes, a photomultiplier tube, a crystal, silicone-grease interface material, potting compound, solder, and miscellaneous hardware.

The modes of failure associated with the detector include power shorts and signal loss or degradation. Specific causes of failure are discussed in Section 8.2. A power short, including arcing, occurring ahead of R12 will result in a total loss of the system. Other power shorts, opens, or parameter drifts will cause loss or degradation of the particular detector channel only. The effects of degradation can be removed by ground and flight calibration adjustment of the output data.

---

[*]*Failure of Electronic Equipment and High Voltage Circuitry*, NASA Literature Search Number 5337, NASA Scientific and Technical Information Facility, 4 Dec. 1967.

The detectors as a group account for 96% of the system
failures. Each detector unit represents about 16% of the total
system failure rate. This percentage of failure rate is quite
sensitive to the failure rate assigned to the photomultiplier
tube.

8.1.2 Electronics Unit

The electronics unit consists of a container, three
dc-to-dc power supplies, twenty-four potted modules, printed
circuit boards, connectors, wiring, and miscellaneous hard-
ware. The potted modules include such discrete parts as
integrated circuits, potentiometers, resistors, and con-
densers.

The principal electronics-unit failure modes include:

1. Loss of signals (18) to telemetry.

2. Degradation of signal, e.g. intermittent noise,
   distortion, or shift of scale factor.

3. Loss of power to detectors (6).

4. Loss of input power.

5. Loss of 3- or 6-V internal power.

Failure modes 1 and 2 will result in a partial loss of
data, and modes 3,4, and 5 will result in a total loss of the
system. The electronics unit as a whole comprises 4% of the
total system failure rate.

8.2 Piece Parts

8.2.1 Detector Container

This unit houses the crystal, the photomultiplier tube,
and the voltage divider network in a manner that precludes
failures caused by shock, vibration, humidity, and contamina-
tion. Particular attention was given to providing (1) ade-
quate insulation of the high-voltage circuits, (2) mechanical
stability of the crystal-tube optical interface, (3) mechani-

cal support of discrete parts, and (4) exclusion of possible contamination.

8.2.2 Electronics Container

This unit houses the electronic assemblies, interconnecting wiring, and connectors for distribution of signals and power. The design provides for exclusion of water and dirt contamination and for mechanical support sufficient to protect the modules and wiring from specified thermal, pressure, shock, and vibration environments.

8.2.3 Connectors

Separate connectors provide electrical isolation between the high-voltage power, the input power, and the signals. Low-pressure environmental tests substantiate the adequacy of the electrical insulation. Note that the connectors must be wired or clamped for mechanical security. Cable connections must be made with care to avoid crossing, which would cause signal loss but no internal damage.

8.2.4 Printed Circuit Boards

Failures caused by shorts, opens, and contamination are precluded by potting the boards within the detector container. Each connection is examined with a 30-power lens prior to potting to ensure solder and board integrity. Printed wiring is exposed within the electronics unit; however, the mechanical construction of the container adequately protects against contamination-caused failures.

8.2.5 Resistors

The principal modes of failure include opens, shorts, and parameter drift. Avoidance of shorts, control of parameter drift, and elimination of mechanical stress result from the use of potting. Shorting of the input of R12 to ground will cause a total system loss. All other resistor failures from all causes will result in only a partial system loss. (Resistors, including potentiometers, account for 2% of the system failure rate.)

8.2.6 Zener Diodes

The principal failure modes are parameter drift, shorts, and opens. Failure results range from calibration shift to loss of detector. (This component accounts for 4% of the system failure rate.)

8.2.7 Photomultiplier Tubes

The RCA-4461 tube employed in this application was designed specifically for use in missiles and rockets. \The design utilizes ruggedized construction so that it will withstand environmental tests equivalent to those specified in MIL-E-5272C for equipment mounted on structures of missiles propelled or launched by high-thrust rocket engines. One hundred percent of all 4461s are shock-tested. Failure modes include noise, opens, shorts, and parameter drift. A worst-case failure will cause loss of the related detector signal. (This component accounts for 93% of the system failure rate.)

8.2.8 Crystals

A Harshaw Chemical Co. sodium iodide single crystal doped with thallium is used with the photomultiplier tube. Silicone grease couples the crystal optically to the tube. The principal failure modes are defects of grease coupling, surface degradation, cleavage, plane separation, radiation-generated color centers, etc. Note that vibration of the crystal/grease/tube, as constructed, is considered necessary to stabilize the interface coupling. Failure results in a degradation of the signal.

8.2.9 Capacitors

Failure modes include opens, leakages, shorts, and parameter drift. Shorts occurring in capacitors C2, 5, 9, and 13 in any channel will short out the 6-V supply; shorts in C4, 7, 11, and 15 in any channel will short out the 3-V supply. Failure of either supply results in total system loss. Note that the leakage current is checked by monitoring the power consumption before encapsulating the capacitors in the modules. (Capacitors account for 0.3% of the system failure rate.)

8.2.10 Power Supplies

The dc-to-dc converters are used to obtain 3, 6, and 1500 V from the 28-V input. Power supplies are designed to MIL-E-5272. Short-circuit, transient, and reverse-polarity protection are provided. Modes of failure include loss of regulation, loss of output power, and increased noise. Since the power supplies are common to all channels, total system failure or degradation occurs from malfunctioning of the power supplies. Power-supply malfunction will result if shorts or excessive leakage occurs in any of the six high-voltage power cables to the detectors. Failures affect the total system. (The power supplies account for 0.5% of the system failure rate.)

8.2.11 Integrated Circuits

A Fairchild µA702 integrated circuit is used in each of the twenty-four potted amplifier modules. This integrated circuit is a complete dc amplifier constructed on a single silicone chip for use as an operational amplifier. Failure modes include loss or degradation of the signal. Failure of an integrated circuit in the preamplifier or in amplifier A results in loss or degradation of the affected channel. Failure of the integrated circuit in amplifier B or C results in only a partial loss of the affected channel. (The integrated circuits account for 0.7% of the system failure rate.)

8.3 Mathematical Prediction

The analysis results in a Mean Time To Failure prediction of 770 hours for total system operation. The reliability model uses the product rule for computing reliability. All components are required to operate in order for the system to function properly. This prediction reflects expectations for a mature design, manufactured and quality-controlled to high standards. The mathematical predictions are summarized in Tables 8-1 through 8-5 as follows:

1. Total System by Major Modules

2. Total System by Piece Parts

3. Detector

4. Common Items in the Electronics Unit

5. Amplifiers in the Electronics Unit

    a. Preamplifier

    b. Output Amplifier A

    c. Output Amplifiers B and C

8.4 Implication of Analysis

8.4.1 Total Loss of System

Subsections 8.1.1, 8.1.2, 8.2.5, 8.2.9, and 8.2.10 cite failures that result in total system failure. If ultra-reliability is required, judiciously applied use of redundancy could be applied to provide means of reducing the hazards of total system loss.

8.4.2 Partial System Operation

Most failures (99.4%) result in loss of a single channel or, in some cases, degradation of a single channel. This implies that a higher reliability exists for data that do not depend on the operation of all six detectors. As an example, slant range can be obtained if all but one detector fail.

8.4.3 Precautionary Statements

Subsections 8.2.3, 8.2.8, and 8.2.9 contain precautionary statements related to the manufacture or application of the system. These precautions need to be observed to preclude reliability degradation.

Table 8-1

RELIABILITY PREDICTION: TOTAL SYSTEM BY MAJOR MODULES

Component	Quantity	Unit Failure Rate[a]	Total Failure Rate[a]	% of System Failures
Detector	6	207.860	1247.160	96.3
Common Items - Elec Sep Unit	1	6.300	6.300	0.5
Preamplifier - Elec Sep Unit	6	1.660	9.960	0.8
Output Amplifier A	6	1.720	10.320	0.8
Output Amplifiers B and C	12	1.760	21.120	1.6
			1294.860	

MTBF = 770 Hours

a Failure rates stated in parts per million hours.

Table 8-2

RELIABILITY PREDICTION: TOTAL SYSTEM BY PIECE PARTS

Component	Quantity	Unit Failure Rate[a]	Total Failure Rate[a]	% of System Failures
Integrated Circuit	24	0.400	9.600	0.74
Capacitors C12 thru C15	90	0.040	3.600	0.27
Signal Connectors	27	0.020	0.540	0.04
3-V Converter	2	1.500	3.000	0.23
1500-V Converter	1	3.000	3.000	0.23
Resistor	48	0.100	4.800	0.37
Potentiometer	24	1.00	24.000	1.85
Photomultiplier Tube	6	200.000	1200.000	92.67
Zener Diode	66	0.700	46.200	3.56
Crystal	6	0.020	0.120	0.01
Total	294		1294.860	

MTBF = 770 Hours

a   Failure rates stated in parts per million hours.

Table 8-3

RELIABILITY PREDICTION: DETECTOR

Component	Quantity	Unit Failure Rate	Total Failure Rate
Crystal	1	0.020	0.020
Photomultiplier Tube	1	200.000	200.000
Zener 200-V Diode	1	0.700	0.700
Zener 100-V Diode	10	0.700	7.000
Resistor R12	1	0.100	0.100
Power Connector	1	0.020	0.020
Signal Connector	1	0.020	0.020
Total	16		207.860
		MTBF = 4810 Hours	

Table 8-4

RELIABILITY PREDICTION: ELECTRONICS UNIT

Component	Quantity	Unit Failure Rate	Total Failure Rate
Common Items			
6-V Converter	1	1.500	1.500
3-V Converter	1	1.500	1.500
1500-V Converter	1	3.000	3.000
Power Connectors	6	0.020	0.120
Signal Connectors	6	0.020	0.120
28-V Input Connector	1	0.020	0.020
Telemetry Connector	2	0.020	0.040
Total	21		6.300
		MTBF = 158,730 Hours	
Preamplifiers			
Capacitors C1 Thru C4	4	0.040	0.160
Potentiometer R1	1	1.00	1.000
Resistor R11	1	0.100	0.100
Integrated Amplifier	1	0.400	0.400
Total	7		1.660
		MTBF = 602,000 Hours	

Continued

80

Table 8-4 (Cont'd)

Component	Quantity	Unit Failure Rate	Total Failure Rate
Amplifier A			
Capacitors C5 Thru C7	3	0.040	0.120
Potentiometer R2	1	1.000	1.000
Resistors R3 and R4	2	0.100	0.200
Integrated Amplifier	1	0.400	0.400
Total	7		1.720
		MTBF = 581,000 Hours	
Amplifier B or C			
Capacitors C8 Thru C11	4	0.040	0.160
Potentiometer R5	1	1.000	1.000
Resistors R6 and R7	2	0.100	0.200
Integrated Circuit	1	0.400	0.400
Total	8		1.760
		MTBF = 568,000 Hours	

IX. ENVIRONMENTAL QUALIFICATION TESTS

The separation measuring device was designed to meet the environmental requirements set forth in the contract. These requirements are those experienced during a Saturn V launch, when the vibration is extremely severe (32-G peak at 2000 Hz). The device successfully passed the tests after some minor modifications. All tests (vibration, shock, temperature, and pressure) were witnessed and approved by the local MSFC representative and the Fort Worth Division's Quality Assurance Department.

9.1 Vibration and Shock

One detector and one electronics unit, which houses the detector power supplies and all the amplifiers, were subjected to vibration and shock tests as individual test specimens.

9.1.1 Electronics Unit

The electronics unit was sandwiched between two layers of 0.5-in. silicone rubber padding and enclosed in a test fixture, as shown in Figure 9-1. The fixture and specimen were then attached to a vibration machine and subjected to one complete cycle of vibration - 5 to 2000 to 5 Hz - in each of three mutually perpendicular axes. The rate of cycling was 1 octave/min. Amplitudes of vibration over the frequency range, as set forth in the contract, were as follows:

Frequency (Hz)	Amplitude
5-20	0.5 in., Double Amplitude
20-100	$\pm$ 10Gs, peak
100-160	0.019 in., Double Amplitude
160-2000	$\pm$ 32Gs, peak
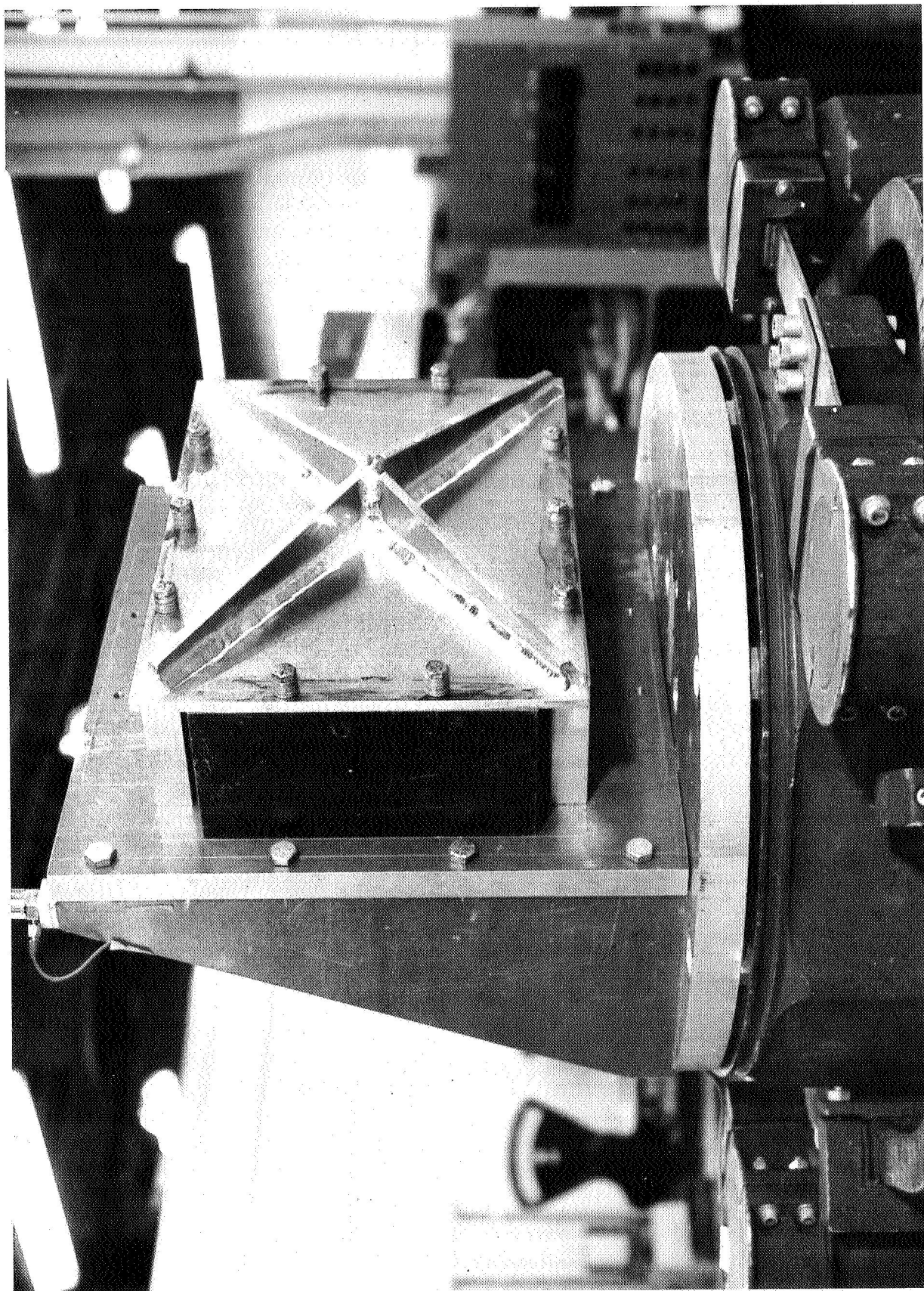
Figure 9-1 Electronics Unit Vibration Mount

Inspection of the electronics unit following the vibration test revealed several broken wires. The wires were repaired and their support modified by the addition of a potting compound. The unit was subjected to the vibration cycling again and inspected. This time it met the requirements of the functional test. The results of the test are given in Table 9-1.

The electronics unit was mounted in the vibration fixture and subjected to a total of six shock pulses, one in each direction, in each of its three axes. The shock waveform configuration was a half-sine pulse with an amplitude of 50 Gs and a duration of 8 msec. The electronics unit met the requirements of the functional test following the shock exposures. The results are given in Table 9-2.

9.1.2 Detector

Detector No. 5 was clamped inside a 0.5-in. silicone rubber pad and mounted to the vibration table, as shown in Figure 9-2. One cycle of vibration, as described for the electronics unit, was applied in each of three mutually perpendicular areas. Functional tests following the vibration exposure revealed a decrease in sensitivity of approximately 15%. A careful inspection and additional functional tests revealed no damage to the detector. It was suspected that the seating fit between the crystal and the photomultiplier tube was altered during vibration. The vibration tests were rerun on the detector and no further sensitivity decrease was noted.

Detector 5 was subjected to six impact shocks as described for the electronics unit. Functional tests following the shock test were satisfactory and no reduction in sensitivity was noted. The data obtained from both the vibration and shock tests are given in Table 9-3.

9.2 Temperature Test

Extensive temperature tests were conducted in the development phase of this program and the results of these tests are given in Section IV. However, temperature tests from -20°C to +60°C were conducted on the final electronics unit and repeated on the detector. The data given in Tables 9-4 and 9-5 show that the response changes are due primarily to the detector.

Table 9-1

VIBRATION TEST DATA ON ELECTRONICS UNIT

Test: Vibration   Supply Voltage: +28.5 V

Date: 1-24-68   High Voltage: -1480 V

Source: G-2 (Cs-137)   B+ Voltage: +6.73 V

Detector No.: 5   B- Voltage: -3.15 V

Source-Detector Distance (cm)	Amplifier Response (volts)																	
	Channel 1						Channel 2						Channel 3					
	Pre-Test			Post-Test			Pre-Test			Post-Test			Pre-Test			Post-Test		
	A	B	C	A	B	C	A	B	C	A	B	C	A	B	C	A	B	C
8	4.93	5.34	5.42	4.88	5.35	5.43	4.99	5.36	5.43	5.02	5.37	5.43	5.00	5.39	5.39	4.91	5.40	5.40
15	1.95	4.87	5.41	1.91	4.78	5.42	2.00	5.03	5.42	1.97	4.99	5.44	2.00	5.00	5.39	1.95	4.92	5.40
27	0.69	1.75	4.55	0.70	1.77	4.51	0.72	1.80	4.55	0.72	1.82	4.59	0.72	1.80	4.85	0.72	1.83	4.85
45	0.24	0.63	1.58	0.24	0.61	1.60	0.26	0.64	1.62	0.25	0.63	1.67	0.29	0.68	1.88	0.28	0.70	1.92

Source-Detector Distance (cm)	Amplifier Response (volts)																	
	Channel 4						Channel 5						Channel 6					
	Pre-Test			Post-Test			Pre-Test			Post-Test			Pre-Test			Post-Test		
	A	B	C	A	B	C	A	B	C	A	B	C	A	B	C	A	B	C
8	5.00	5.39	5.40	4.98	5.40	5.42	5.00	5.38	5.46	4.93	5.40	5.47	5.00	5.44	5.43	4.97	5.45	5.45
15	2.00	5.00	5.40	1.95	4.95	5.42	1.98	5.10	5.46	1.95	5.03	5.47	2.00	5.10	5.43	1.97	5.0	5.45
27	0.68	1.71	4.50	0.66	1.71	4.46	0.70	1.82	4.60	0.70	1.83	4.64	0.71	1.80	4.60	0.70	1.80	4.55
45	0.22	0.54	1.35	0.20	0.54	1.40	0.27	0.68	1.70	0.26	0.69	1.79	0.27	0.67	1.72	0.25	0.61	1.77

Notes: With source G-2 located 8 cm from detector face, all preamplifier outputs were set at +1.00 volt before taking readings.

Test Results: No significant changes after vibration.

Test Engineer: _A R Robinson_

Approved:

Fort Worth Engineer: _Ralph Wiley_

Fort Worth Quality Assurance: _H. E. Martin_

Air Force Quality Assurance: _Gus Messick_

Table 9-2

SHOCK-TEST DATA ON ELECTRONICS UNIT

Test_____Shock_____   Supply Voltage____+28.0 V_____

Date_____1-30-68_____   High Voltage_____-1485 V_____

Source_____G-2 (Cs-137)_____   B+ Voltage_____+6.78 V_____

Detector No._____5_____   B- Voltage_____-3.14 V_____

Source-Detector Distance (cm)	Amplifier Response (volts)																	
	Channel 1						Channel 2						Channel 3					
	Pre-Test			Post-Test			Pre-Test			Post-Test			Pre-Test			Post-Test		
	A	B	C	A	B	C	A	B	C	A	B	C	A	B	C	A	B	C
8	4.88	5.35	5.43	5.00	5.36	5.43	5.02	5.37	5.43	5.06	5.37	5.44	4.91	5.40	5.40	4.99	5.40	5.41
15	1.91	4.78	5.42	1.95	4.83	5.43	1.97	4.99	5.44	2.01	5.04	5.44	1.95	4.92	5.40	1.97	4.97	5.41
27	0.70	1.77	4.51	0.68	1.74	4.45	0.72	1.82	4.59	0.71	1.82	4.57	0.72	1.83	4.85	0.72	1.84	4.87
45	0.24	0.61	1.60	0.25	0.55	1.69	0.25	0.63	1.67	0.26	0.66	1.73	0.28	0.70	1.92	0.28	0.72	1.97

Source-Detector Distance (cm)	Amplifier Response (volts)																	
	Channel 4						Channel 5						Channel 6					
	Pre-Test			Post-Test			Pre-Test			Post-Test			Pre-Test			Post-Test		
	A	B	C	A	B	C	A	B	C	A	B	C	A	B	C	A	B	C
8	4.98	5.40	5.42	5.04	5.40	5.42	4.93	5.40	5.47	5.01	5.40	5.48	4.97	5.45	5.45	5.05	5.46	5.45
15	1.95	4.95	5.42	1.97	5.00	5.42	1.95	5.03	5.47	1.97	5.07	5.48	1.97	5.00	5.45	1.98	5.02	5.45
27	0.66	1.71	4.46	0.67	1.74	4.50	0.70	1.83	4.64	0.72	1.88	4.67	0.70	1.80	4.55	0.73	1.86	4.70
45	0.20	0.54	1.40	0.20	0.54	1.41	0.26	0.69	1.79	0.26	0.68	1.78	0.25	0.61	1.77	0.25	0.64	1.72

Notes: With source G-2 located 8 cm from detector face, all preamplifier outputs were set at +1.00 volt before taking readings.

Test Results: No significant changes after vibration.

Test Engineer _A R Robinson_

Approved:

Fort Worth Engineer____Ralph Wiley____

Fort Worth Quality Assurance____H E Martin____

Air Force Quality Assurance____Gus Smasich____
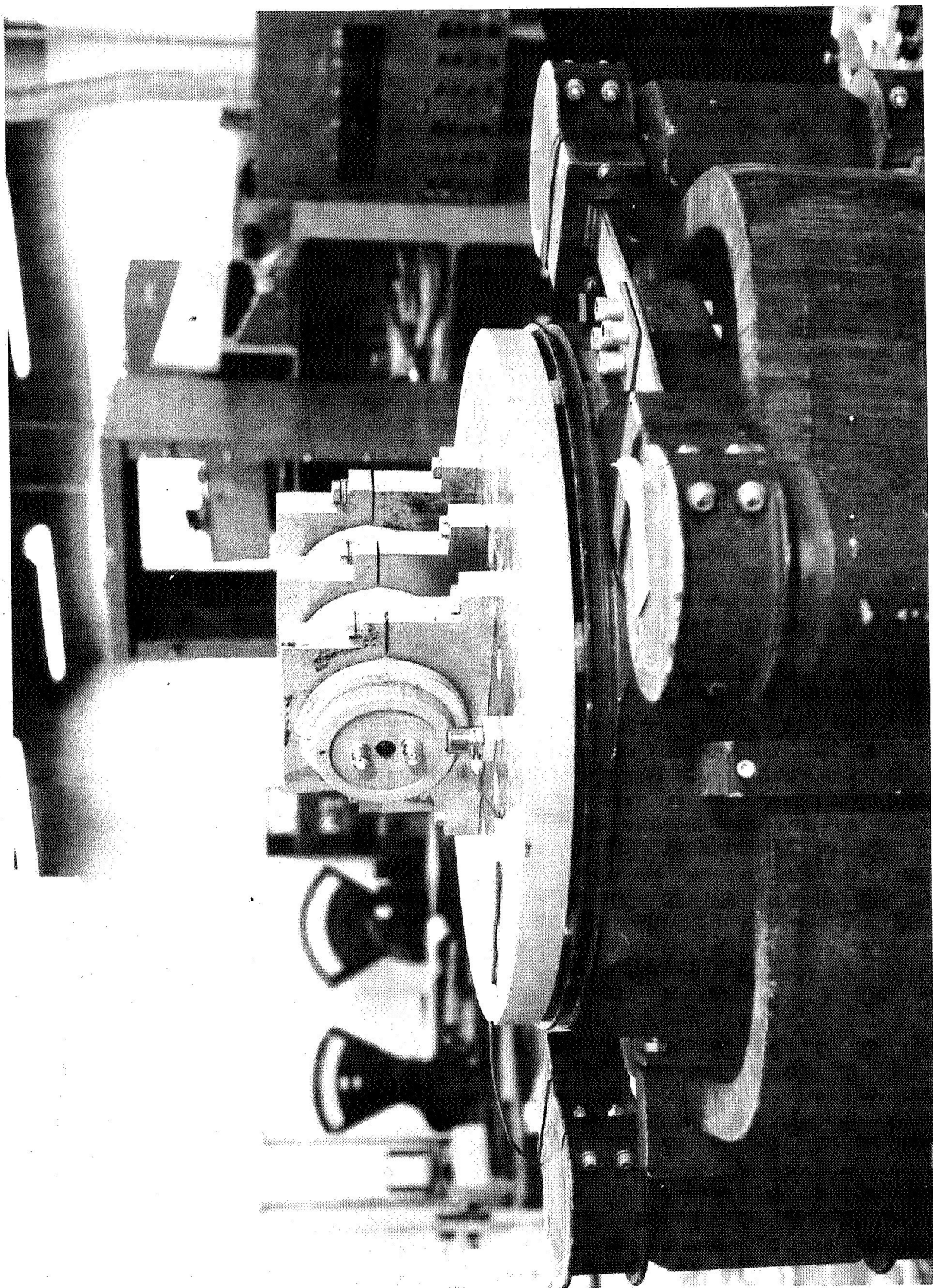
Figure 9-2 Detector Vibration Mount

Table 9-3

VIBRATION- AND SHOCK-TEST DATA ON DETECTOR

Test: ___Vibration___   Detector No. ___5___

Date: ___1-11-68___   High Voltage ___-1500 V___

Source-Detector Distance (cm)	Detector Output (µA)					
	First Vibration		Second Vibration		Shock	
	Pre-Test	Post-Test	Pre-Test	Post-Test	Pre-Test	Post-Test
8	258	235	235	243	243	240
10	193	175	175	183	183	180
12	150	135	135	142	142	140
16	95	86	86	90	90	88
20	67	60	60	63	63	62
26	42	38	38	40	40	39
40	19.8	18.8	18.8	18.8	18.8	18.1
50	13.1	11.8	11.8	12.4	12.4	12.0
60	8.9	8.3	8.3	8.4	8.4	8.2
68	7.5	7.0	7.0	7.2	7.2	7.0

Notes: _____

_____

Test Engineer _A L Robinson_

Approved:

Fort Worth Engineer _Ralph Wiley_

Fort Worth Quality Assurance _/d. E. Martin_

Air Force Quality Assurance _Gus Messick_

Table 9-4

TEMPERATURE-TEST DATA

TEST_____Temperature_____

DATE_____2-24-68_____

SOURCE_____G-2 (Cs-137)_____

DETECTOR NO. _1_ CHANNEL NO. _1_

Temp (°C)	Time	Power Supply (V)			Amplifier Response (V)				Detection Current (µA)
		B+	B-	H.V.	Pre.	A	B	C	
-20	9:04	6.61	3.03	1550	0.25	1.29	3.06	4.65	42
-10	9:42	6.84	3.06	1545	0.25	1.28	3.03	4.85	43
0	10:00	6.86	3.08	1530	0.25	1.28	3.03	4.93	43.5
10	10:15	6.80	3.09	1520	0.25	1.28	3.01	4.93	43.5
20	10:20	6.74	3.10	1515	0.25	1.28	3.00	4.94	43.5
30	3:19	6.72	3.11	1500	0.25	1.28	2.98	4.96	43.5
40	3:48	6.63	3.12	1500	0.25	1.29	3.01	4.94	43.5
50	4:10	6.58	3.13	1490	0.25	1.29	2.99	4.93	43
60	4:40	6.52	3.14	1480	0.25	1.28	2.96	4.91	42

Notes:_____

_____

Test Engineer _A R Robinson_

Approved:

Fort Worth Engineer _Ralph Wiley_

Fort Worth Quality Assurance _W. E. Martin_

Air Force Quality Assurance _Gus Messick_

Table 9-5

PRESSURE-TEST DATA

TEST   Pressure

DATE   2-27-68

SOURCE   G-2 (Cs-137)

DETECTOR NO.   1

CHANNEL NO.   3

Pressure (mm-Hg)	Power Supply (V)		Amplifier Response (V)			
	B+	B-	Pre.	A	B	C
Atmospheric	6.71	3.11	0.22	1.17	2.52	4.84
40	6.71	3.11	0.23	1.21	2.59	4.95
30	6.71	3.11	0.23	1.21	2.60	4.97
20	6.70	3.11	0.23	1.21	2.61	4.98
10	6.70	3.11	0.23	1.22	2.62	5.00

Notes: _____

_____

Test Engineer _A R Robinson_

Approved:

Fort Worth Engineer _Ralph Wiley_

Fort Worth Quality Assurance _H E Martin_

Air Force Quality Assurance _Gus Messick_

91

Thermocouples were mounted inside the detector and electronics packages to monitor internal temperatures and ensure thermal equilibrium at each temperature point. The responses of the detector and the electronics unit were monitored independently in order to observe their individual characteristics. A current of 25 μA was supplied to the electronics unit input in order to simulate the detector output current.

The detector output current and the potentials throughout the electronics unit were recorded at 10°C intervals after the temperature was allowed to stabilize (Table 9-4).

9.3 Pressure Test

The detector and electronics unit were placed in a Tenney environmental chamber and subjected to pressures ranging from atmospheric to 10 mm-Hg. In order to prevent corona discharge at high altitudes, the high-voltage output terminal of the dc-to-dc converter, which is inside the electronics package, and the associated internal high-voltage wiring were encapsulated in Sylgard 185.

As can be seen from the test data in Table 9-5, the outputs from amplifiers A, B, and C changed about 4%, while the supply voltages did not change at all over the entire pressure range.

9.4 Test Equipment

Below is a listing of the major items of equipment used in the vibration, shock, temperature, and pressure tests.

Vibration Test

Item	Manufacturer and Model No.	Rating
Shaker	MB Model C-25H	3500 lb
Amplifier	Ling Model PP 20/20	20,000 watts
Control Console	Ling Model R1007	± 3%
Accelerometer	Endevco Model 2234	± 2%
Charge Amplifier	Endevco Model 2710	± 3%
Voltmeter	Ballantine Model 300	± 2%

Shock Test

Item	Manufacturer and Model No.	Rating
Shock Machine	Barry Model 150-400	400 lb
Accelerometer	Endevco Model 2252	± 2%
Shock Amplifier	Endevco Model 2718	± 2%
Peak Holding Meter	Endevco Model 2954	± 1%
Storage Oscillo-scope	Tektronix Model 549	± 3%

Temperature and Pressure Tests

Item	Manufacturer and Model No.	Rating
Environmental Chamber	Tenney Model TMST	± 10%
Temperature Recorder	Mineapolis-Honeywell Brown Temperature Recorder	± 3%
Voltmeter	Fairchild Model 7050	± .01V
Voltmeter	Hewlett-Packard 412A VTVM	± 3%
Voltmeter	Sensitive Research Instrument Corp. Electrostatic Voltmeter Model ESD	± 5%
Power Supply	Kepco Model CK64-05	± 5%

X. RECOMMENDATIONS

10.1 Source-Detector Array

Although the initial approach of using one distance and one angle measurement is appealing from the standpoint of telemetry and data reduction, it is severely limited in the types of movement it can detect. Consequently, the angle-distance array was discarded for the six distance-measurement array, by means of which the spatial orientation of the two stages can be completely defined within the limits specified in Section VI.

The array of three sources on one stage and six detectors on the other stage appears to be the best approach for the situation studied in this project. However, any change in measurement requirements or geometrical arrangements may dictate the use of a different array. Thus all aspects of any future application will require careful consideration.

10.2 Source Type

The cesium-137 source proved to be workable in this application, but required a relatively large amount of shielding. It is possible that americium-241 would work satisfactorily and, if so, would require much less shielding. The scattering effects of the lower-energy americium could prove to be detrimental to system accuracy, especially with regard to the rocket exhaust gases present upon separation. No attempt was made to calculate the effects of scattering for various source energies, since such calculations are complex and somewhat uncertain. It is recommended that americium-241 be considered for any future application, especially if accuracy requirements can be reduced. The use of a lower energy source should be experimentally evaluated.

10.3 Shielding

The shielding design is very dependent on the geometrical relationship of the source-detector array and the movements to be measured. Any change in the system geometry will necessitate a change in shielding. The limits of movement of the

particular system studied can be increased by increasing the angle of the upward radiation of the sources, but this would result in increased scattering effects.

If a lower-energy source were used, the thickness of the shielding could be decreased. The thickness of the shields used for this task was approximately 2 in. for each of the detectors and sources. If americium-241 were used, the shielding could be reduced to 0.4 in. in thickness.

10.4 Electronics

All of the circuitry was exceptionally insensitive to temperature changes, and the components proved resistant to vibration, shock, and pressure changes.

The use of three spreader amplifiers in the basic design provides little increase in accuracy for the increase in the number of components. More important, the spreader amplifier requires the use of more telemetry channels. If the accuracy of one amplifier per detector was sufficient, the electronics could be simpler and more reliable.

10.5 Fabrication Techniques

The "bolt-down" modular construction developed by Boehm and Herrmann of MSFC proved to be resistant to the severe vibration and shock tests. The electronics unit would be still more sturdy if its size were reduced, as would be the case if one amplifier system were used in place of the three spreader amplifiers.

The detector fabrication presented numerous problems. Initially, a hard potting compound was used to hold the photomultiplier tube to the crystal, but the heat and stresses developed in curing the compound damaged the tube. The final method employed a small amount of the hard potting compound near the tube interface and a soft potting compound to finish the embedding of the photomultiplier tube and its voltage divider network. This method resulted in a 15% decrease in sensitivity after one vibration test. A second vibration on the same unit

did not change its sensitivity. The 15% decrease in sensitivity could be tolerated, since the system calibration is known after launch or immediately before separation. Also, the detectors could be "pre-vibrated."

The fact that the sensitivity of the detector changes with the initial vibration leaves one doubtful about their reliability. Research and development in integrating a crystal and photomultiplier tube during manufacture might prove fruitful.

APPENDIX A

PROPERTIES OF ANGLE-DISTANCE ARRAY

APPENDIX A

PROPERTIES OF ANGLE-DISTANCE ARRAY

The most practical array for one angle measurement and two distance measurements between the S-IVB and S-11 stages is shown in Figure A-1. Since the S-IVB engine is in the center, the angle measurement must be made off center. In addition, the source of the angle pair must be on the opposite stage from the near-distance pair to eliminate interference between the distance and source pairs.

A-1 Distance Relationships

The following conditions must be made in utilizing the angle-distance array:

1. The sources and detectors on a given vehicle must lie in a straight line.

2. Before the vehicles are separated, the source and detector of each source-detector pair must be located opposite each other. The lines connecting the pairs of sources and detectors (i.e., p and p', q and q', s and s') will be then parallel to the vehicles' axes, which are coincident.

3. The relative motion of the vehicles is pitching (or yawing) and slipping motion, but no roll. Therefore, the axes of the two vehicles will intersect, and the axes form a plane designated the x-z plane.

Figure A-2 is a three-dimensional view of detector-source pairs p-p', q-q', and s-s', on the two separating vehicles. The plane of the mating surface of one vehicle is designated the x-y plane. The other mating surface lies in the x'-y' plane. The axes of the vehicles are designated z and z'. The angle between the axes is designated as α.

Since the axes z and z' define the x-z plane, the vertical distance from the x-z plane to points p and p' are equal. That is, the y component is equal to the y' component. Therefore, the projected image of p-p' on the x-z plane is equal
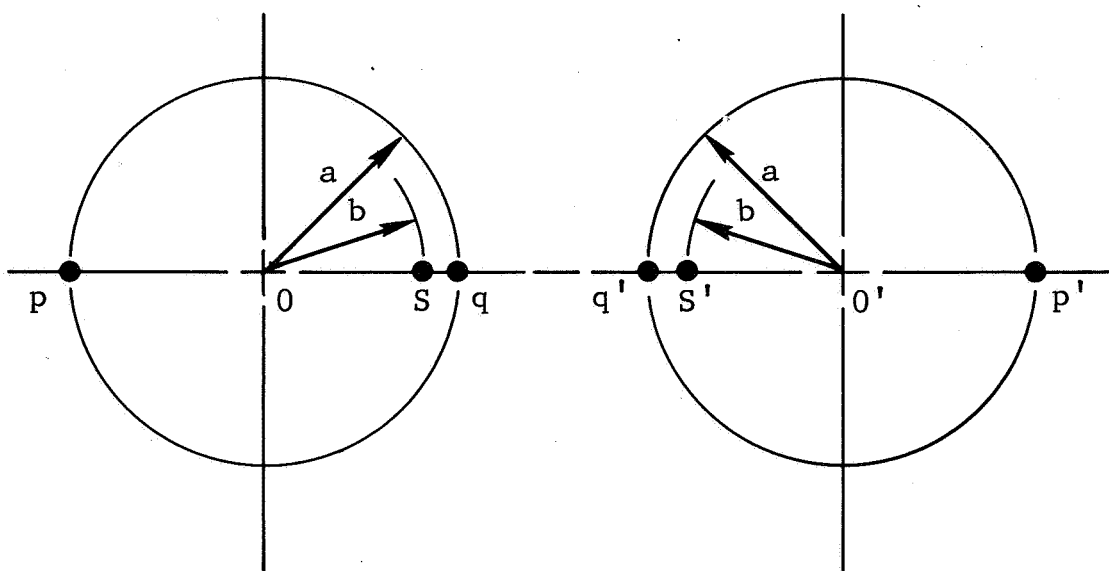
101

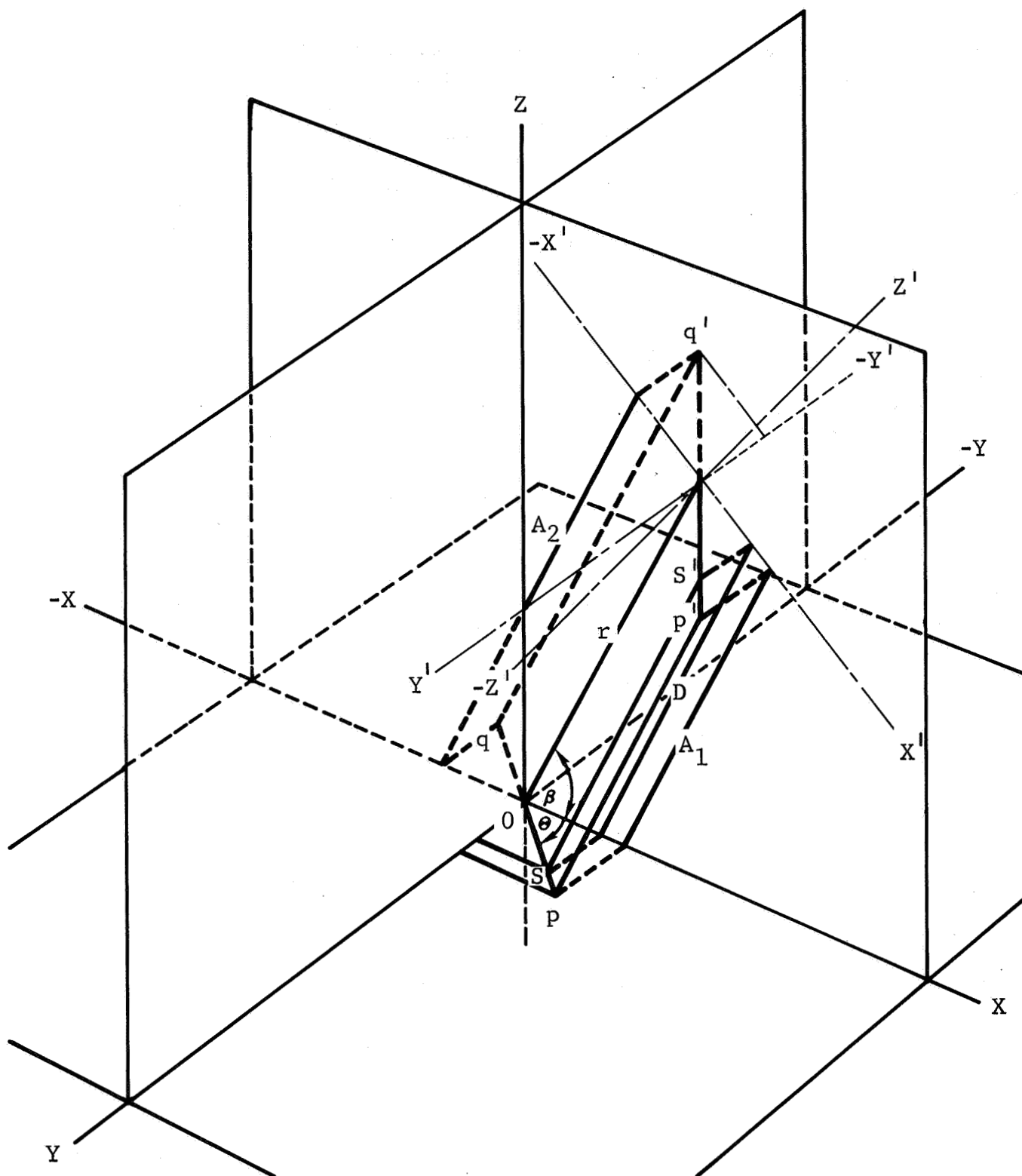Figure A-1   Source and Detector Relationship
for Angle-Distance Array

Figure A-2   Three-Dimensional View of
Angle-Distance Array

103

in length to the separation distance between p and p'. The same is true for q-q' and s-s'. Therefore,

$$A_1 = \text{distance between p and p'}$$

$$A_2 = \text{distance between q and q'}$$

$$D = \text{distance between s and s'}$$

In addition,

$$r = \text{distance between 0 and 0'}.$$

The distance between the centers of the mating planes is approximately the average of the distances between the two detector-source pairs, p-p' and q-q'. The error in determining the distance in this manner is very small - less than 0.2% for the worst case. The computation of this error is discussed below.

Figure A-3 shows the geometrical relations within the x-z plane of Figure A-2. By letting

$$a_1 = \text{distance from 0 to p}$$

$$a_2 = \text{distance from 0' to p}$$

the following equations may be written:

$$\frac{a_1}{r} = \cos \beta \left(1 + \frac{\tan \beta}{\tan \alpha}\right)$$

$$\left(\frac{a_2}{r}\right)^2 = \cos^2 \beta \left[\left(1 + \frac{\tan \beta}{\tan \alpha}\right)^2 - 2\left(1 + \frac{\tan \beta}{\tan \alpha}\right)\right] + 1$$

$$\left(\frac{A_1}{r}\right)^2 = \left(\frac{a_1}{r} - \frac{a}{r} \cos \theta\right)^2 + \left(\frac{a_2}{r} - \frac{a}{r} \cos \theta\right)^2$$

$$- 2\left(\frac{a_1}{r} - \frac{a}{r} \cos \theta\right) \cdot \left(\frac{a_2}{r} - \frac{a}{r} \cos \theta\right) \cos \alpha$$

104
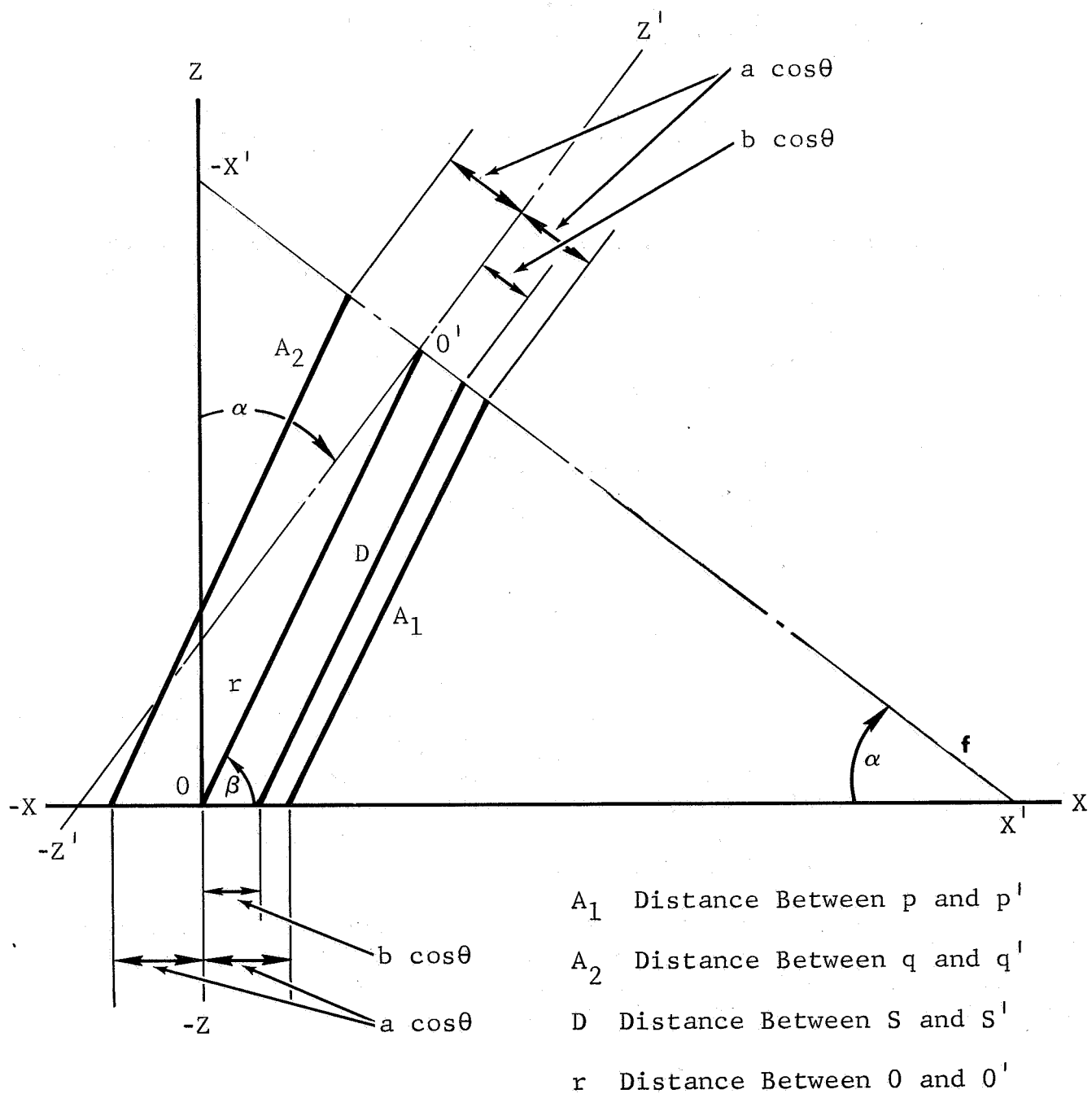
Figure A-3   Geometrical Relationship in the
            x-y Plane

$$\frac{A_2}{r} = \left(\frac{a_1}{r} + \frac{a}{r}\cos\theta\right)^2 + \left(\frac{a_2}{r} + \frac{a}{r}\cos\theta\right)^2$$

$$- 2\left(\frac{a_1}{r} + \frac{a}{r}\cos\theta\right)\left(\frac{a_2}{r} + \frac{a}{r}\cos\theta\right)\cos\alpha$$

From the above equations, values may be calculated for A_1/r and A_2/r if values are given for a/r, θ, α, and β. From these, the error, δ, may be determined.

$$\delta = \frac{1}{2}\left(\frac{A_1}{r} + \frac{A_2}{r}\right) - 1$$

where the error is defined as the ratio, to r, of the difference between the average of A_1 and A_2 and the actual distance r between mating-plane centers, that is

$$\delta = \left(\frac{A_1 + A_2}{2} - r\right)/r$$

To visualize the case resulting in the maximum error, see Figure A-4. These cases are based on $\theta = 0^\circ$, which causes the greatest difference between A_1 and A_2 and thus a maximum effect on the value of θ on δ. Obviously in cases a and b the center-separation distances are equal to the averages of A_1 and A_2. In the remaining cases, they are not equal. But, within practical limits, they are.

The limiting case which results in maximum δ is illustrated in cases d and e which are, in principle, the same. For the limiting case, the following conditions are chosen, based on Saturn V geometry and specific values.

$$\theta = 0^\circ$$

$$\alpha = 15^\circ$$

$$r_0 = 225 \text{ in.}$$

$$r = r_0 + 15 \text{ ft} = 408 \text{ in.}$$

$$a = 130 \text{ in.}$$

$$\beta = \sin^{-1}\left(\frac{a}{r}\sin\alpha + \frac{r_0}{r}\right)$$

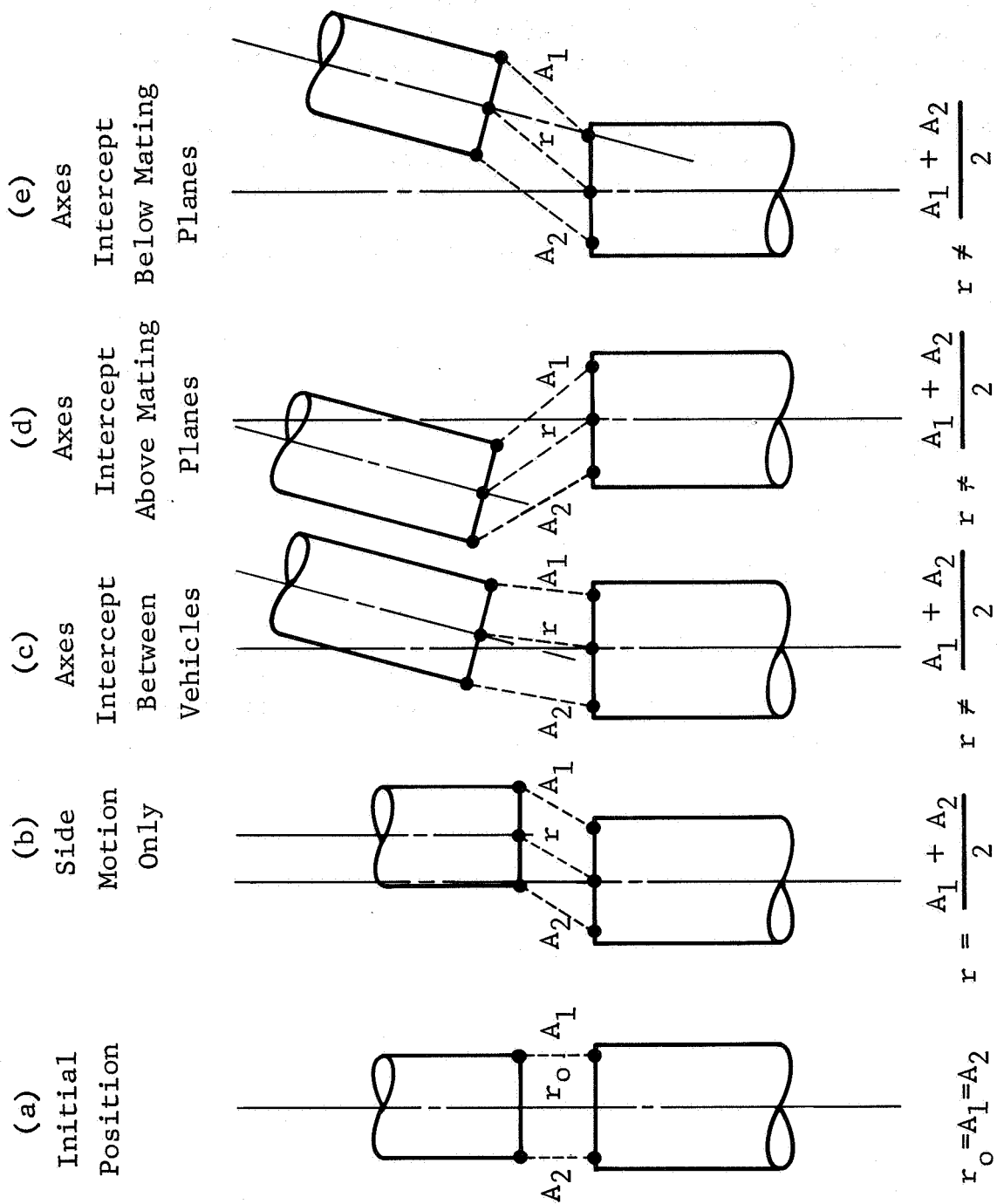Figure A-4 Example of Positions of Vehicles

107

A-2 Angle Measurement

A source and detector can be made sensitive to the angle between their centerlines by providing identical shields on the source and detector. The most simple shield, which proved to be quite satisfactory, was a right cylindrical collimator.

The expression for the intensity of radiation through one right cylindrical collimator as a function of angle from its centerline is

$$\frac{I}{I_o} = 2\left(\frac{180 - 2 \text{ arc } \sin(h/2r) \, \sin\theta}{360}\right)\cos\theta$$

$$- \frac{h\left(r^2 - h^2/4 \, \sin^2\theta\right)^{1/2}}{2r^2} \, \sin\theta$$

where h = collimator height

   r = collimator radius

   θ = incident angle from axis

A collimator 5.08 cm in height and 0.835 cm in radius was used to shield a detector from a distant Ce^{144} source. The results of this test show an almost linear response as a function of angle, as can be seen in Figure A-5.
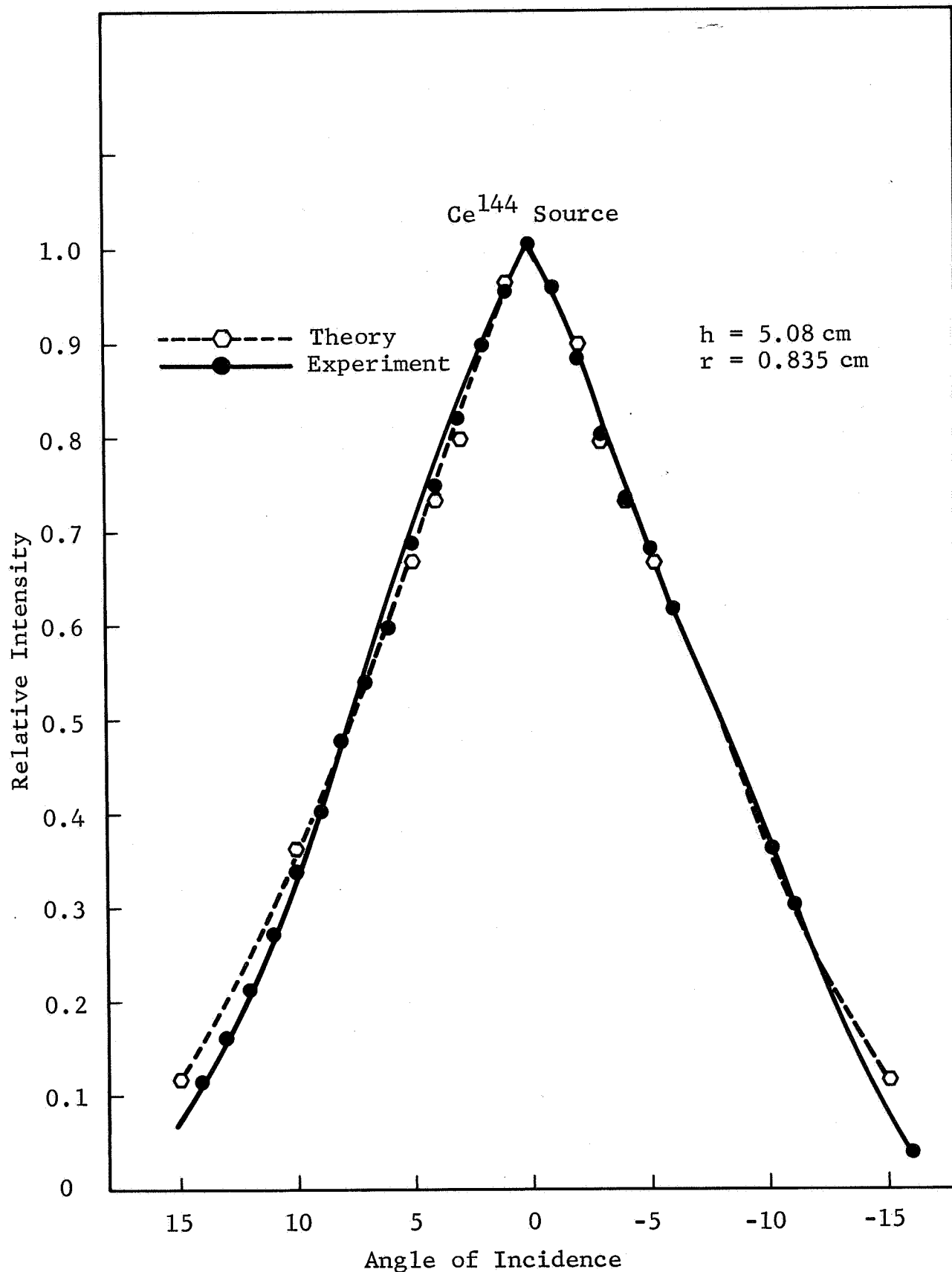
Figure A-5 Angle Measurement